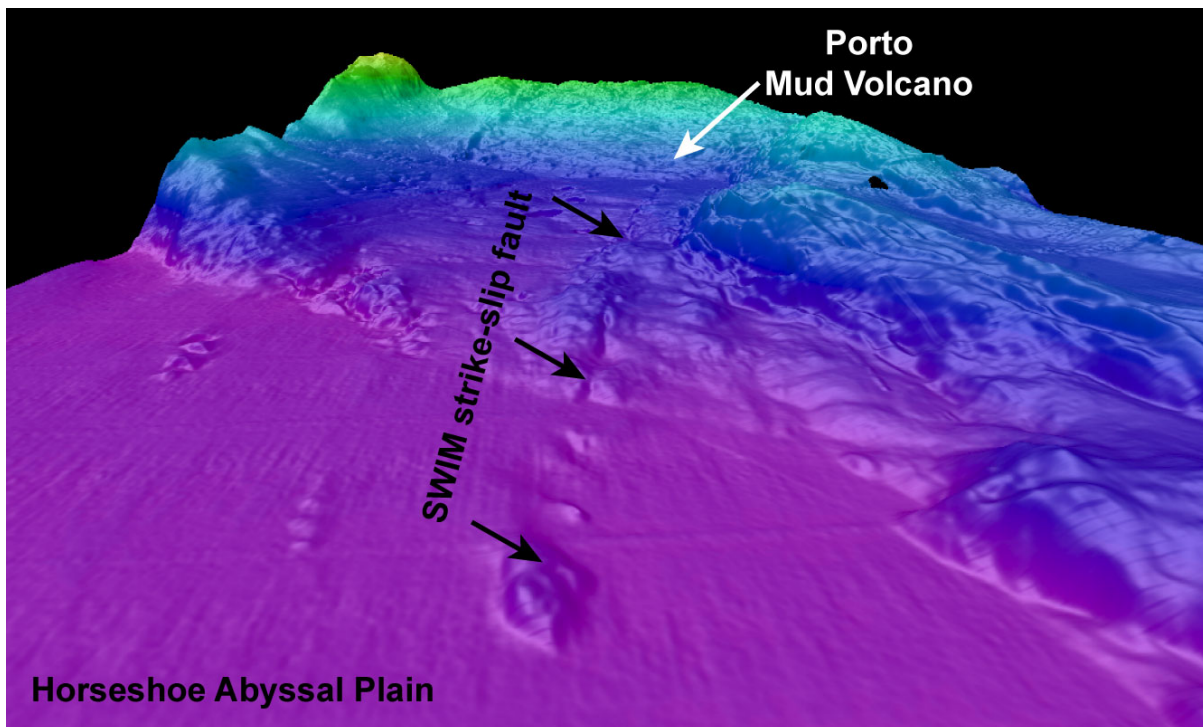


TransFlux

Tracing for active dewatering sites along deep-reaching transform faults in the western Gulf of Cadiz

Cruise 86, Leg 5, Palma de Mallorca – Lisbon, February 23 –March 16, 2012



Dr. C. Hensen and cruise participants
GEOMAR Helmholtz-Zentrum für Ozeanforschung Kiel

Editorial Assistance:

Senatskommission für Ozeanographie der Deutschen Forschungsgemeinschaft
MARUM – Zentrum für Marine Umweltwissenschaften der Universität Bremen

Leitstelle Deutsche Forschungsschiffe
Institut für Meereskunde der Universität Hamburg

2013

Table of Contents

Leg 86/5

1. Summary	4
2. Participants.....	6
3. Narrative	8
4. Preliminary Results	10
4.1 Shipboard Hydroacoustic Systems	10
4.2 AUV	25
4.2.1 AUV “ABYSS” dives	25
4.2.2 AUV Data Processing	31
4.3 CTD and Water Column sampling	42
4.4 Sedimentology and Coring	49
4.5 Biology.....	59
4.6 Pore Water Geochemistry	64
4.7 Organic Geochemistry	71
4.8 Heat flow measurements.....	73
4.9 Measurement of thermal conductivity on sediment cores	78
5 Cruise and weather report M86/5	80
6. List of Stations	81
7. Acknowledgments.....	89
8. Data and sample storage and availability.....	89
9. References.....	89
Appendix:	92

1. Summary

Cruise M86/5 aimed at collecting data from potential fluid dewatering sites located in the deep-sea region of the western part of the Gulf of Cadiz and the adjacent deep sea plain. Previous work on mud volcanoes (cruises SO175 and MSM1/3) located on the accretionary wedge in the Gulf of Cadiz showed that mud volcano fluids are typically sourced at several km depth below the seafloor. In addition, the geochemical composition of fluids from the deepest mud volcano in this area which is located on a west-east trending transform lineament (SWIM1) indicated that these fluids are typical for having been altered by the reaction with oceanic crust. This implies that there is active flow connecting the oceanic basement and the seafloor. To date, such kind of hydrothermal circulation is only known for relatively young oceanic crust (<60 Ma). Hence, the existence of a hydrological connection between old, sedimented oceanic crust and the seafloor is a phenomenon, which essentially has not been investigated in the past, and may represent a (missing) link between hot vents at mid-ocean ridges and cold seeps at continental margins. On the cruise, we followed an interdisciplinary approach characterized by extensive geochemical sampling in the water column and the sediment, heat flow measurements, and detailed mapping with AUV and ship-based hydroacoustic systems. We mainly investigated selected sites with conspicuous backscatter anomalies recorded on previous cruises along the SWIM1 lineament: (i) within the transition between the accretionary prism and the Horseshoe Abyssal Plain and (ii) on seafloor highs within the Horseshoe Abyssal Plain itself. The geotectonic environment in both sections is completely different from the situation on the accretionary wedge, where numerous mud volcanoes were detected on previous cruises. Within the transition zone three new mud volcanoes were discovered and extensively sampled during M86/5. Typical chemoautotrophic organisms were found here together with conspicuous methane anomalies in the water column. Preliminary pore water analyses show that the fluids indicate a deep origin, but show distinctive differences to those found on the mud volcanoes on the wedge. Future analyses will show, if this phenomenon is - as hypothesized - due to decreasing sediment thickness with increasing westward distance from the wedge, and hence decreasing sediment-water interaction overprinting the original fluid composition. On the seafloor highs along the SWIM1 lineament in the Horseshoe Abyssal Plain no seeps or mud volcanoes were discovered. However, the lineament seems to be active in terms of fluid flow as indicated by pore water and heat flow anomalies as compared to values measured off the lineament. Overall, the major goal of the cruise could be fulfilled: fluid seeps related to active faults were discovered in a new geotectonic environment. The overall significance in terms of fluid transport in old oceanic crust and/or the role of deeply-rooted fault systems needs to be further addressed in subsequent studies.

Zusammenfassung

Ziel der Meteor Reise M86/5 war die Untersuchung potentieller Entwässerungsstrukturen westlichen Teil des Golfes von Cadiz und der darin anschließenden Tiefseeebene. Vorarbeiten an Schlammvulkanen im Golf von Cadiz während der Reisen SO175 und MSM1/3 hatten gezeigt, dass dort entlang von Transformstörungen Fluide aus mehreren Kilometern Tiefe mobilisiert werden. Die geochemische Zusammensetzung der Schlammvulkan-Fluide im westlichen Teil des Akkretionskeils weist eindeutig auf Alterationsprozesse und damit Zirkulation in der ozeanischen Kruste hin. Die Fluidzirkulation zwischen ozeanischer Kruste und dem

Meeresboden, verbunden mit hydrothormaler Alteration von Krusten-gestein und Sediment, ist bislang nur für relativ junge Plattenalter (<60 Ma) nachgewiesen. Solche hydrologischen Verbindungen zwischen alter, sedimentbedeckter ozeanischer Kruste und dem Meeresboden könnten ein bislang unbekanntes Bindeglied zwischen Hydrothermalquellen an Spreizungsachsen und kalten Quellen an Kontinentalrändern darstellen. Während der Ausfahrt wurden ausgewählte Lokationen - im Bereich der sich nach Westen in die Tiefsee-Ebene hinein erstreckenden Transformstörungen - mit einem interdisziplinären Ansatz erkundet. Wegen der nach Westen abnehmenden Sedimentbedeckung konnte hier mit einer geringeren Überprägung und somit klareren Fluid-Signalen aus der ozeanischen Kruste gerechnet werden. Es wurden geochemische Beprobungen der Wassersäule und der Sedimente, Wärmestrom-Messungen sowie Kartierungen mit dem AUV sowie den schiffseigenen hydroakustischen Systemen durchgeführt. Es wurden vornehmlich Stationen entlang des SWIM 1 Lineamentes ausgewählt, die eine deutliche Anomalie in der Rückstreu-Intensität aufwiesen. Hierbei wurden sowohl Strukturen innerhalb der Übergangzone zwischen dem Akkretionskeil und der Horsehoe Tiefseebene als auch bathymetrische Erhebungen am Meeresboden in der Horsehoe Tiefseebene selbst ausgewählt. Das geotektonische Umfeld ist hier grundsätzlich anders als auf dem östlich gelegenen Akkretionskeil, auf dem in der Vergangenheit bereits zahlreiche Schlammvulkane nachgewiesen werden konnten. Innerhalb der Übergangzone zwischen dem Akkretionskeil und der Horsehoe Tiefseebene wurden auf M86/5 drei neue Schlammvulkane entdeckt und intensiv beprobt. Typisch sind eine entsprechende Besiedlung des Meeresbodens mit chemoautotrophen Organismen, sowie auffällige Methananomalien in der Wassersäule. Erste Porenwasseranalysen weisen auf eine tiefe Quelle der mobilisierten Fluide hin, zeigen aber auch auffällige Unterschiede zu den bislang untersuchten Fluid-Proben von Schlammvulkanen auf dem Akkretionsrücken. Weitergehende Analysen werden Aufschluß darüber bringen, wie diese Unterschiede hinsichtlich der aufgestellten Hypothesen einzuordnen sind. Weitere Schlammvulkane oder „Cold Seeps“ konnten auf der Tiefseebene nicht nachgewiesen werden, allerdings weisen geochemische Anomalien im Porenwasser und erhöhte Wärmestromwerte an einzelnen Strukturen darauf hin, dass auch hier das SWIM 1 lineament „fluid-aktiv“ ist. Insgesamt wurden alle wesentlichen Ziele der Ausfahrt erreicht; herausragend ist hierbei die Entdeckung neuer Schlammvulkane in der Tiefsee. Die Erkenntnis, dass diese Fluidquellen auch abseits der dafür typischen geologischen Strukturen existieren, muss nun hinsichtlich ihrer Bedeutung bezüglich des Fluidtransportes in alter Kruste und der Rolle tiefreichender Störungssysteme weiter untersucht werden.

2. Participants

1. Christian Hensen, Dr.	Chief scientist	GEOMAR
2. Florian Scholz, Dr.	Pore water geochemistry	GEOMAR
3. Bettina Domeyer	Pore water geochemistry	GEOMAR
4. Ulrike Lomnitz	Pore water geochemistry	GEOMAR
5. Verena Thönißen	Pore water geochemistry	GEOMAR
6. Ann-Marie Völsch	Pore water geochemistry	GEOMAR
7. Lorenzo Rovelli	CTD sampling	GEOMAR
8. Anke Bleyer	Gas geochemistry	GEOMAR
9. Marianne Nuzzo, Dr.	Organic geochemistry	LNEG
10. Erica dos Santos Godinho	Organic geochemistry	LNEG
11. Hector Perea, Dr.	Hydroacoustics	CSIC / CMIMA
12. Vasco Valadares, Dr.	Hydroacoustics	FCUL / LNEG
13. Pedro Terrinha, Dr.	Hydroacoustics	LNEG
14. Andreas Prokoph	Hydroacoustics	GEOMAR
15. Klas Lackschewitz, Dr.	AUV	GEOMAR
16. Fred Wendt	AUV	GEOMAR
17. Marcel Rothenbeck	AUV	GEOMAR
18. Norbert Kaul, Dr.	Heat Flow	GeoB
19. Bernd Heesemann	Heat Flow	GeoB
20. Tobias Kulgemeyer	Heat Flow	GeoB
21. Elena Pinero, Dr.	Sedimentology	GEOMAR
22. Vitor Magalhães, Dr.	Sedimentology	CESAM / UA
23. Asmus Petersen	Coring	GEOMAR
24. Claus Hinz	Sensorics, video technics	GEOMAR
25. Marina Cunha, Dr.	Benthos Biology	CESAM / UA
26. Ana Hilario, Dr.	Benthos Biology	CESAM / UA
27. Elger Esser	Photographer	
28. Andreas Raeke	Bordwetterwarte / Meteorology	DWD
29. Juliane Hempelt	Bordwetterwarte / Meteorology	DWD

GEOMAR

Helmholtz-Zentrum für Ozeanforschung Kiel
Wischhofstr. 1-3
D-24148 Kiel
www.geomar.de

LNEG

Laboratório Nacional de Energia e Geologia
Estrada da Portela - Bairro do Zambujal
Alfragide - Apartado 7586

FCUL

Faculdade de Ciências
da Universidade de Lisboa
Campo Grande
1749-016 Lisboa, Portugal

CESAM / UA

Centro de Estudos do Ambiente e do Mar
Universidade de Aveiro
Campus Universitario de Santiago
3810-193 Aveiro, Portugal

CSIC / CMIMA

Unitat de Tecnologia Marina – CSIC
Centre Mediterrani d’Investigacions Marines i Ambientales
– CMIMA
Passeig Maritim de la Barceloneta, 37-49
08003 Barcelona, Spain

GeoB

Fachbereich 5 - Geowissenschaften
Universität Bremen
Klagenfurter Straße
28359 Bremen, Germany
<http://www.geo.uni-bremen.de/>

DWD

Deutscher Wetterdienst
Seeschiffahrtsberatung
Bernhard-Nocht-Straße 76
20359 Hamburg / Germany
Internet: www.dwd.de
e-mail: seeschiffahrt@dwd.de



Fig. 2.1: Scientific party of M86/5

3. Narrative

(C. Hensen)

FS Meteor arrived at Palma de Mallorca in the morning of the 20th of February 2012. Most of the scientific equipment could be loaded within the following two days. However, the container with the AUV Abyss arrived only in the morning of the 23rd of February due to logistical problems. Since a harbor test of this device was obligatory the departure had to be postponed by one day. Meteor left the port of Palma de Mallorca in the morning of the 24th of February 2012 with an international group of 28 scientists onboard and on a transit of about 3 days into the working area, the western extension of the Gulf of Cadiz. The time during the transit was used to set up laboratories and prepare scientific equipment. One important aspect was to check and fix important working modes of the AUV. These tasks could successfully be fulfilled during the first 2 days of the transit and a technician of the company Remus, producing the multibeam-bathymetry device mounted on the AUV, could leave the ship during a stopover in Cadiz.

In the early morning of the 27th of February the station work started with recording a number of Multibeam and Parasound (MB/PS) transects across 3 preselected sites, which were considered as potential seep locations. Ground-truthing by gravity corer, however, did not reveal evidence for active seepage here. On the following two days station work was mostly dedicated to run and test all gears and scientific devices at Porto mud volcano (MV), a known active seep site located at the western margin of the accretionary wedge. In spite of minor problems all station work could be successfully carried out at this position. Thereafter, new potential mud volcano sites were explored along the E-W trending SWIM1 fault north of Coral Patch Ridge. On the 1st of March the first successful deployment of a gravity corer at 35°44.3'N and 10°12.1' W retrieved sediments from an active mud volcano located at about 30 nautical miles west of Porto MV. Almost coincident, the existence of another two mud volcanoes could be confirmed on an AUV sidescan survey a few miles further to the west. During the following days the mud volcanoes were intensively sampled by gravity corer, box corer, CTD, and heat flow probe. In addition, all three structures were mapped during high resolution side scan and bathymetry surveys. Unfortunately, on the 2nd of March the coaxial cable broke, and as a consequence the TV-guided multicorer could not be deployed further on.

Almost parallel to the sampling of the known sites, new sites were explored further to west in the Horseshoe Abyssal Plain and to the north along the Horseshoe fault. However, those backscatter anomalies in the north were abandoned after some surveys with the Parasound sub-bottom profiler system as they could be identified as being related to morphological features at the seafloor and not to fluid emanation. Hence, most of the working time was thereafter dedicated to the study of seafloor highs and other conspicuous sites in the Horseshoe Abyssal Plain along the SWIM 1 lineament. Although no further seepage sites could be found here, the major fault line could be proven to be active in terms of recent tectonics, heat flow and fluid flow. In addition, a number of backscatter anomalies were investigated at the southern slope of the Gorringer Bank and the northwestern slope of Coral Patch Ridge. These backscatter anomalies, however, turned out to be caused either by outcrops of consolidated sediments, slope morphology or even ship wrecks. Two wrecks were mapped in detail during AUV surveys. During the last 2 days of the cruise one of the M. Ivanov MV was revisited in order fill in the remaining sample gaps. As a highlight, a gravity core of approximately 1m length containing a massive piece of gas hydrate

could be retrieved. Finally, a photo survey with the AUV was performed here in order to compensate for the lack of other video guided instruments. At the end of this station the AUV had to be recovered by zodiac because the messenger line of the device was twisted around its propeller. Station work of a successful cruise ended in the morning of the 15th of March. After a transit of about 20 hours RV Meteor moored at the pier “Terminal de Cruzeiros da Rocha Conde de Óbidos” in Lisbon at 08:00 on the 16th of March.

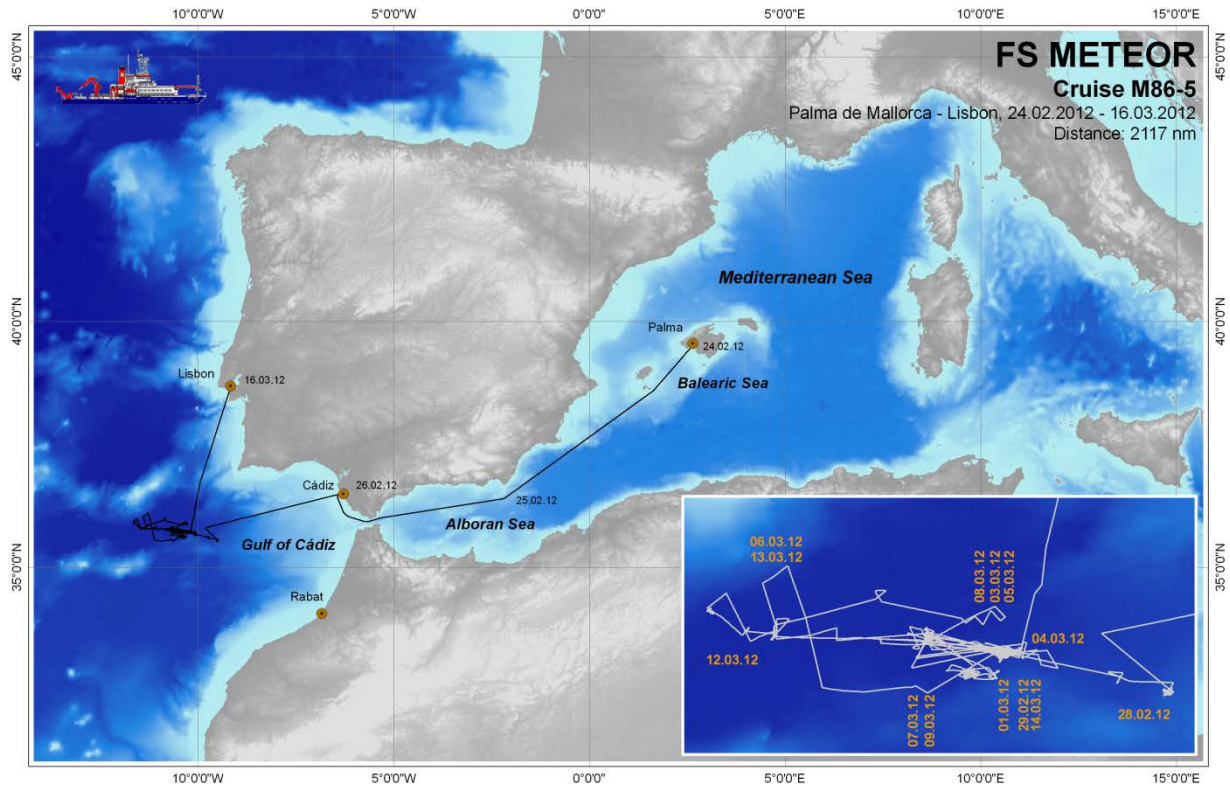


Fig. 3.1: Cruise plot of M86/5

4. Preliminary Results

4.1 Shipboard Hydroacoustic Systems

(M. Terrinha, H. Perea, A. Prokoph, V. Valadares)

EM 122 bathymetric and backscatter mapping

Two multibeam systems are available onboard R/V METEOR for bathymetric mapping of the seafloor: a KONGSBERG EM122 for deep-water mapping and a KONGSBERG EM710 for shallow water. Due to depths between 3500 m and 4900 m in the western Gulf of Cadiz, only the EM122 System was used for surveying the seafloor. There were no measurements carried out with the shallow water echosounder EM710 during the whole cruise.

The EM122 system is a deep-water multibeam echosounder that provides accurate bathymetric mapping of the seafloor. (Fig. 4.1.1) Basic components of the system are two linear transducer arrays in a Mills cross configuration with separate units for transmitting and receiving. The nominal sonar frequency is 12 kHz with an angular coverage sector of up to 150° and 256 beams per ping. The emission beam is 150° wide across track, and 1° along track direction. The reception is obtained from 256 beams, with widths of 2° across track and 20° along track. Thus, the actual footprint of a single beam has a dimension of 1° by 2°. Achievable swath width on a flat bottom will normally be up to six times the water depth depending on the character of the seafloor. The angular coverage sector and beam pointing angles may be set to vary automatically with depth according to achievable coverage. This maximizes the number of usable beams. The beam spacing can be chosen to be equidistant or equiangle at the seafloor, in addition a “high-density-equidistant” mode is available. Using this mode 432 independent depth values (soundings) are obtained perpendicular to the track for each ping. Using the 2-way-travel-time and the beam angle known for each beam, and taking into account the ray bending due to refraction in the water column by sound speed variations, depth is calculated for each beam. A combination of amplitude (for the central beams) and phase (slant beams) is used to provide a measurement accuracy that is practically independent of the beam-pointing angle.

Common for the system is the “dual swath” technology, which means that two pings (rather than one) are simultaneously transmitted and recorded, one slightly tilted forward and one backward, thus enabling a denser bottom coverage along track, or allowing for a higher survey speed. So 864 independent depth values are achieved with each record. The system also applies CW (continuous wave) pulses in shallow modes and FM pulses in deep modes. FM or “chirp” pulses transmit more energy to the water, thus enabling greater ranges of the beams, in turn leading to better across-track coverage of the seafloor, particularly at greater depths. On the other hand, systems applying FM pulses demand additional features of the motion reference unit because the acoustic signals travel a longer time through the water while the vessel is moving. Consequently, the motion sensor of R/V METEOR was recently upgraded to a Seapath-300, an inertial motion-reference unit, which is augmented by GPS-signals.



Fig. 4.1.1: Basic principle of a multibeam echosounder

In addition to travel times, the Simrad EM122 also records the amplitude of the backscattered signal that is used to produce seafloor backscatter maps. The acoustic backscatter acquired by multibeam carries important information about the seafloor geomorphology and physical properties. With the proper radiometric and geometric correction, acoustic backscatter mosaics can aid in the mapping of surficial seafloor features and facies, an important task toward remote seafloor characterization. Backscatter mosaics can also provide important auxiliary information not only for marine geological and environmental studies but also for hydrographic surveys (Fonseca 2005). The principle of sonar imaging is the same for multibeam sounders and sidescan sonars. The signal backscattered by the seabed is recorded as a function of time, and its instantaneous intensity represents irregularities (i.e. seabed structure) if the ground strip swept by the signal. When constructing a sonar image from multibeam sounder data, time signals are available after beam forming. They must therefore be recombined so as to provide a continuous image all along the swath. The multibeam sidescan represents the echo amplitude on a time reference. The echo amplitudes of all pre-formed beams are combined and densely sampled to derive the cross profile of amplitude values for each ping. This provides acoustic imagery that is comparable to regular sidescan systems that are towed close to the bottom and that transmit short pulses in a slant direction that sweep the bottom. The multibeam sidescan performance is reduced in comparison to towed sidescan systems because the acoustic pulse is longer, less grazing and affected by larger movements of the ship. (Lurton 2002)

Multibeam Data Processing

Processing multibeam data involves two steps: a profile-oriented processing followed by area-based processing. The former requires checking navigational data, interpolating missing navigational values, calculating water depth in order to determine the location of the beam swaths by ray-tracing through the water-column (taking into account the sound velocity profile) and finally, data cleaning by removing artefacts and erroneous data points. Area-based processing comprises the calculation of a digital terrain model (DTM) and the visualisation of the data. For these purposes, the R/V METEOR is equipped with the NEPTUNE software package from KONGSBERG. However, mainly for easier integration of other data from different systems in various data formats, we processed the multibeam data with the “open source software” packages MB-SYSTEM (Caress and Chayes, 1996) and GMT (Wessel and Smith, 1995). The processing of the acoustic backscatter data was carried out with IVS 3D Fledermaus.

Results

Most of the study area had already been mapped during various cruises in the past. Consequently, acquiring new bathymetry was not a major objective of this cruise. To achieve improved results a reduced swath opening angle of max. 120° was chosen. The gathered bathymetry and backscatter information was used to support the search for possible mud volcanoes in the area under investigation. (Fig. 4.1.2) All mud volcanoes are located at great depth, around 4500 mbsl. For that a detailed mapping with the hull mounted hydroacoustic systems was not possible. High resolution surveys were realized by deploying the AUV. During the cruise two different sound velocity profiles were used: the first one was measured at the 27th of February at Porto MV, the second profile was taken at the 1st of March near M. Ivanov, Abzu and Tiamat MV.

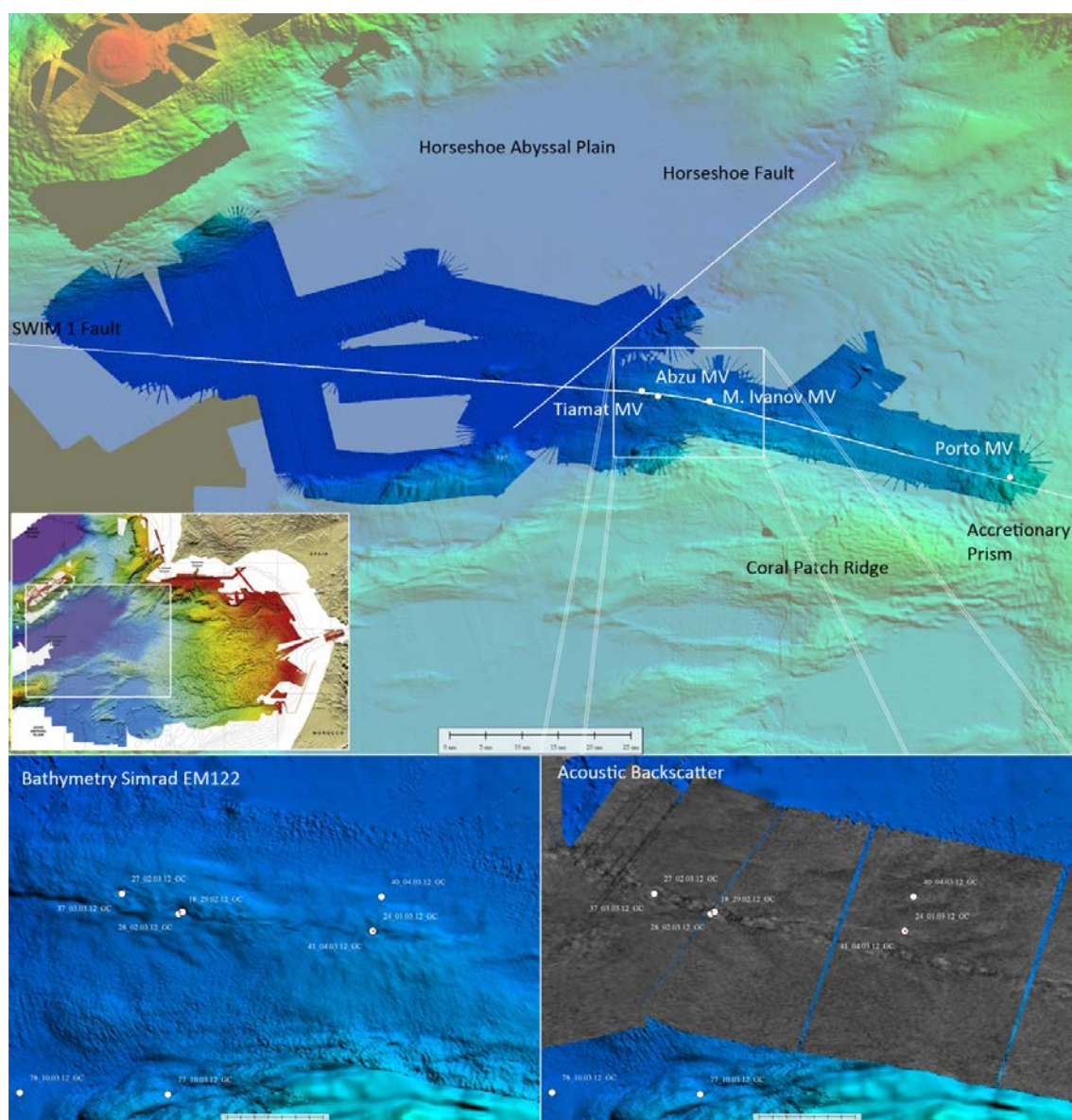


Fig. 4.1.2: Bathymetry acquired in the western Gulf of Cadiz; the small pictures display the area around the three discovered mud volcanoes, M. Ivanov, Abzu and Tiamat.

Sub-bottom profiling – Parasound

In parallel to the bathymetric mapping, the hull mounted parametric sub-bottom profiler Parasound P70 (Atlas Hydrographic GmbH, Bremen) was operated to provide high resolution information of the uppermost 50-100 m of the sediments. Parasound P70 works as a narrow beam sediment echo-sounder, providing primary high frequencies (PHF) of 18 kHz and adjustable to 18.5-28 kHz, thus generating parametric secondary low frequencies (SLF) in the range of 0.5-10 kHz and secondary high frequencies (SHF) between 36.5-48 kHz. The secondary frequencies develop through nonlinear acoustic interaction of the primary waves at high signal amplitudes. This takes place only in the emission cone of the PHF signal, which is limited to an aperture angle of only 4° for the Parasound P70. This is achieved by using a transducer array of 128 transducers on a rectangular plate of approximately 1 m² in size. Therefore the footprint size is only 7% of the water depth and vertical and lateral resolution is significantly improved compared to conventional 3.5 kHz echosounder systems. The fully digital system provides important features like recording of the 18 kHz PHF signal and both secondary frequencies, SLF and SHF, continuous recording of the whole water column, beam steering, different types of source signals (continuous wave, chirp, barker coded) and signal shaping. However, many of the new features are still in an experimental state. Digitization takes place at 96 kHz to provide sufficient sampling rates for the SHF. A down-mixing algorithm in the frequency domain is used to reduce the amount of data and allow data distribution over ethernet. For the standard operation a parametric frequency of 4 kHz and a sinusoidal source wavelet of 2 periods was chosen to provide a good relation between signal penetration and vertical resolution. The transmission sequence was established as a single pulse mode with manual system depth at the beginning of the acquisition and afterwards controlled by the PHF arrival. The PHF signal was recorded permanently. All raw data were stored in the ASD data format (Atlas Hydrographic), which contains the data of the full water column of each signal as well as the full set of system parameters. Additionally, a 200 m long reception window of the onboard processed data was recorded in compressed PS3 data and SEG Y format. All lines were then loaded to a Kingdom Suite Project. A total of 108 profiles of high-resolution ATLAS Parasound parametric sub-bottom profiler were acquired in the Gulf of Cadiz, 42 coinciding with M86-5 stations and 66 corresponding to transits between stations. In total, around 669 nm during the M86-5 cruise were acquired. Most of the profiles corresponding to stations were acquired at speed of 5 to 7 knots. However, profiles corresponding to transits were acquired at 10 to 12 knots.

The survey concentrated mainly along the SWIM Fault described by Terrinha et al. (2009) and Zitellini et al. (2009) searching for fluid escape structures, such as mud volcanoes. The SWIM Fault cuts across various morpho-tectonic regions, three of which were studied during this mission, the Gulf of Cadiz Accretionary Wedge (specifically the zone of the Porto mud volcano), the Horseshoe Valley and the Horseshoe Abyssal Plain. Thus the survey extended along the SWIM Fault for a total length of approximately 250 km, from the Porto mud volcano in the east to the southwestern slope of the Gorringer Bank in the west (Fig. 4.1.3).

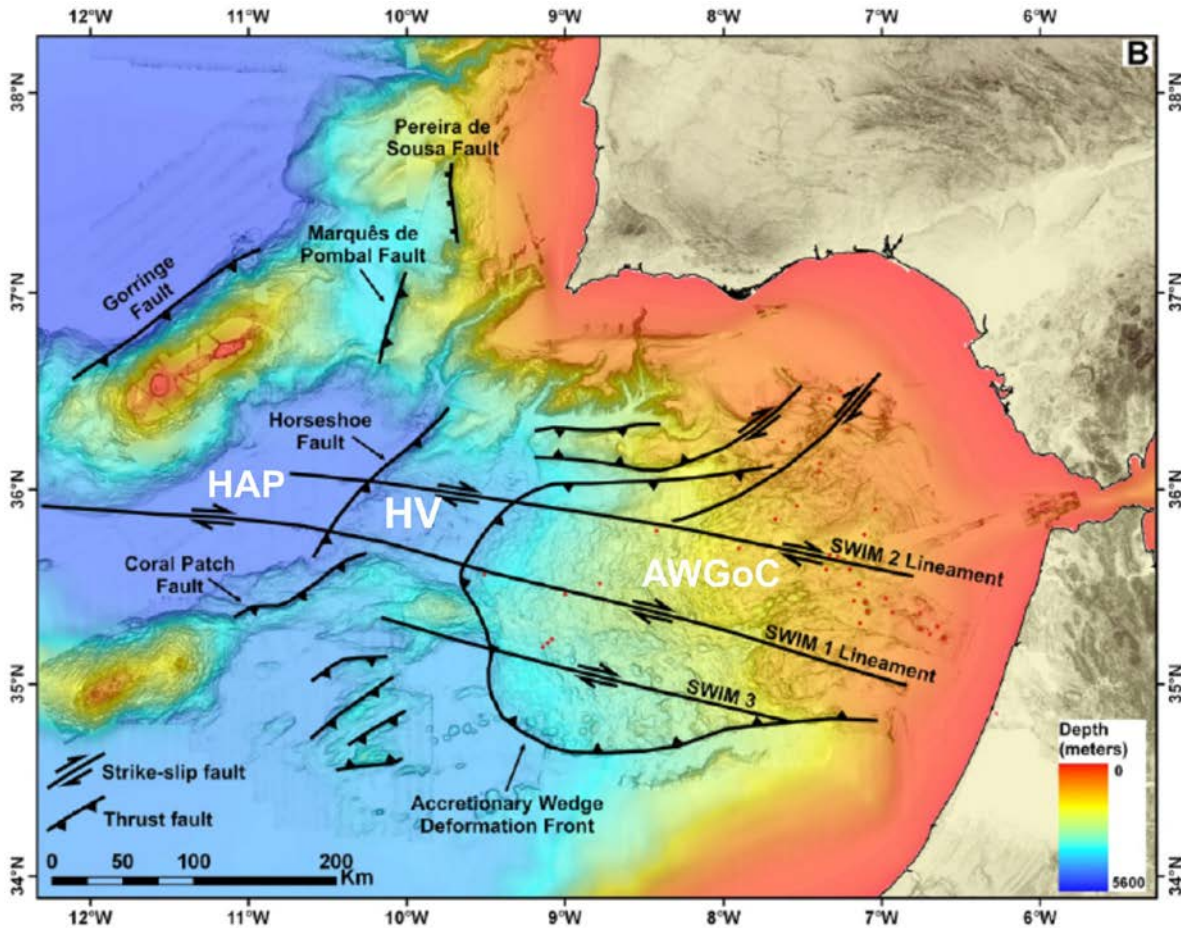


Fig. 4.1.3: Bathymetric and simplified tectonic map of the Gulf of Cadiz study area adapted from Duarte et al. (2010). HAP, Horseshoe Abyssal Plain; HV, Horseshoe Valley; AWGoC, Accretionary Wedge of the Gulf of Cadiz.

The ATLAS Parasound parametric data show detailed stratigraphic information of the uppermost tens of metres below the seafloor (up to 75 m at an assumed sediment velocity of 1.5 km/s). These new data provide new insights into the Pliocene-Quaternary sedimentary architecture over the surveyed zones, as well as into the subsurface tectonic geometry of the faults and fault systems observed there. The best results were obtained in the flat areas of the Horseshoe abyssal Plain with highly penetrative sediments, while abrupt slopes displayed very low penetration, as in the Gulf of Cadiz Accretionary Wedge and the Horseshoe Valley. Figure 4.1.4 displays PARASOUND stations recorded during this mission and the following examples refer to this figure.

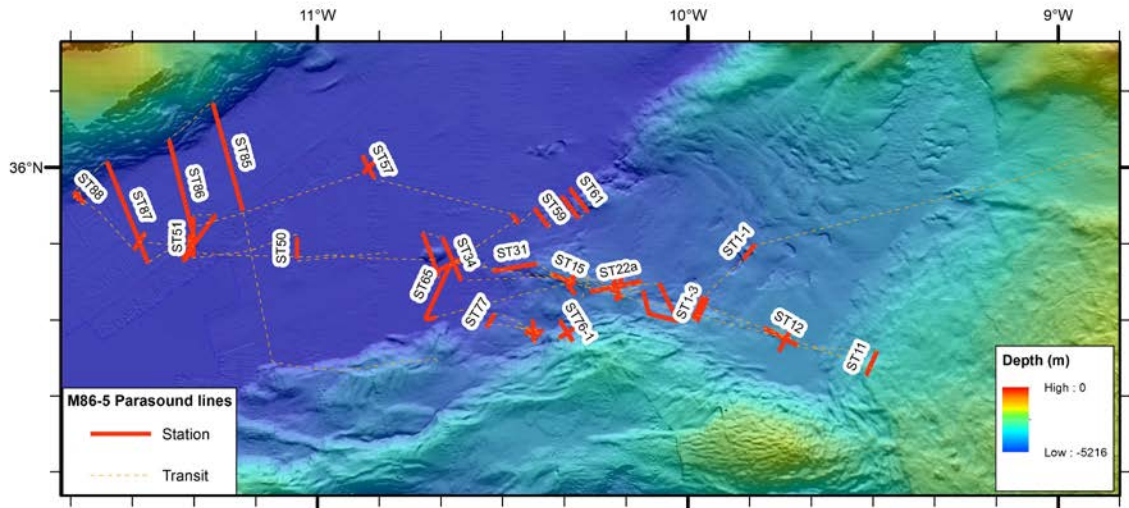


Fig. 4.1.4: Location of the PARASOUND stations profiles recorded during the TRANSFLUX mission. Labels correspond to the longest profiles.

Results from the Parasound acoustic survey

The Mediterranean Outflow Water Contourites

On the transit from Cadiz to the study area a transit profile was acquired in Portuguese territorial waters, from approximately 900 m to 1600 m water depths. This profile yielded the best results of all despite the general acquisition speed of 12 kn; this was due to the low shallower water depths and nature of the sediments (Fig. 4.1.5). The sediments are little disturbed by tectonic deformation and display high lateral continuity. The three imaged peaks correspond to diapiric structures.

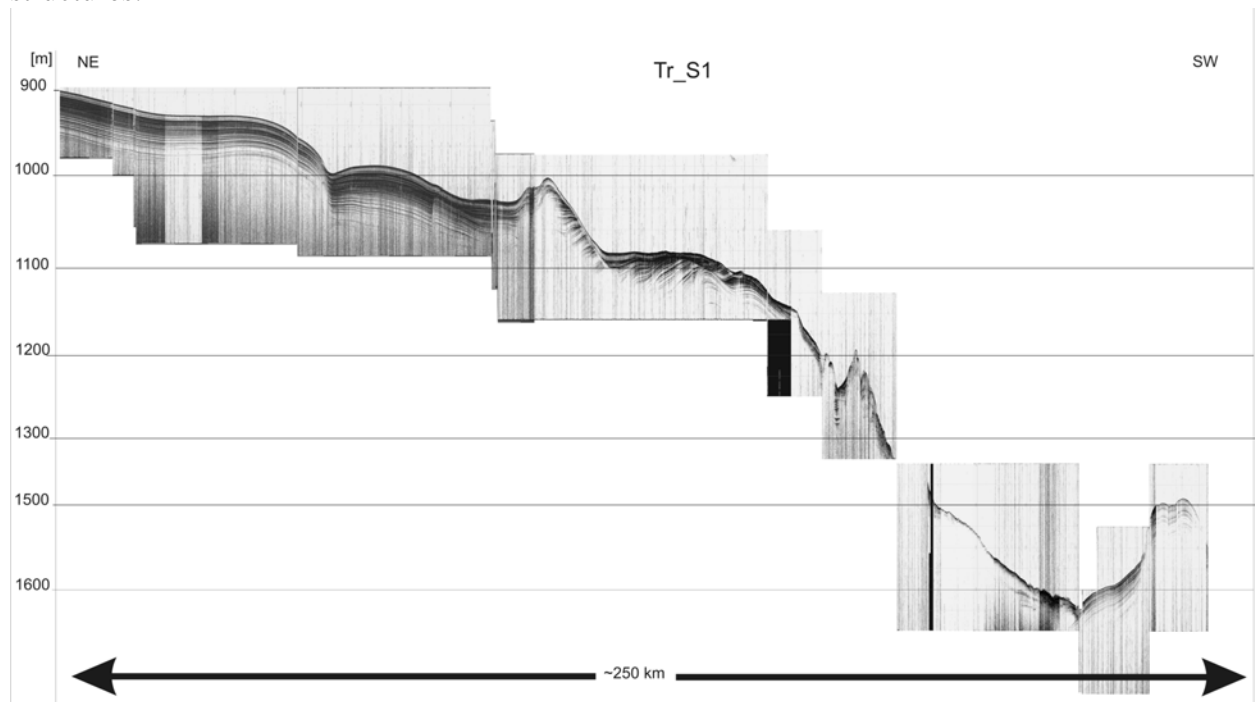


Fig. 4.1.5: Parasound profile acquired during the transit along the Portuguese continental slope. This profile images mainly the contourite deposits associated with the Giant Contourite System of SW Iberia (Hernandez-Molina et al., 2006, Roque et al., 2011).

The Horseshoe Valley

The Horseshoe Valley (HV) is the area comprised between the Accretionary Wedge of the Gulf of Cadiz (AW) and the Horseshoe Abyssal Plain (HAP). Only one target was initially planned to be surveyed station #1 (Fig. 4.1.6).

A NNE-SSW Parasound line, station #1, was acquired across the initial target 14, which corresponds to a localized morphological high in the Horseshoe Valley at the side of a crescent shaped scour, 5 000 m x 2 500 m, at ca. 4 600 m water depth (Duarte et al., 2010). The seamount has an elliptical outline (~2km x ~3.3km) and rises around 110 m above seafloor. The acoustic facies observed in the profile are very reflective and the slopes of the high yielded refractions systematically. The flat segments at the base of the high are also highly reflective and no internal structure of the sediments is observed, probably because this is a zone of active sediment by-pass towards the Horseshoe Abyssal Plain.

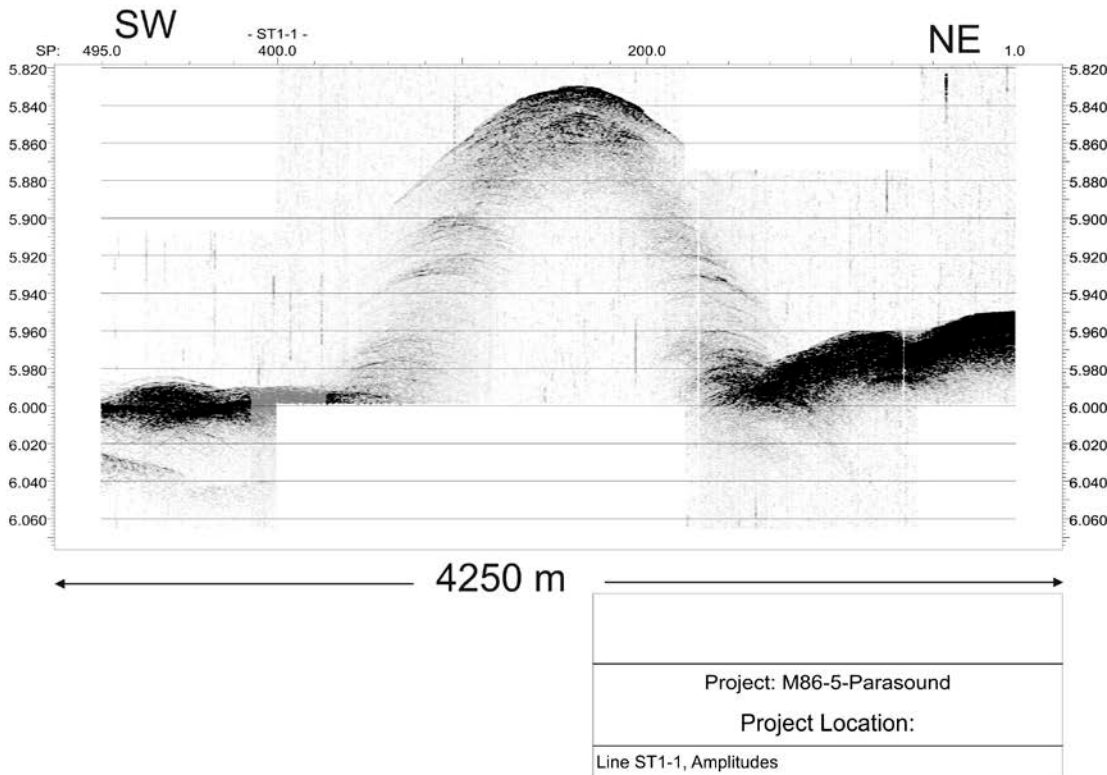


Fig. 4.1.6: Parasound profile Station 1 across the isolated hill located adjacent to a crescent shaped scour in the HV (Duarte et al., 2010). The internal structure of the ca. 130 m high hill is not visible, either due to the lack of penetration of the signal or to its chaotic nature. This target was not cored during this mission. Also note the highly reflective sediments at the sides of the hill. The HV is flushed by turbidites and mass transport processes that apparently do not favour the setting of continuous well stratified sediments.

The Accretionary Wedge of the Gulf of Cadiz and the Porto mud volcano

The AW has been described by various authors (under different designations and geodynamic interpretations (e.g. Gutscher et al., 2002, Iribarren et al., 2007, Zitellini et al., 2009) as a morpho-tectonic unit consisting of a stack of imbricated thrusts, whose thickness varies from virtually nil at its limit up to more than 10 km near the Gibraltar Straits. This unit hosts a series

of mud volcanoes whose location is associated with active thrusts driven by the westward push of the Gibraltar Arc and the SWIM 1 Fault (Fig. 4.1.3).

The acoustic facies of the Porto mud volcano and of the AW are highly diffractive and transparent. The foot of the slope of the AW where it is cut by the SWIM 1 Fault (Fig. 4.1.7) displays a syncline with a top sedimentary unit made up of high amplitude continuous reflections that are interrupted by segments of transparent bodies, that can be interpreted as consisting of debris and blocks fallen from the AW due to its progression onto its foreland.

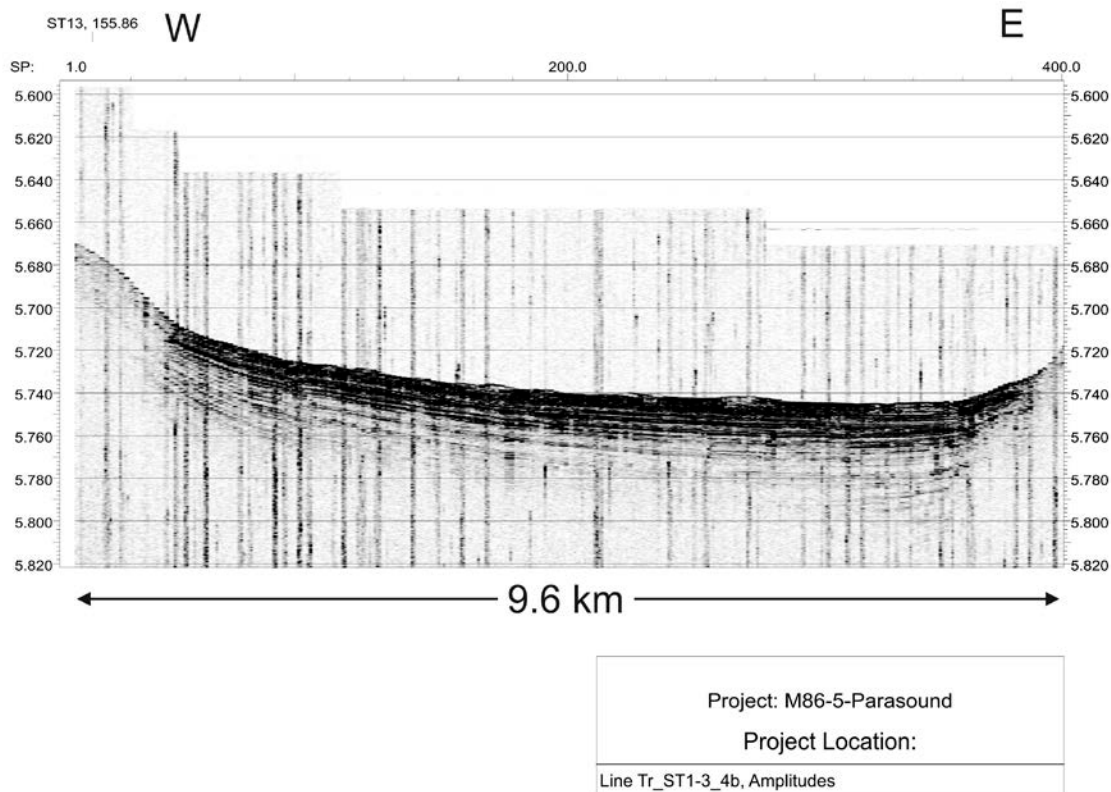


Fig. 4.1.7: PARASOUND profile imaging the gentle syncline in front of the AW (East) and the slope towards the elevated hills of the SWIM 1 Fault (West). Note the continuous high amplitude reflections of the top units interrupted by possible mass transport deposits associated to overthrusting to the West of the AW.

The SWIM 1 Fault mud volcanoes in the Horseshoe Valley

Three mud volcanoes (MV) were found for the first time outside the AW. They are located along the SWIM 1 Fault in the HV and were named as Michael Ivanov, Abzu and Tiamat.

The search for these MVs was initially made on the basis of inspection of the backscatter map of previous multibeam swath bathymetry surveys of this area. During this mission, PARASOUND profiles were run on top of the selected sites before attempting gravity coring. Although three MVs were found, it is clear from AUV side scan sonar surveys (section 4.2) that the PARASOUND profiles were not run across their centres. Despite this fact the structural and lithologic disturbances associated with mud volcanism are still detected on the PARASOUND profiles as shown in figures 4.1.8 and 4.1.9.

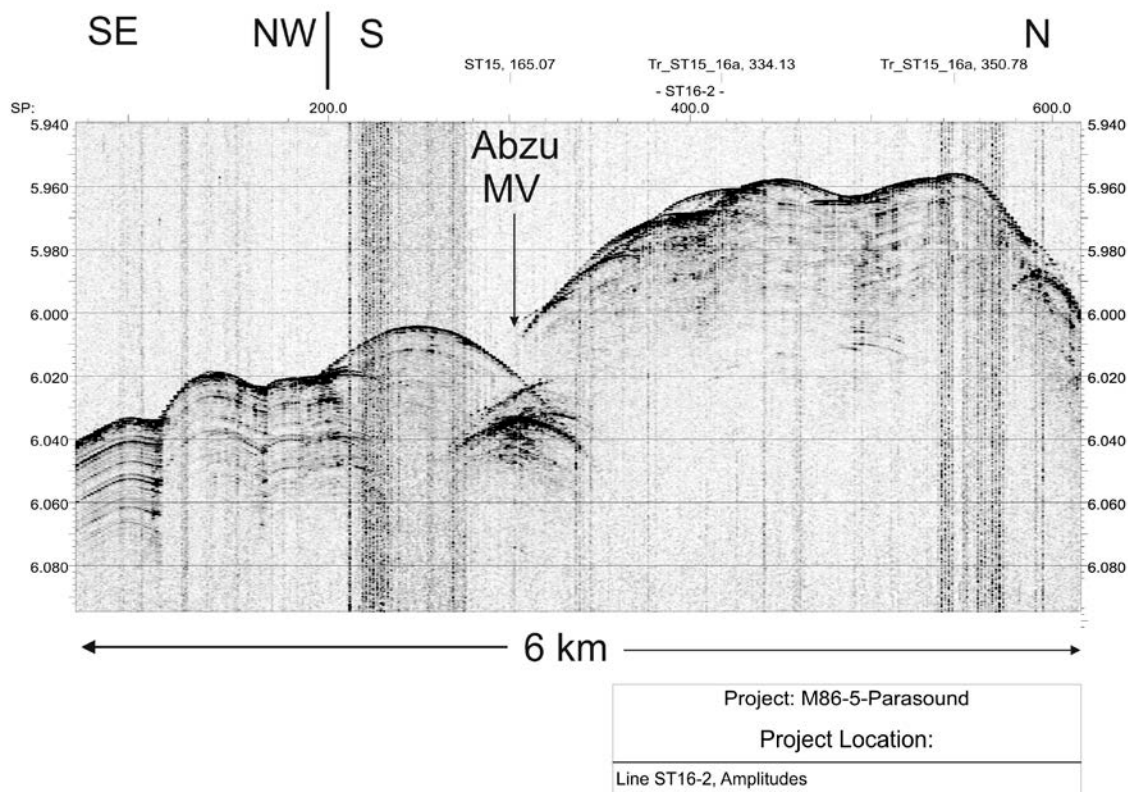


Fig. 4.1.8: PARASOUND line run across the SWIM 1 Fault over MV Abzu. Despite the fact that the line missed the MV by a few tens a metres, it is noticeable that the sedimentary layering observed at the two adjacent sides of the MV is not existent at the Abzu. Also note the highly reflective surface of its top.

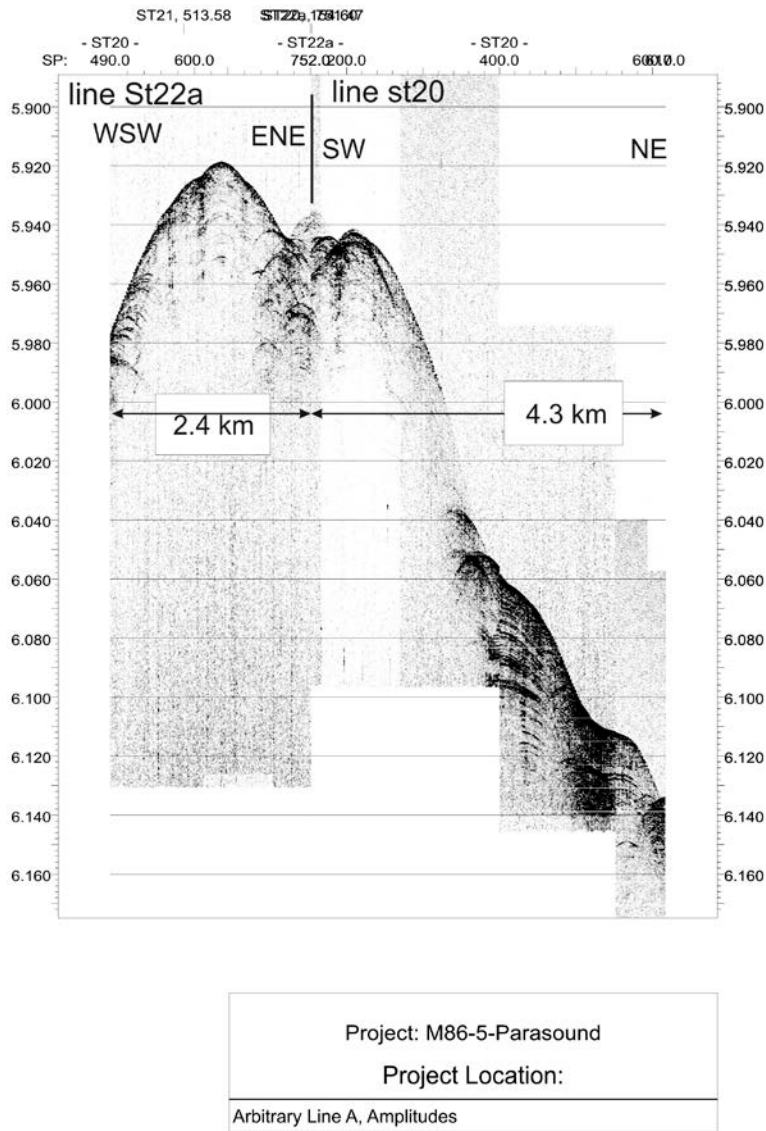
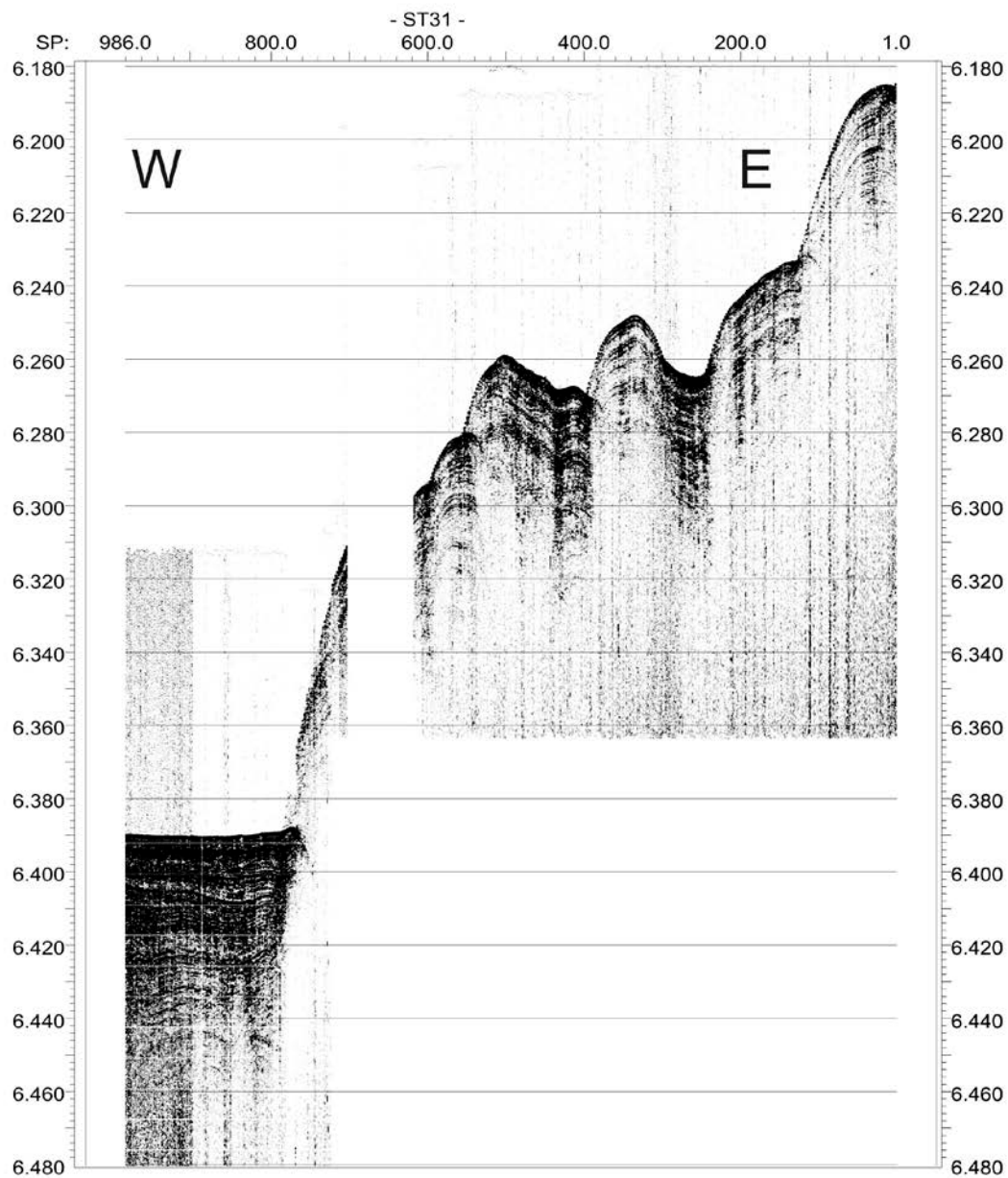


Fig. 4.1.9: Mosaic of two PARASOUND intersecting lines across MV Michael Ivanov. Similarly to MV Abzu, note the lack of internal structure of this MV that is surrounded by hills whose internal structure is barely displayed due to the slope gradients.

The Horseshoe Abyssal Plain

The divide of the HAP and HV is marked by an escarpment that coincides with the Horseshoe Fault (see figure 4.1.3 for location), which is eroded in its central part where sedimentary mass transport processes have occurred (figures 4.1.10 and 4.1.11). As a result of this the stratigraphy of this transitional area is fairly well imaged in the south, close to the SWIM 1 Fault (figure 4.1.10), than in the north, close to another fault of the SWIM fault system (figure 4.1.11).



10.5 km

Project: M86-5-Parasound
Project Location:
Line ST31, Amplitudes

Fig. 4.1.10- PARASOUND profile across the Horseshoe Fault in the SWIM 1 Fault. The stratigraphic record is well imaged with respect to the northern surveyed area (see figure 4.1.8).

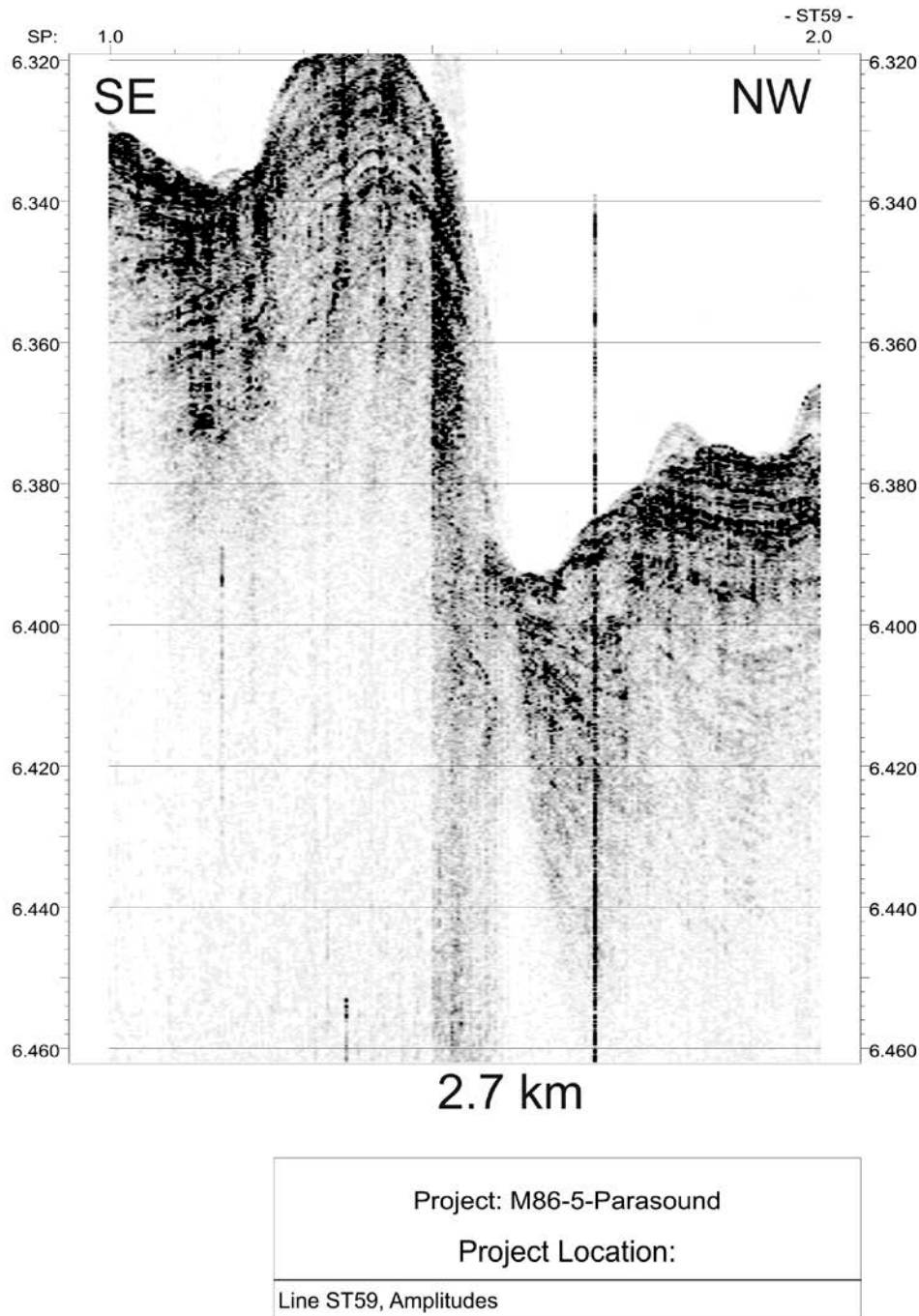


Fig. 4.1.11: PS profile across the Horseshoe Fault. The superficial profile is irregular and off-section echoes were recorded in the hanging-wall and footwall, where the stratigraphic reflections are not as continuous as in the profile to the south (figure 4.1.7).

This survey also imaged various tectonic structures along the SWIM 1 Fault, with the purpose of selecting the best places for seafloor physical sampling (gravity, box multicore cores, AUV surveys and CTDs). As a result of this new information on the SWIM 1 Fault was acquired showing that:

- i) despite the general transpressive deformation behaviour of this fault there are evidences for extensional deformation, probably associated with transtension on en echelon faults and releasing fault bends (figure 4.1.12).

ii) the SWIM1 Fault is active as a strike-slip fault in the approaches of the Goringe-Hirondelle seamounts (longitude $\sim 11^{\circ}30'$) as shown in figure 4.1.13.

iii) across the SWIM 1 Fault upthrust displacement of the northern flank of the fault is usually observed (Fig. 4.1.14).

iv) the existence of a very low amplitude package of sediments, up to 10 mili-seconds of TWT record is widespread in the HAP. According to the published results of Gràcia et al. (2010) this layer is more than 16 ky old, i.e. could be associated with the last Glacial Maximum (e.g. the “white layer” underneath the topmost “black package” in figures 4.1.12, 4.1.13 and 4.1.14).

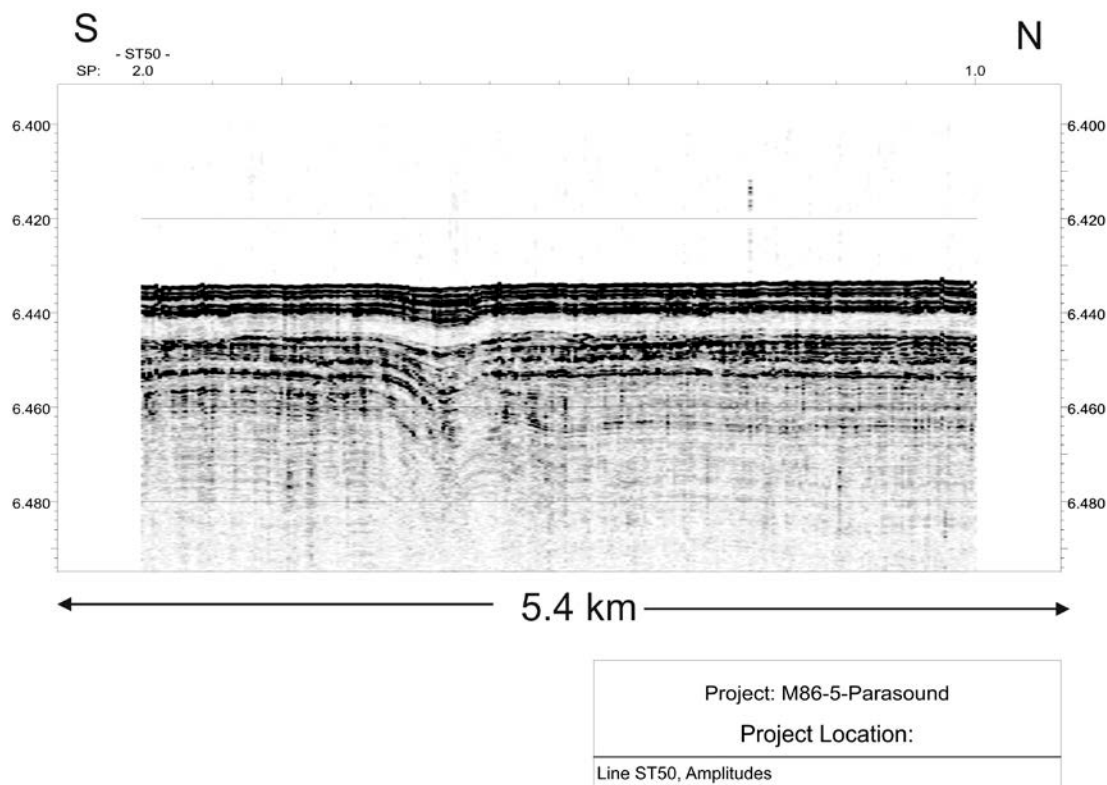


Fig. 4.1.12: Parasound profile across the SWIM1 Fault showing localized subsidence in a graben-like structure. Note that in depth compressive-like structures are observed. The existence of compressive and extensional deformation on vertical profiles across a strike-slip fault is an evidence of the successive role of different fault segments with different strike and dip, i.e. with different orientations to the main horizontal compression.

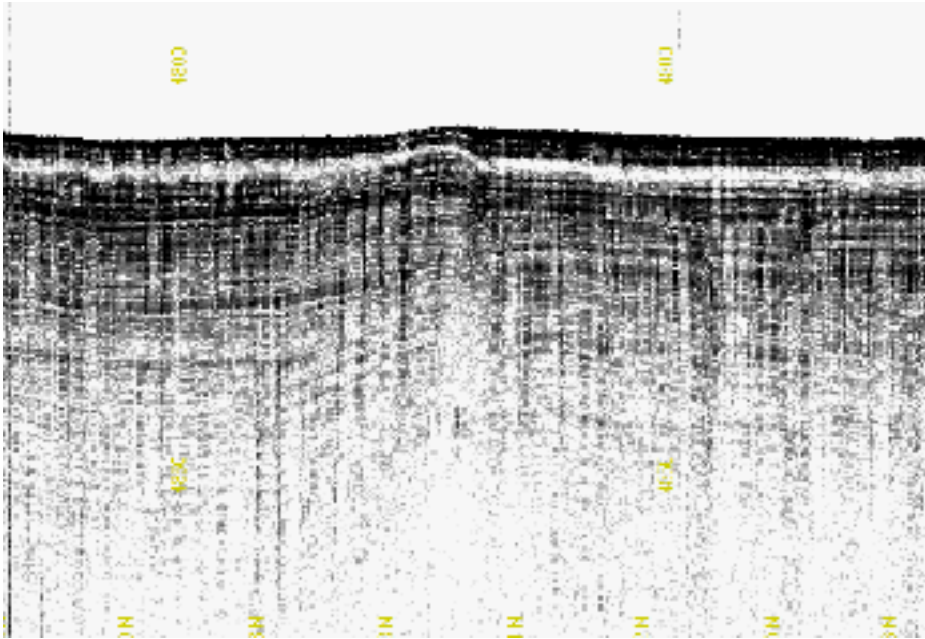


Fig. 4.1.13: Parasound profile at the foot of the SW flank of the Goringe Bank showing clear evidence of compressive deformation with little vertical displacement, another indication for strike-slip faulting along the SWIM 1 Fault.

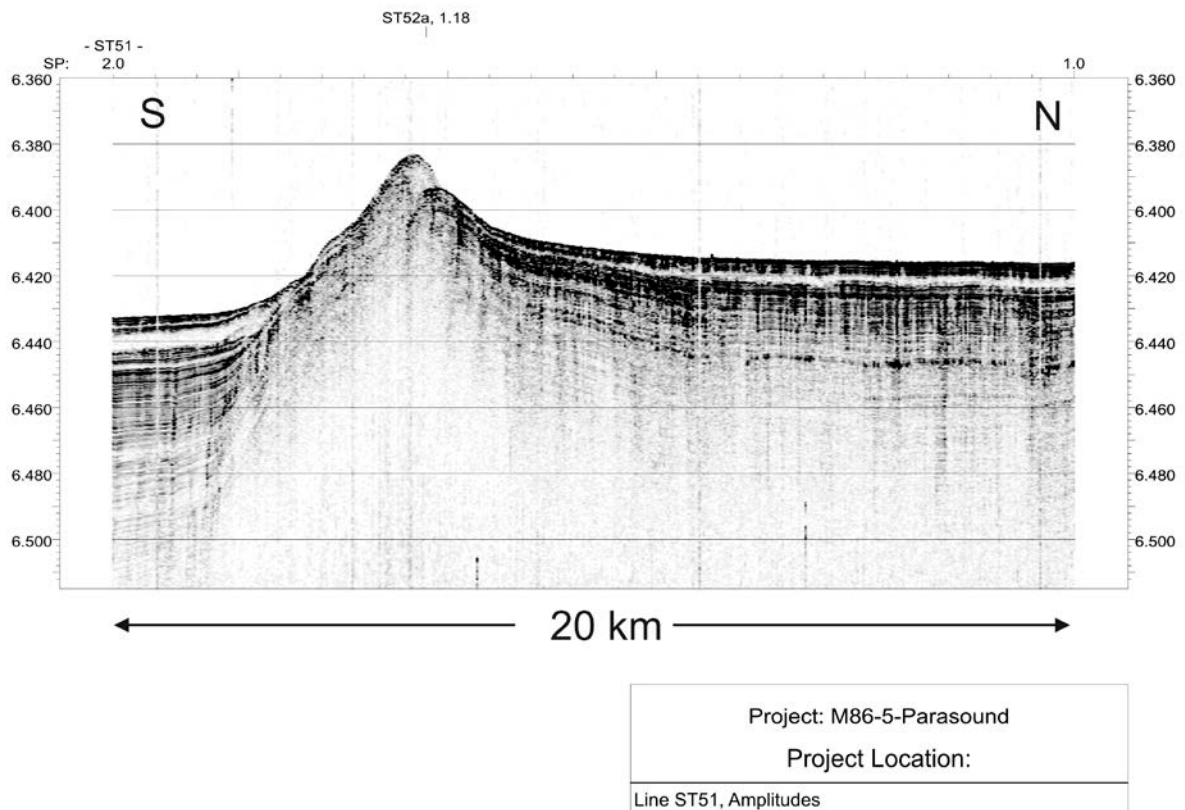


Fig. 4.1.14: Parasound profile across the SWIM 1 Fault showing vertical displacement of the northern block. This was observed at various places of the fault.

Acoustic signal for the detection of ship wrecks

The joint experience of the side scan sonar record from the AUV, inspection of the map with reported ship wrecks (www.wrecksite.eu) and observation of the Parasound record allowed to conclude that clear individual echoes/reflections standing approximately 10 to 20 mili-seconds TWT above sea floor were reflected from ship wrecks. These echoes were clearly observed on approximately perpendicular profiles and corresponded to ship wrecks in two cases (figure 4.1.15). One of these cases was confirmed by the AUV survey. The use of this criterion as an indicator for ship wrecks can be used as a quick decision indication for finding or avoiding ship wrecks.

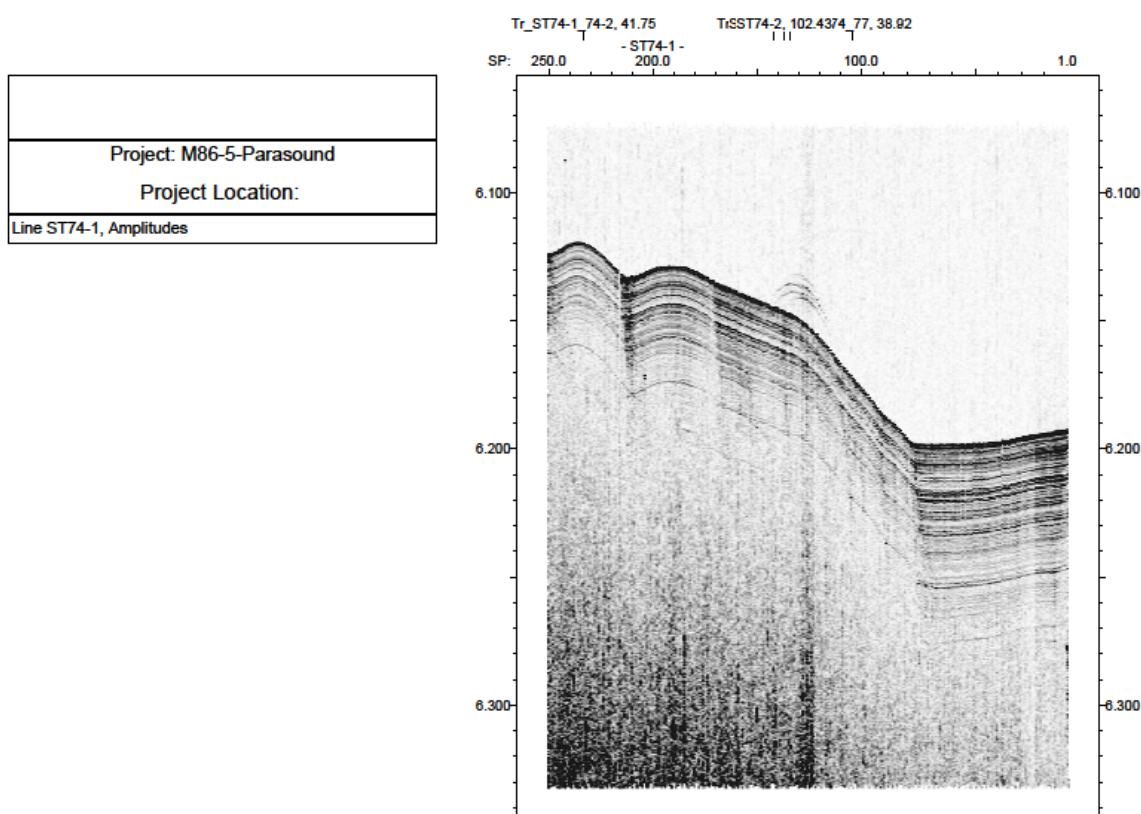


Fig. 4.1.15: Parasound profile showing individual echoes 10 to 20 mili-seconds above the sea floor. This site was surveyed with the AUV side scan sonar showing the presence of a 120 m wreck of a ship.

4.2 AUV

4.2.1 AUV “ABYSS” dives

(K. Lackschewitz, M. Rothenbeck, F. Wendt)

Technical description

The Autonomous Underwater Vehicle (AUV) ABYSS from Helmholtz Centre for Ocean Research Kiel (GEOMAR) can be operated in water depth of up to 6000 m. The ABYSS system comprises the AUV itself, a control and workshop container, and a mobile Launch and Recovery System (LARS) with a deployment frame that was installed on steel plates at the stern of R/V METEOR. During M86/5, we have deployed and recovered the AUV at weather conditions with a swell of up to 2.5 m and wind speeds of up to 6 beaufort. For the recovery the nose float pops off when triggered through an acoustic command. The float and the 20 m long recovery line drift away from the vehicle so that a grappnel hook can snag the line (Fig. 4.2.1.1A). The line is then connected to the LARS winch, and the vehicle is pulled up (Fig. 4.2.1.1B). Finally, the AUV is brought up on deck and safely secured in the LARS (Fig. 4.2.1.1C). During M68/5 no problems were encountered during any deployment and most of the recoveries with the LARS system. Only during the last dive the nose float has popped off during ascent and the recovery line has twisted 2 times at the propeller. Thus, a zodiac has set outboard to remove the line.

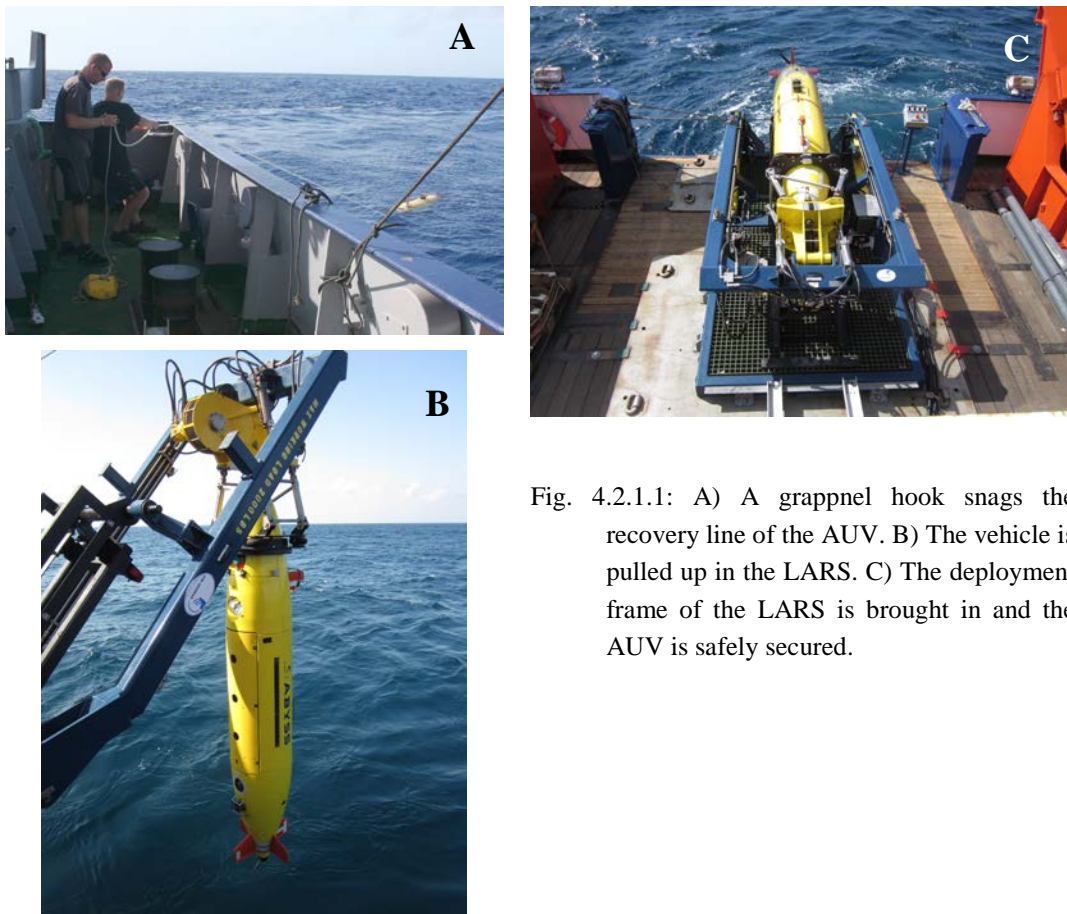


Fig. 4.2.1.1: A) A grappnel hook snags the recovery line of the AUV. B) The vehicle is pulled up in the LARS. C) The deployment frame of the LARS is brought in and the AUV is safely secured.

The vehicle has navigated autonomously using a combination of navigation methods:

- **GPS** - Works only on the surface, GPS determines the vehicle's location on Earth. GPS determines the "initial position" before the vehicle submerges, and verifies or corrects the vehicle's position when it surfaces during the mission. GPS also plays a critical role during INS alignment.
- **Inertial Navigation System (INS)** - After alignment on the surface, INS continuously integrates acceleration in 3 axes to calculate the vehicle's position. It uses input from the DVL and the GPS to maintain its alignment.

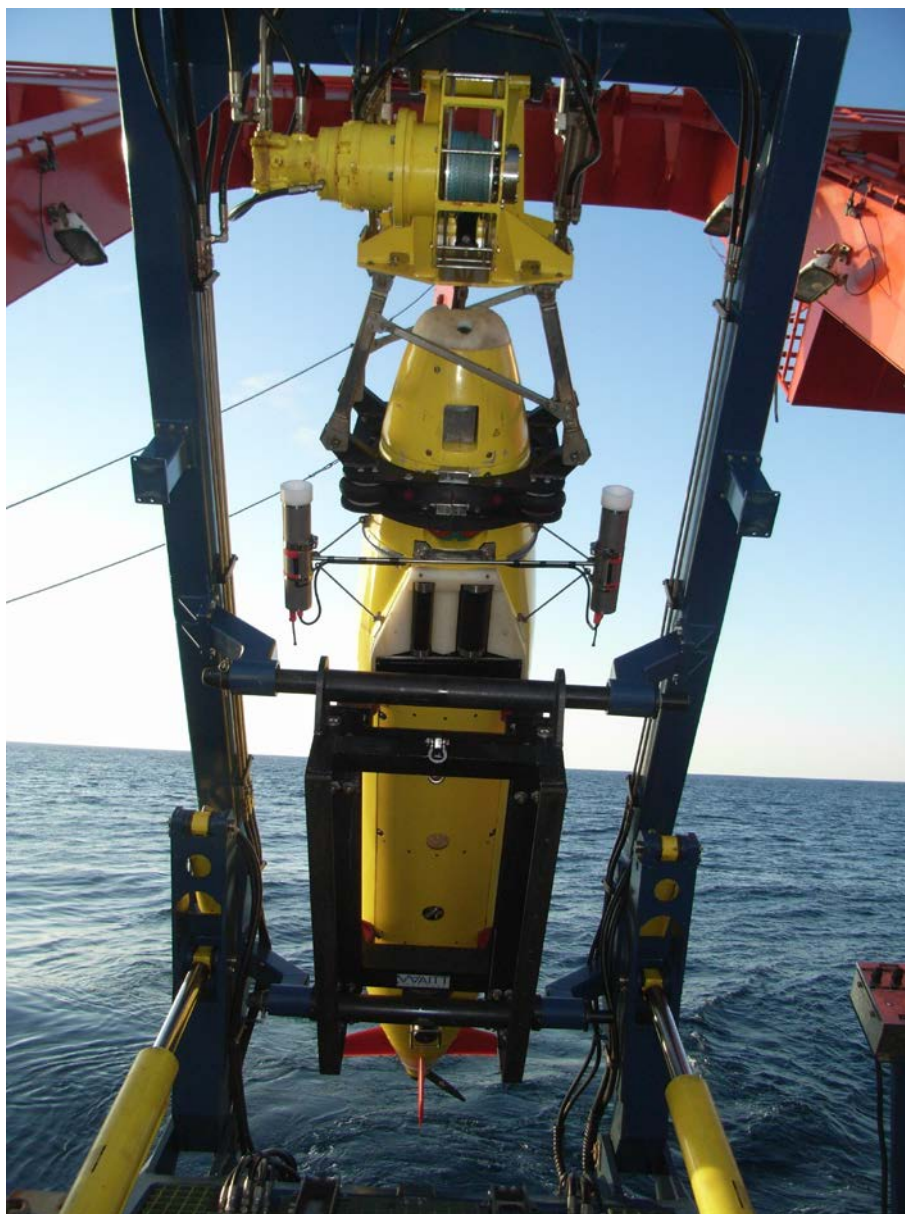


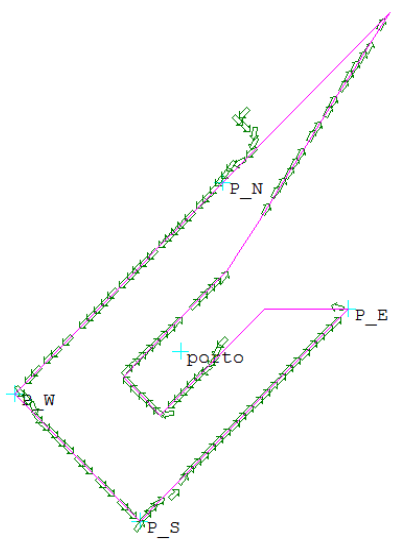
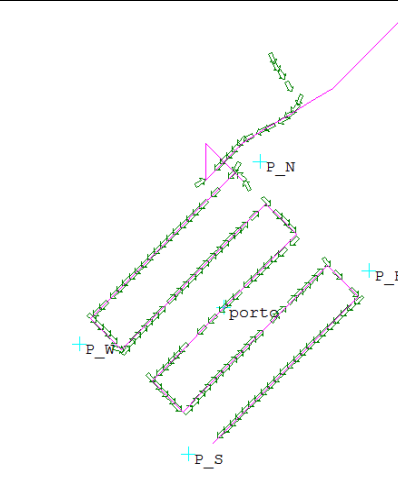
Fig. 4.2.1.2: AUV with attached CH₄ and CO₂ sensors.

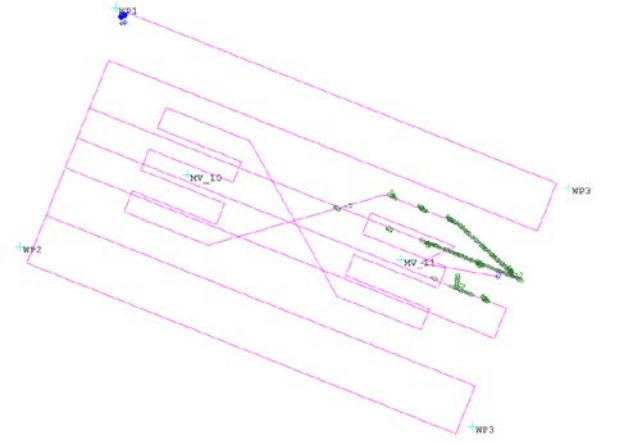
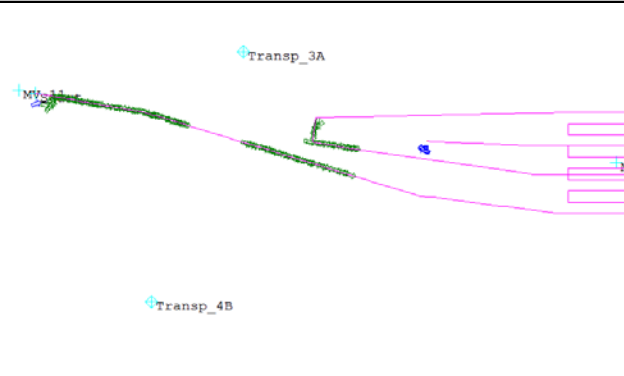
- **Doppler Velocity Log (DVL)** - Continuously measures altitude and speed over ground whenever the vehicle can maintain bottom-lock. The DVL receives temperature and salinity data from the CTD Probe to calculate sound speed. The DVL must be within range of the bottom to measure altitude and provide bottom-lock for the INS.

• **Long Baseline Acoustic Navigation (LBL)** - The vehicle has also used the LBL navigation by computing its range to two moored acoustic transponders.


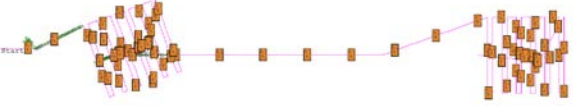
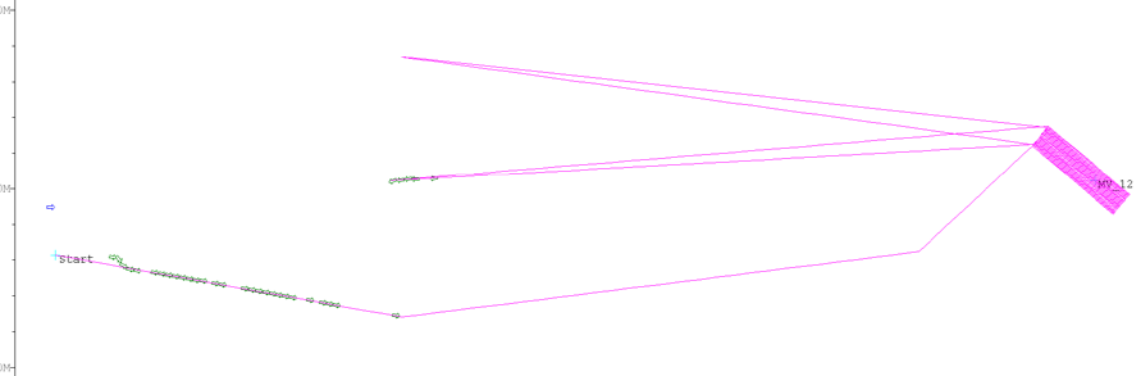
The vehicle has collected data using the following sensors: A SEABIRD Fastcat SBE49, a WETLABS ECO FLNTU optical backscatter/fluorometer, an Edgetech Sidescan system and a b/w camera system. In addition, a HydrosC™ CH₄ and a HydroC™ CO₂ sensor from CONTROS Systems and Solutions GmbH were mounted on the AUV Abyss (Fig. 4.2.1.2). The mounting brackets were designed such, that the sensors would fit inside the LARS for launch and recovery purposes. The sensors were incorporated in pressure housings. Power (24V) is supplied by the AUV, but data is stored internally in the sensor electronic system. The sensors are used to measure the CH₄ and CO₂ content in the areas of mud volcanoes. In total, 7 dives were completed in the Gulf of Cadiz. ABYSS dives 82-89 were dedicated to mud volcano exploration, high-resolution seafloor mapping and photographic documentation.

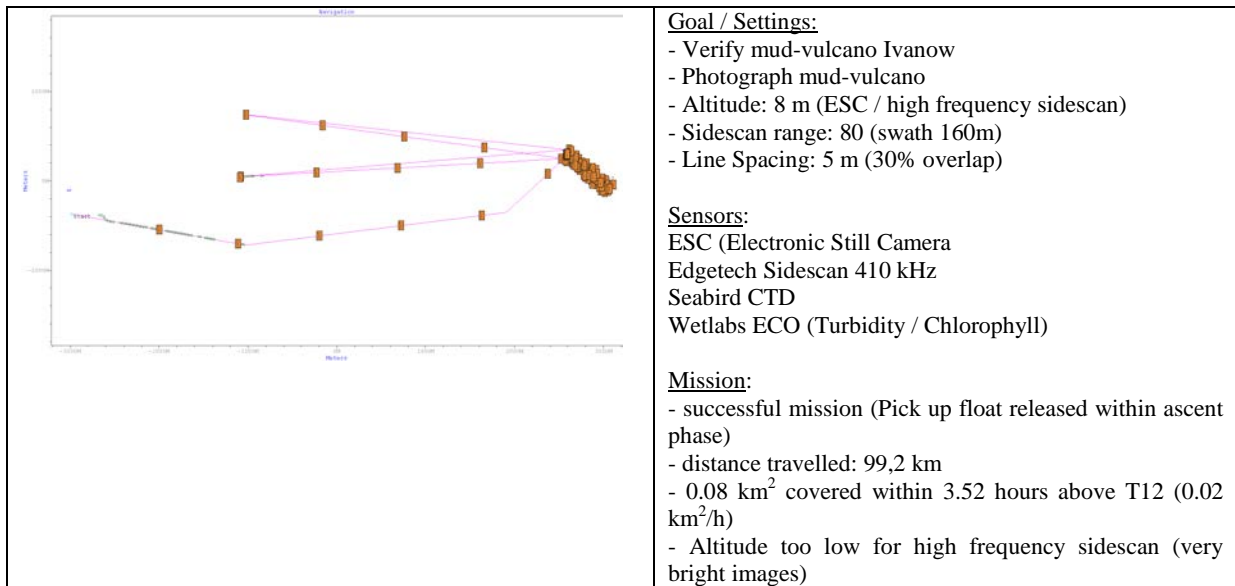
Event list for M86/5

Dive number / station number / Target	Date / Mission start / on bottem / off bottem / Mission end
Dive Abyss 82-1 / Station 7 / MV Porto	28.02.12 / 08:22 / 09:53 / 10:57 / 12:22
	<p><u>Goals / Settings:</u></p> <ul style="list-style-type: none"> - First part of dive above known mud-vulcano Porto - Map vulcano Porto - Verify acoustic image of known mud-vulcano <p><u>Sensors:</u> Edgetech Sidescan 120/410 kHz Contros HydroC-CO₂ II Contros HydroC-CH₄S II Seabird CTD Wetlabs ECO (Turbidity / Chlorophyl)</p> <p><u>Mission notices:</u></p> <ul style="list-style-type: none"> - Successful mission - Vehicle stayed on surface waiting for next mission
Dive Abyss 82-2 / Station 7 / MV Porto	28.02.12 / 12:44 / 14:20 / 15:38 / 17:03
	<p><u>Goals / Settings:</u></p> <ul style="list-style-type: none"> - Second part of dive above known mud-vulcano Porto - Map vulcano Porto - Mission was loaded and started just after dive 82-1 without recovery - Altitude: 50 m (high frequency bathymetry) - Swath width: 200 m - Line Spacing: 170 m (15% overlap) <p><u>Sensors:</u> RESON Multibeam Seabat 7125 400 kHz Contros HydroC-CO₂ II Contros HydroC-CH₄S II Seabird CTD Wetlabs ECO (Turbidity / Chlorophyl)</p> <p><u>Mission notices:</u></p> <ul style="list-style-type: none"> - No useful bathymetry files logged (vehicle records not logged)

Dive Abyss 83 / Station 16 / MV 10, MV 11	29.02.12 / 21:48 / 23:39 / 15:20 / 15:38
	<p>Goals / Settings:</p> <ul style="list-style-type: none"> - Verify targets T10, T11 - Verify anomalies in ship based backscatter - high frequency sidescan on top of targets - Altitude: 50 m (low freq. sidescan) / 20 m (high freq. sidescan) - Sidescan range: 500 m (low freq.) / 200 m (high freq.) - Line Spacing: 350 m (17% overlap → high freq. sidescan on top of targets) - Line Spacing: 800 / 500 m (20% / 100% overlap → low freq. sidescan) <p>Sensors: Edgetech Sidescan 120/410 kHz Contros HydroC-CO₂ II Contros HydroC-CH₄S II Seabird CTD Wetlabs ECO (Turbidity / Chlorophyl)</p> <p>Mission notices:</p> <ul style="list-style-type: none"> - Successful mission (aborted to end position due to battery capacity) - Vehicle stopped frequently during mission due to motor controller board failure - 3 km² covered in high frequency sidescan within 2.33 hours above T10 (1.28 km²/h) - 3 km² covered in high frequency sidescan within 1.62 hours above T11 (1.85 km²/h)
Dive Abyss 84 / Station 29 / T12, T13	02.03.12 / 18:18 / 20:07 / 10:34 / 10:36 (Mission over (deep))
	
<p>Goal / Settings:</p> <ul style="list-style-type: none"> - Verify targets T12, T13 - Verify anomalies in ship based backscatter - Altitude: 50 m (low freq. sidescan) / 20 m (high freq. sidescan) - Sidescan range: 500 m (low freq.) / 200 m (high freq.) - Line Spacing: 200 m (100% overlap → high freq. sidescan on top of targets) <p>Sensors: Edgetech Sidescan 120 / 410 kHz Contros HydroC-CO₂ II Contros HydroC-CH₄S II Seabird CTD Wetlabs ECO (Turbidity / Chlorophyll)</p> <p>Mission:</p> <ul style="list-style-type: none"> - Successful mission (in spite of abort at the end) - Aborted to end position on the last leg due to battery capacity - distance travelled: 88.5 km - 3.74 km² covered in high frequency sidescan within 3.13 hours above T12 (1.19 km²/h) - 3.74 km² covered in high frequency sidescan within 3.52 hours above T13 (1.06 km²/h) - constant ground fault between 20 and 30% (caused by either pencil beam or Contros sensors) 	

<p>Dive Abyss 85 / Station 39 / T10, T11, T12</p>	<p>04.03.12 / 06:21 / 08:19 / 19:56 / 20:17 (Mission over (deep))</p>
<p>Goal / Settings:</p> <ul style="list-style-type: none"> - Map known Mud-vulcanoes 10, 11, 12 - Altitude: 50 m (high frequency bathymetry) - Swath width: 200 m - Line Spacing: 150 m (25% overlap) <p>Sensors:</p> <p>RESON Multibeam Seabat 7125 400 kHz Contros HydroC-CO₂ II Contros HydroC-CH₄S II Seabird CTD Wetlabs ECO (Turbidity / Chlorophyll)</p> <p>Mission:</p> <ul style="list-style-type: none"> - Aborted to end position on top of T10 due to battery capacity - distance travelled: 74.8 km - No useful bathymetry files logged (probably beam steering issue) <p>→ First approach to mission 86 were stopped because of not working ADCP → Contros sensors and belonging outrigger disassembled → Vehicle turned to Camera configuration</p>	
<p>Dive Abyss 86 / Station 49 / T1, T2, T9</p>	<p>08.03.12 / 19:04 / 20:19 / 06:51 / 08:30</p>
<p>Goal / Settings:</p> <ul style="list-style-type: none"> - Verify targets T1, T2 and T9 - Verify anomalies in ship based backscatter - Altitude: 50 m (low frequency sidescan) - Sidescan range: 500 (swath 1000m) - Line Spacing: 300 / 700 m (100% overlap) <p>Sensors:</p> <p>Edgetech Sidescan 120 kHz Seabird CTD Wetlabs ECO (Turbidity / Chlorophyll)</p> <p>Mission:</p> <ul style="list-style-type: none"> - successful mission (no faults) - distance travelled: 74,2 km - 6 km² covered within 2.32 hours above T2 (2.59 km²/h) - 12 km² covered within 4.65 hours above T9 (2.58 km²/h) - 4 km² covered within 1.63 hours above T1 (2.45 km²/h) 	

Dive Abyss 87 / Station / T94, T102	10. March 2012 / 02:28 / 03:40 / 10:55 / 17:22
	
	<p>Goal / Settings:</p> <ul style="list-style-type: none"> - Verify targets 102 and 94 - Acoustical image (410 kHz) of targets 10 and 11 (each 3.2 km²) - Photo survey on top of targets - Altitude: 20 m (Sidescan) / 8 m (Camera / Sidescan) - Sidescan range: 200 m (80 m on photo survey) - Line spacing: 100/ 200 m (100 % overlap) <p>Sensors:</p> <p>Edgetech Sidescan 410 kHz Electronic Still Camera Seabird CTD Wetlabs ECO (Turbidity / Chlorophyll)</p> <p>Mission notices:</p> <ul style="list-style-type: none"> - Successful mission - Distance travelled: 82.3 km - 3.2 km² covered in high frequency sidescan within 4.25 hours above T102 (0.75 km²/h) - 3.2 km² covered in high frequency sidescan within 3.73 hours above T94 (0.86 km²/h)
Dive Abyss 88 / Station	11. March 2012 / 15:00 / - / - / 15:14
Mission aborted due to leak in oil filled tail section (propulsion)	
Dive Abyss 89 / Station / MV Ivanow (MV12)	14. March 2012 / 15:05 / 16:22 / 07:42 / 09:14
	



4.2.2 AUV Data Processing

(V. Valadares)

AUV processing was only carried out on sidescan sonar imagery as the two site surveys for bathymetry acquisition yielded no useful data. AUV was also able to take near seabottom photographs on 3 sites.

Sidescan sonar imaging was conducted on pre-selected targets identified on backscatter data derived from the previous MATESPRO multibeam swath bathymetry and backscatter survey. It was carried in 2004 aboard R/V NRP D. Carlos I, PIs: P. Terrinha and L. Matias from IDL, Lisbon, Portugal. The reflectivity data was derived from a Simrad EM120 and processed using Caribes software.

Sidescan data was recorded by the AUV in JSF file format and data processing was carried out using Chesapeake software, SonarWiz, version 5.04.0018.

Lines were run in two different modes: high resolution (410kHz) and low resolution (120kHz). The files had to be imported separately but with the same settings; these were: importing 100% of the sonar range, auto jsf scalar, a linear TVG and an ADC gain (derived from jsf sonar packet). The position and navigation was smoothed using an envelope of 10 pings and importation was done using group coordinates and heading source was taken from the value stored with the ping data.

Processing of the data consisted in removing data bad positioned due to the AUV correcting its positioning, AUV navigation malfunctioning, data acquired in sharp turns and removal of data acquired while descending and ascending from the target area. All data was scanned for bottom tracking with the disadvantage of not being possible to select two different tracks for port and starboard sides of the imaged data. Mosaics were produced with a grey standard color palette with no histogram compression and contrast and brightness in middle values. Overlapping images had no transparency and the segments that image the features the best were chosen to be on top in the order of display.

Ten different targets were inspected with sss imagery on 6 different site surveys (Fig. 4.2.2.1 and 4.2.2.2). One additional site survey was carried out on Porto mud volcano in order to test the equipment.

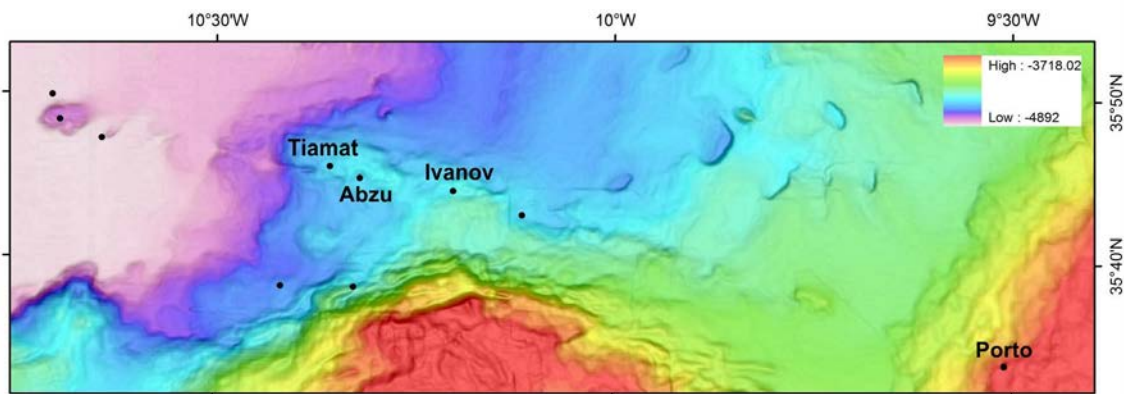


Fig. 4.2.2.1 – Map of the selected targets for AUV surveying.

Three of the pre-selected targets were proved to correspond to mud volcanoes, three to shipwrecks and others to steep slopes or rock outcrops.

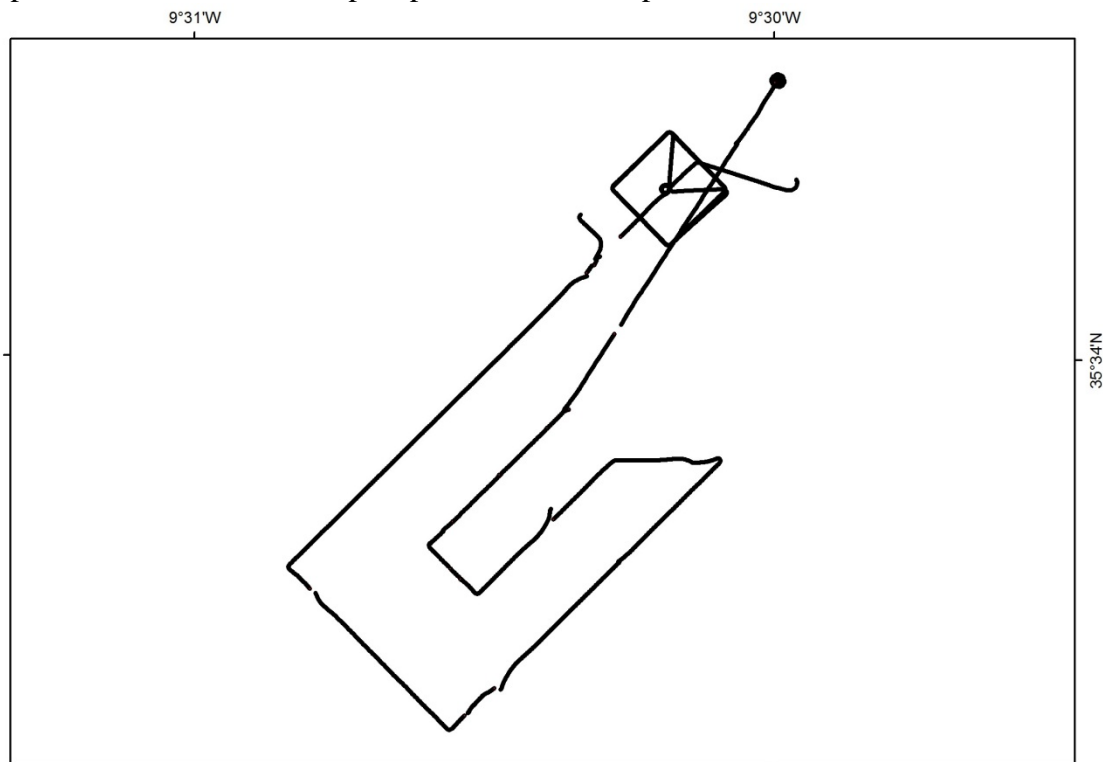


Fig.: 4.2.2.2: AUV navigation tracks for the Porto Mud Volcano.

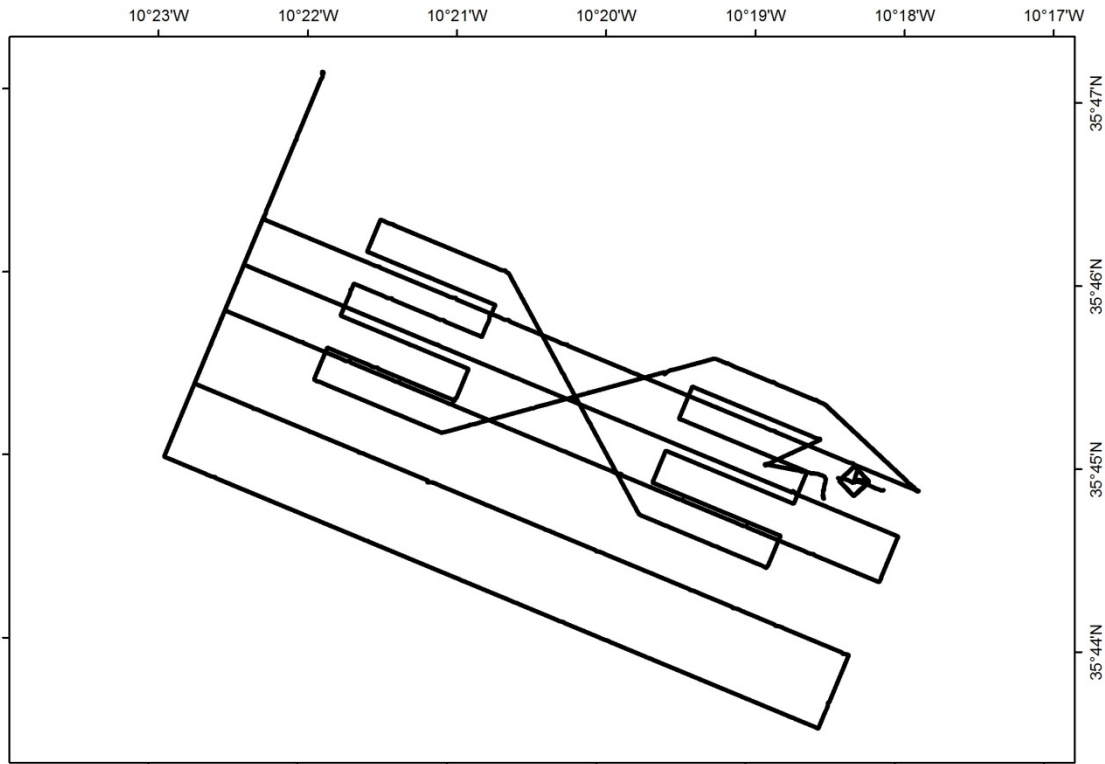


Fig.: 4.2.2.3: AUV navigation tracks for the Tiamat and Abzu Mud Volcanoes.

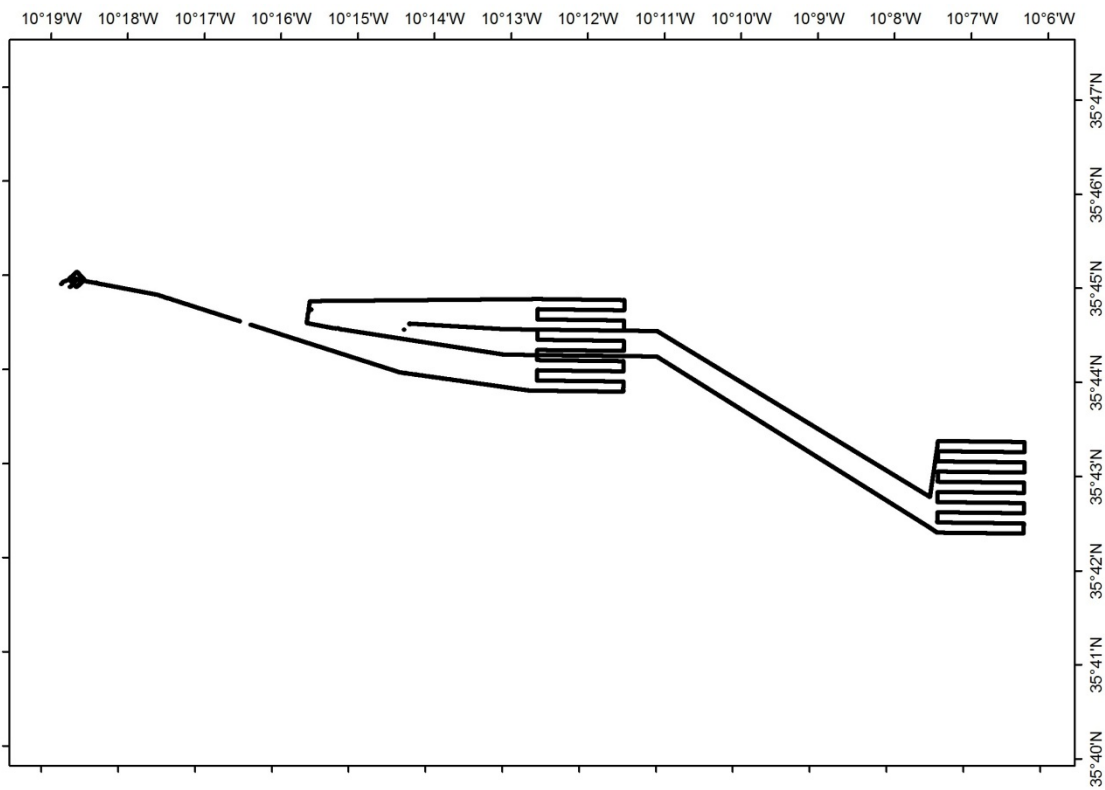


Fig. 4.2.2.4: AUV navigation tracks for the Ivanov Mud Volcano and the site eastward of it.

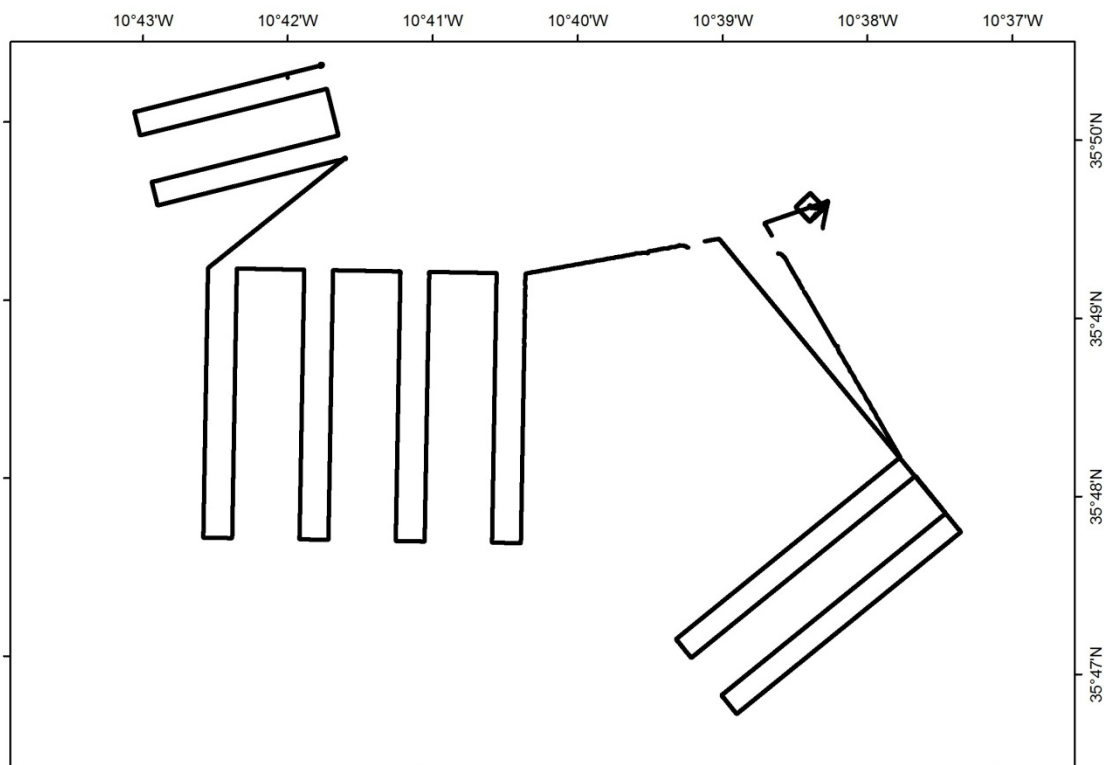


Fig. 4.2.2.5: AUV navigation tracks for the survey near the bathymetric high on the Horseshoe Abyssal Plain.

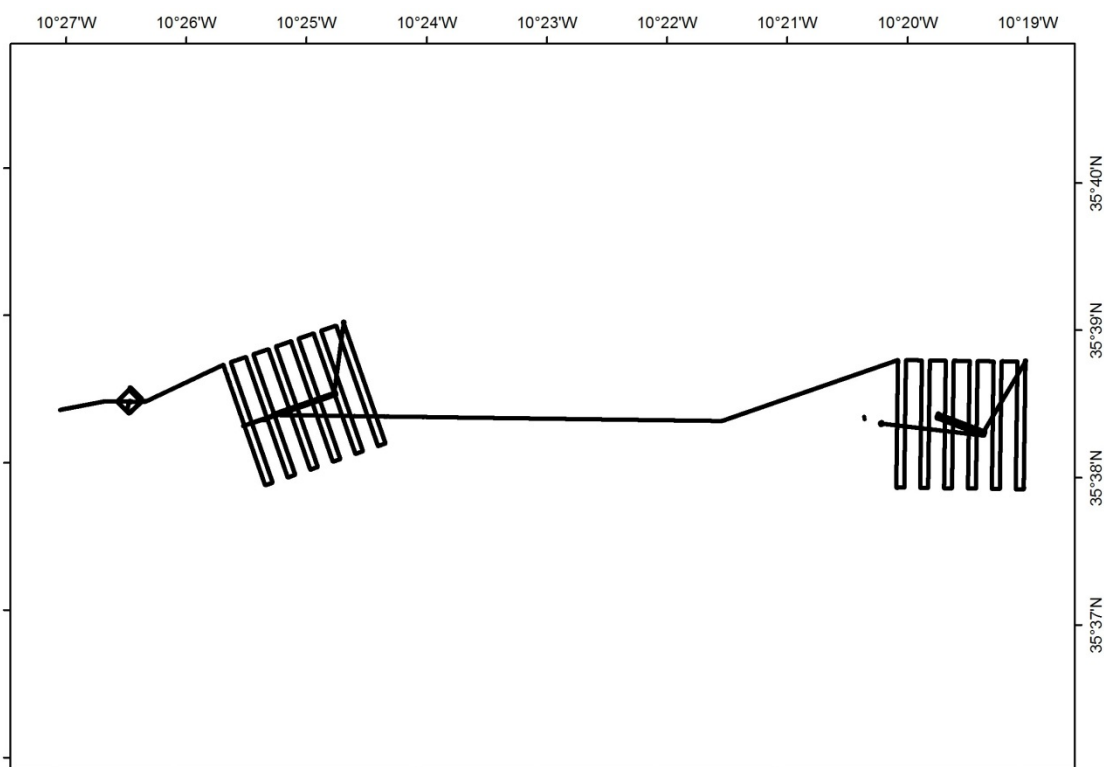


Fig. 4.2.2.6: AUV navigation tracks for the targets south of Tiamat and Abzu Mud Volcanoes.

Site Survey for targets on the Horseshoe Abyssal Plain

Two of these sites were surveyed because they displayed a high reflectivity patch on the backscatter map, another was also imaged because it is the most prominent bathymetric high in the Horseshoe Abyssal Plain. One target corresponds to a shipwreck that was found to be broken in two parts. Another site shows no special feature and the backscatter anomaly probably corresponds to a slope of an elevation close by or to some coarser materials found beneath the seafloor. The large bathymetric high revealed no special features.

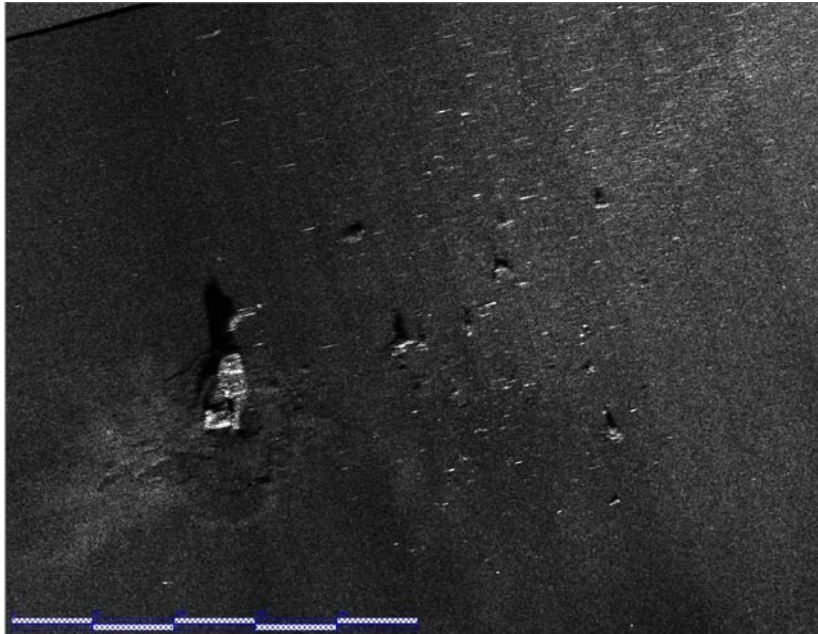


Fig. 4.2.2.7: Shipwreck found in one of the targets for this site survey.

“Tiamat” Mud Volcano

It is located at 4560 mbsl near the top of a WNW-ESE elongated bathymetric high. It displays an elliptic shape with the major axis trending NW-SE; is 600 meters long and 420 meters across. Its elevation displays a rugged seafloor (not present on the NE sector) that is well depicted from the smooth textured seafloor all around it. On its NW tip, a small depression is present and it seems to be related with erosion from near seabottom currents. Near its top, several patches of more reflective material can be found indicating that more coarse/compact materials are present. Some marginal elevations are depicted near the top, especially in the NE side, clearly identifiable on the mosaic shown by the shadows (Figure 4.2.2.8).

Several circular depressions are present on both the flanks and the top, ranging from almost 20 meters to less than 1 meter. These features may be pockmarks and therefore be related with focalized fluids' escape.

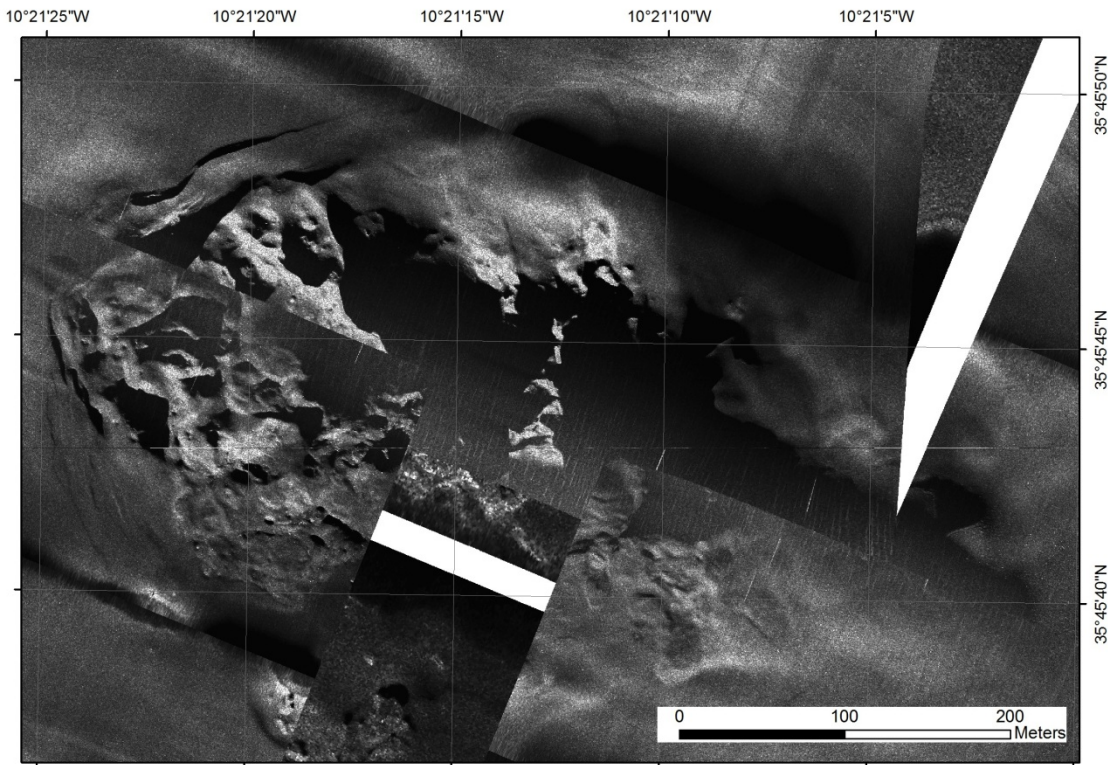


Fig. 4.2.2.8: Side scan processed mosaic of MV10, the Tiamat mudvolcano. Acquisition lines were run at 410kHz. Black colors are low reflectivity areas or shadows, white stripes are “no data” areas. Lines imaging the mud volcano were run on both sides imaging towards the elevation. Sonar imaging shows the rugged seafloor pattern on the top, the marginal elevated areas in the north and the scattered circular depressions.

“Abzu” Mud Volcano

“Abzu” is located about 3600 meters to the ESE of “Tiamat” and seats on the same bathymetric high. It displays a sub circular shape and is about 100 meters in diameter. In the center of the top a small elevation is present. The acquired sss imagery (Fig. 4.2.2.9) shows a distinct pattern for the sides and the top of this mud volcano; the slopes display a smooth texture while the top displays a punctuated and rugged seafloor with high reflectivity. There seems to be a small depression on the top area with respect to the top of the sides. The all-around smooth sides are disturbed in the eastern side where a depression is carved connecting the upper part with the surrounding lower parts. This feature may derive from erosion caused by a mud flow expelled from the central part. To the east of the mud volcano two depressions are present, of about 50 meters each. Also to the east but in the vicinities of “Abzu” some smaller circular depressions reaching up to 6 meters in diameter can be found, probably are pockmarks.

Around the mud volcano, some smooth features can be tracked on the seafloor probably corresponding to sedimentary features related with bottom currents flowing around the elevation.

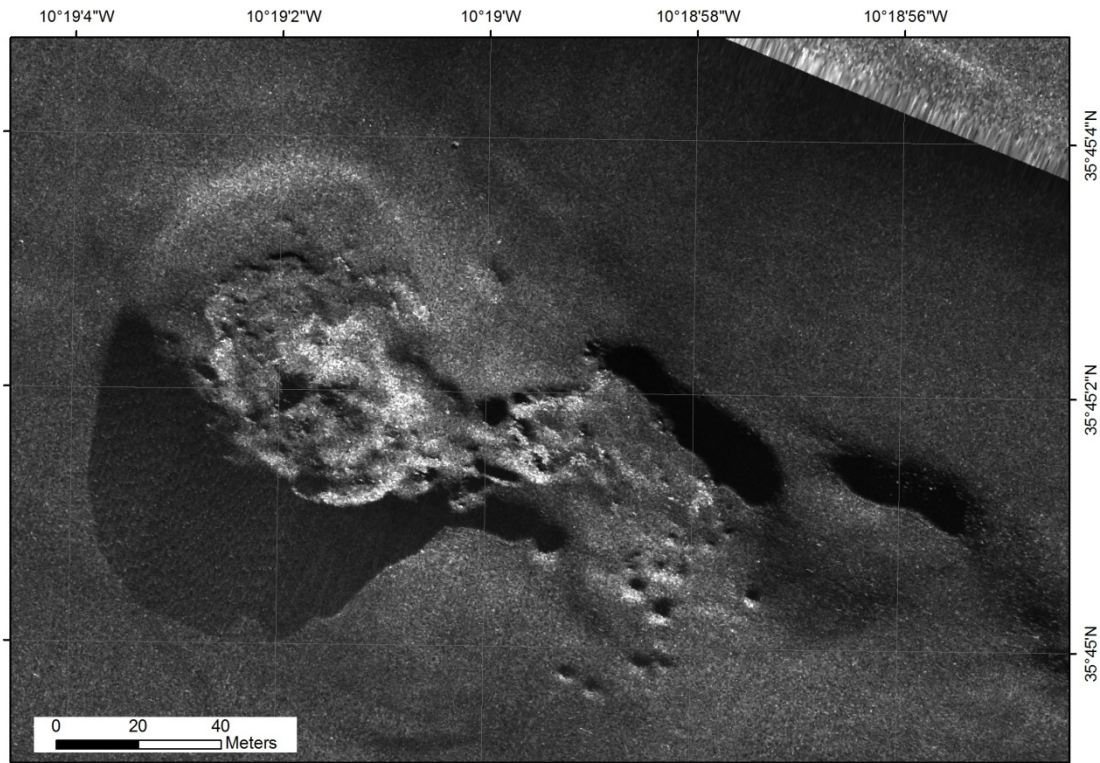


Fig. 4.2.2.9: Sidescan processed mosaic of Abzu. Acquisition lines were run at 410kHz. Black colors are low reflectivity areas or shadows. Line imaging the mud volcano was run from the north side. To be noted the different pattern on the top and sides of the elevation, the carved channel on the eastern side and the small circular depressions more to the east.

“Ivanov” Mud Volcano

“Ivanov” mud volcano lies at 4500 meters of water depth, east of Tiamat and Abzu, on a small flat in the middle of the slope that connects the Coral Patch Ridge to the Horseshoe Valley. Overall it extends for about 450 meters and is made up of several minor edifices. In the eastern part two small elevations are present, both reach around 50 meters in diameter and to the west there is an elongated elevation with a NW-SE trend (Figure 4.2.2.10). The first two are very well defined and at least one of them is cone-shaped with a flatter area on top and a minor central depression. The other major elevation to the NW is punctuated by minor features that seem to be elevations with a subsided top (caldera).

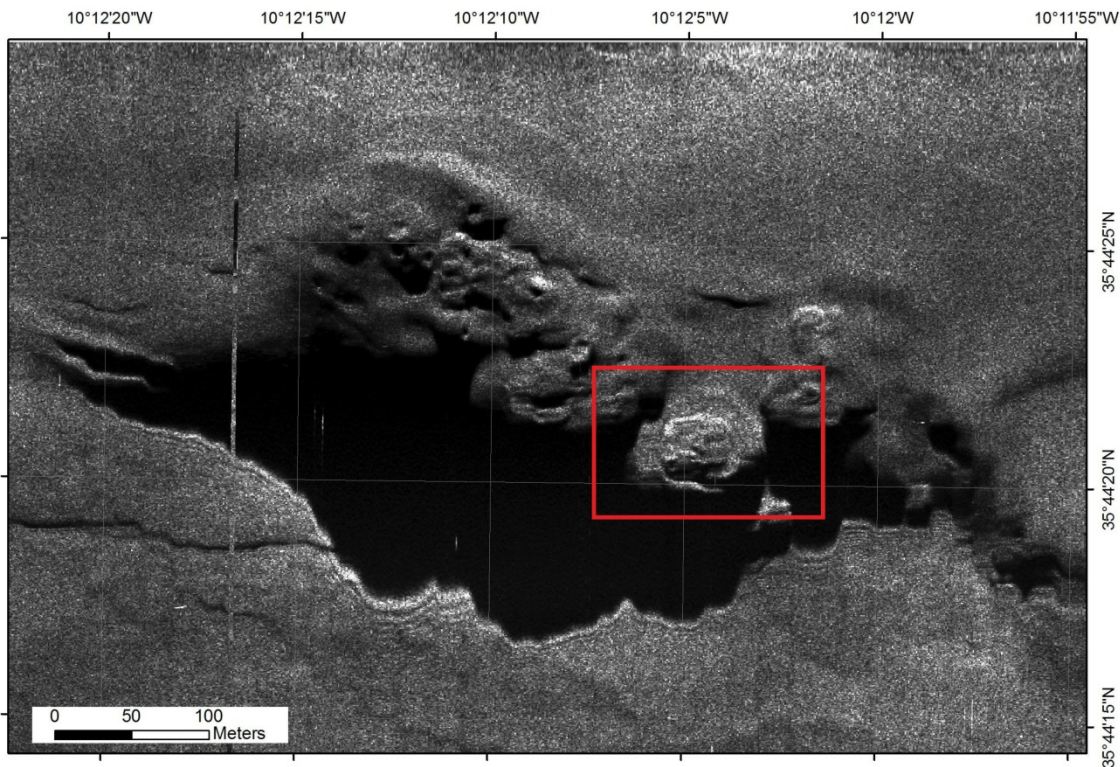


Fig. 4.2.2.10: Sidescan processed mosaic of MV12. Acquisition lines were run at 120kHz. Black colors are low reflectivity areas or shadows. The image presented was collected with the AUV to the North of the mud volcano. It is noticed that the seafloor texture is different from the two edifices in the east and the major elevation to the west, where the small circular depressions are scattered. Red box depicts area of figure 4.2.2.11 acquired at higher resolution.

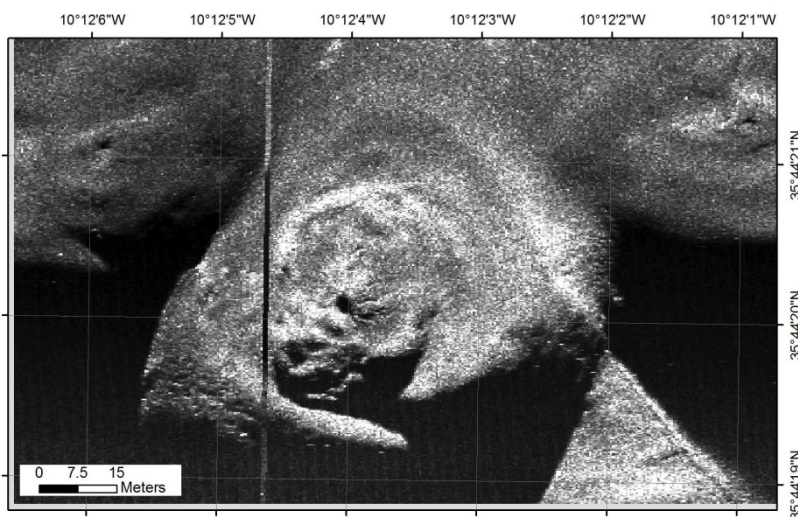


Fig. 4.2.2.11: Sidescan sonar processed data of MV Ivanov acquired at high resolution (410kHz). In this area (imaged from the north) is displayed one of the singular heights in the east with the high reflective patches near the top.

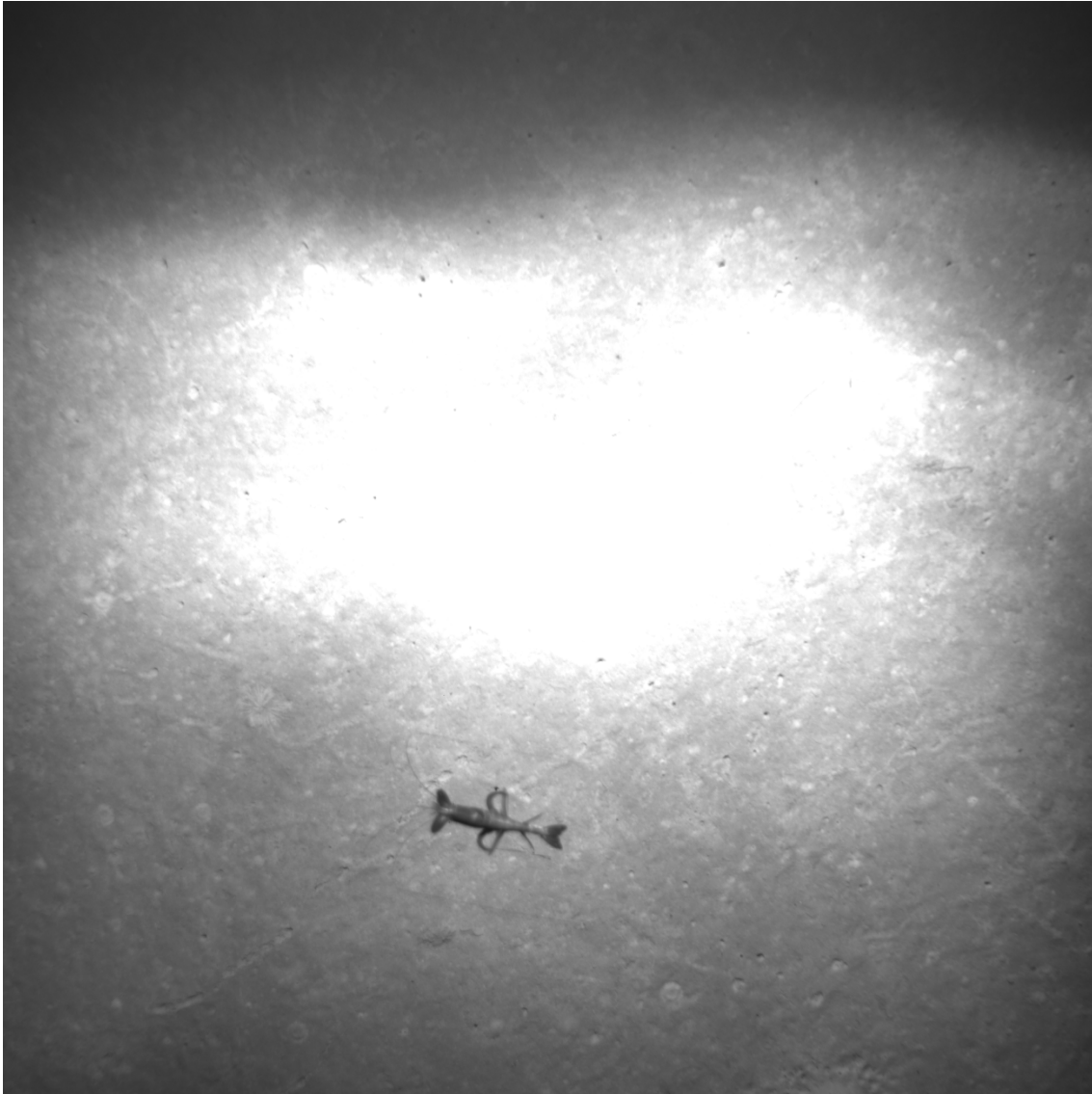


Fig. 4.2.2.12: Photograph taken at Ivanov Mud Volcano.

Site Survey for target east of Ivanov Mud Volcano

This site revealed no special features and the detected high reflectivity patch identified in the backscatter map probably corresponds to debris derived from the steep slope located just to the south of this area.

“Porto” Mud Volcano

This site is located at 3880 mbsl, inside the accretionary wedge, one of the main morphotectonic units of the Gulf of Cadiz. It displays a sub circular shape with more than 500 meters in diameter. The top area shows a smoother texture when compared with the flanks. However, in the uppermost part there is a feature that seems to be an emission center that has several minor features related to the material flow originating from there, that define a dissymmetric radial pattern (Figure 4.2.2.13). The sides display a more or less intense network of incised minor

channels. Some areas near the foot of the slope display a more rugged pattern suggesting the presence of another type of materials.



Fig. 4.2.2.13: Sidescan sonar processed mosaic of Porto mud volcano, acquired at both low and high resolution (120kHz, 410kHz). The top displays an asymmetric pattern of flows, it is also clear the network of incised channels in the sides and some areas with different textures near the foot of the slope of this edifice.

Site Survey for target 12 km south of Abzu Mud Volcano

This target was surveyed and the identified backscatter anomaly corresponds to rocks outcropping on a steep slope (Figure 4.2.2.14).



Fig. 4.2.2.14: Rock outcrops imaged from the west, acquisition at 120kHz.

Site Survey for target 14.5 km south of Tiamat

The backscatter anomaly for site corresponds to a shipwreck.

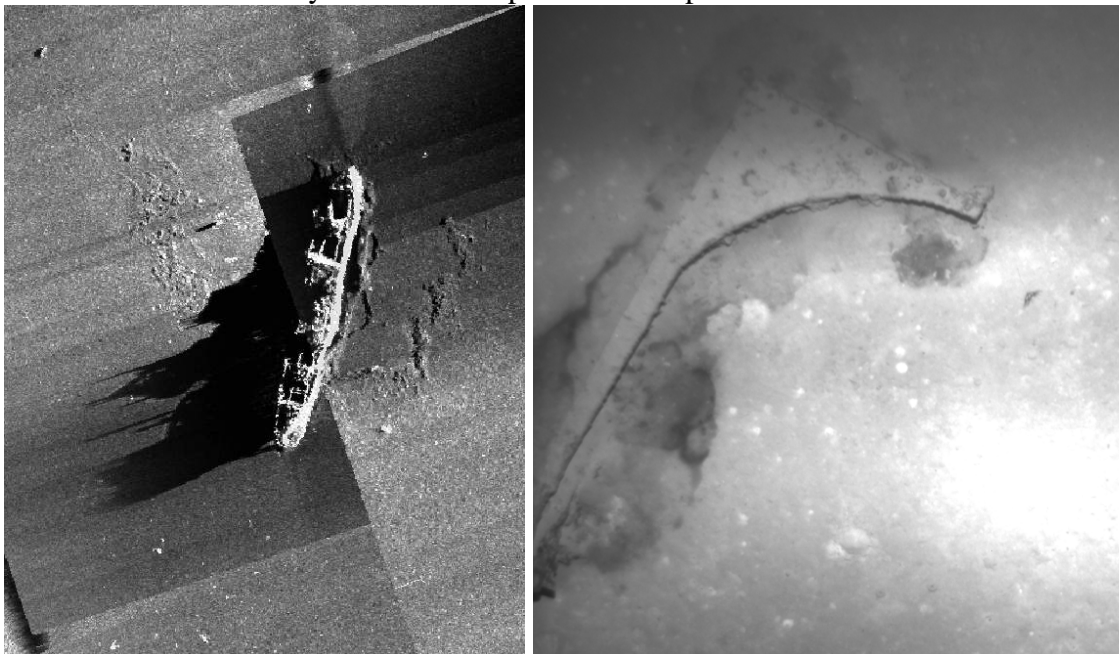


Fig: 4.2.2.15: Shipwreck and scattered debris and a photograph taken at one of these debris located south of the shipwreck.

4.3 CTD and Water Column sampling

(L. Rovelli, C. Hinz, A. Bleyer)

Water column measurements were performed in-situ using standard CTD-Rosette (Conductivity-Temperature-Depth) system as well as with state-of-the-art Methane and Carbon Dioxide sensors (HydroC sensors, CONTROS Systems & Solutions GmbH, Kiel, Germany), which were mounted alternatively on the AUV or the CTD carousel. In addition gas-chromatographic analyses were performed on discrete water samples from the CTD Rosette system to provide accurate methane (CH₄) concentration estimates. The aim was to use these instruments as survey tools to spot the presence of near bottom methane anomalies that would have suggested the presence of active sediment.

Measurements and analysis

CTD

The ship SBE9plus CTD (Seabird, Washington, USA) was the main instrument we used for water column and near bottom measurements (Figure 4.3.1). The SBE9 samples at 24Hz and was equipped with the default sensors (temperature, conductivity, pressure) as well as standard additions (oxygen, altimeter). Furthermore, a 24-Niskin Rosette system was installed for discrete water sampling. The ship navigation data were recorded by the CTD software, which allowed the recording of the sampled Niskin-bottles coordinates. To provide more reliable positioning of both the measurements and the sampling, a Posidonia Transponder (Ixsea SAS, France) was attached on the cable 10 m above the CTD frame. Both Ship navigation and Posidonia positioning data were collected in real time using the OFOP software. The CTD was generally deployed for near bottom surveys in the towed or tojo mode respectively. The downcast was also used to provide valuable sound velocity profiles for both the AUV navigation and the onboard MB system.

Chemical analysis

The discrete water samples analyses were performed in two steps. First the dissolved gasses were extracted from seawater by vacuum degassing of 1.8 L of seawater according to Keir et al. (2008). The extracted gas samples were stored for further quantification and stable isotope measurements in 20 ml head space vials. Concentration of CH₄ was then determined by using a Thermo Finnigan Trace GC 2000 gas chromatographer. Due to an unfortunate series of ruptures and lack of spare parts, the onboard absolute CH₄ estimations were inaccurate. The general trend, meaning relative increases and decreases in the concentrations, were however found to be consistent with both previous studies and thus considered reliable. For this reason the preliminary results will show “normalized“ concentrations (to the local highest concentration) to highlight the concentration changes. All samples will be re-analyzed for CH₄ concentrations at Geomar; furthermore analyses of the isotopic ¹³C/¹²C ratio of CH₄ will be conducted.

Methane and carbon dioxide sensors

Water in the vicinity of subsea mud volcanoes is often characterized by (CH₄) concentrations and carbon dioxide partial pressures (*p*CO₂) that differ from water column background values in the wider area around these hot spots. During this cruise different types of dissolved gas sensors were hence deployed on a number of different mobile platforms to on the one hand foster the

explorations endeavors of new mud volcanoes and on the other hand to sample the water column next to known mud volcanoes. For the first time, a HydroC-CO₂ II instrument for the measurement of $p\text{CO}_2$ as well as a new prototype for the measurement of dissolved CH₄, were integrated into and deployed together with the AUV Abyss (Figure 4.3.1). The instruments were equipped with newly developed flow heads that made use of the platform movement to provide a constant and directed stream of water to the HydroC's membrane. Normally a submersible pump is used to create this water flow that is required to speed up the partial pressure equilibration between dissolved gases in the water and the gaseous headspace behind the membrane. During the dives the instruments were powered by the AUV. A HydroC-CH₄ II was mounted and deployed on a profiling water sampler during CTD-casts (Figure 4.3.1) and on a video multicorer (MUC). In both cases it was equipped with a standard flow-head and an external water pump. Power was provided by an external rechargeable battery pack. The analogue sensor signal was transmitted on deck for live observation. All of the above mentioned HydroC instruments were equipped with an internal data logger.

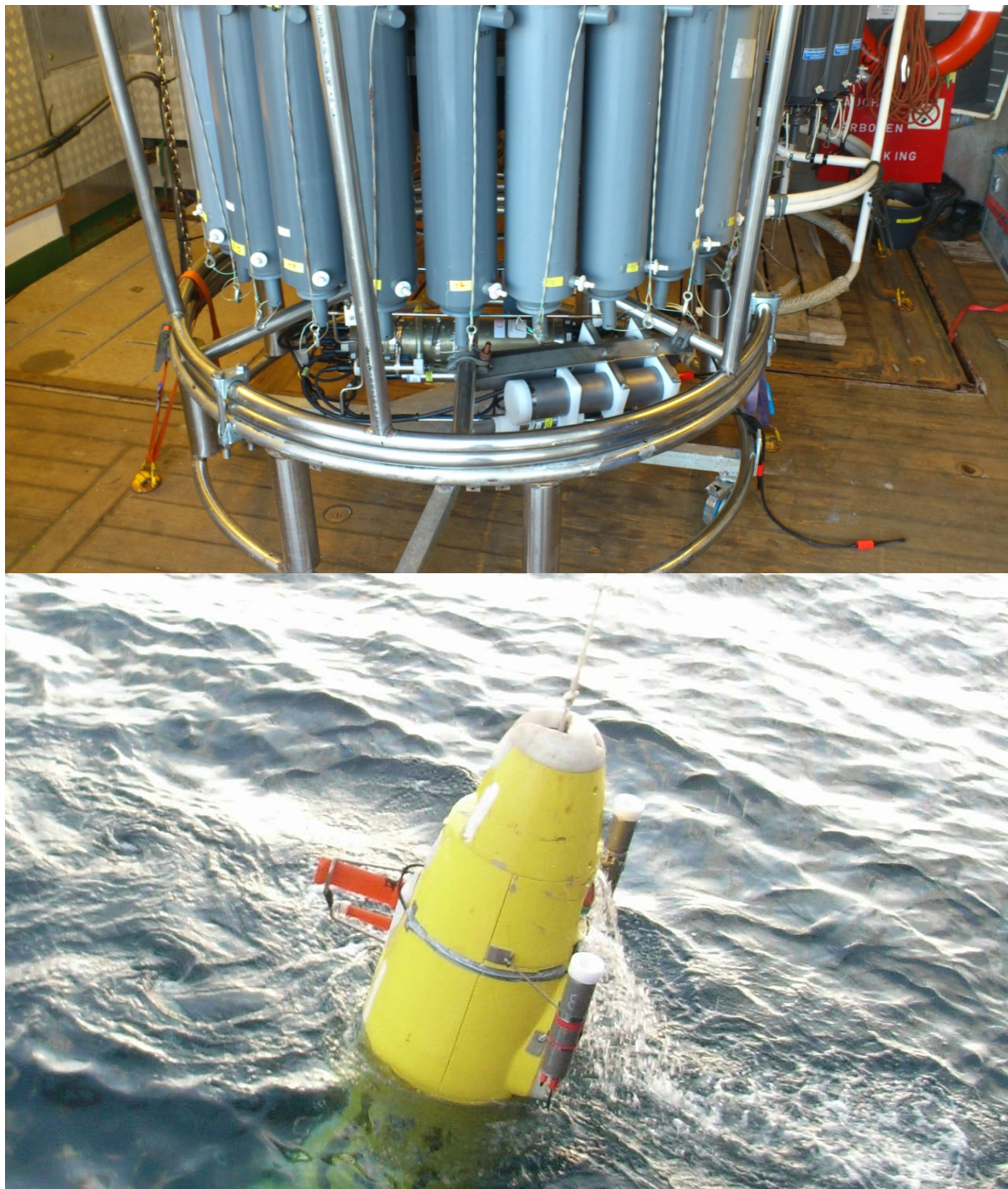


Fig. 4.3.1 Water column measurements tools. Top CTD-Rosette system. It also shows, CH₄ sensor mounted horizontally below the Niskin bottles (front right). Bottom: AUV Abyss at the beginning of the recovery procedure two HydroC instruments: one for CO₂ and one for CH₄ that are mounted on a special frame keeping them at distance of approx. 40 cm from the AUV housing as well as slightly below

Preliminary results

CTD

A total of 8 CTD deployments were performed during the cruise at location 16 (CTD 1, not shown here), as well as at the Porto (CTD 2), Tiamat (CTD 4 and 7), Abzu (CTD 6) and M.

Ivanov (CTD 3, 4 and 8) mud volcanoes respectively. Figure 4.3.2 provides an overview of the main physical parameters collected during the deployments.

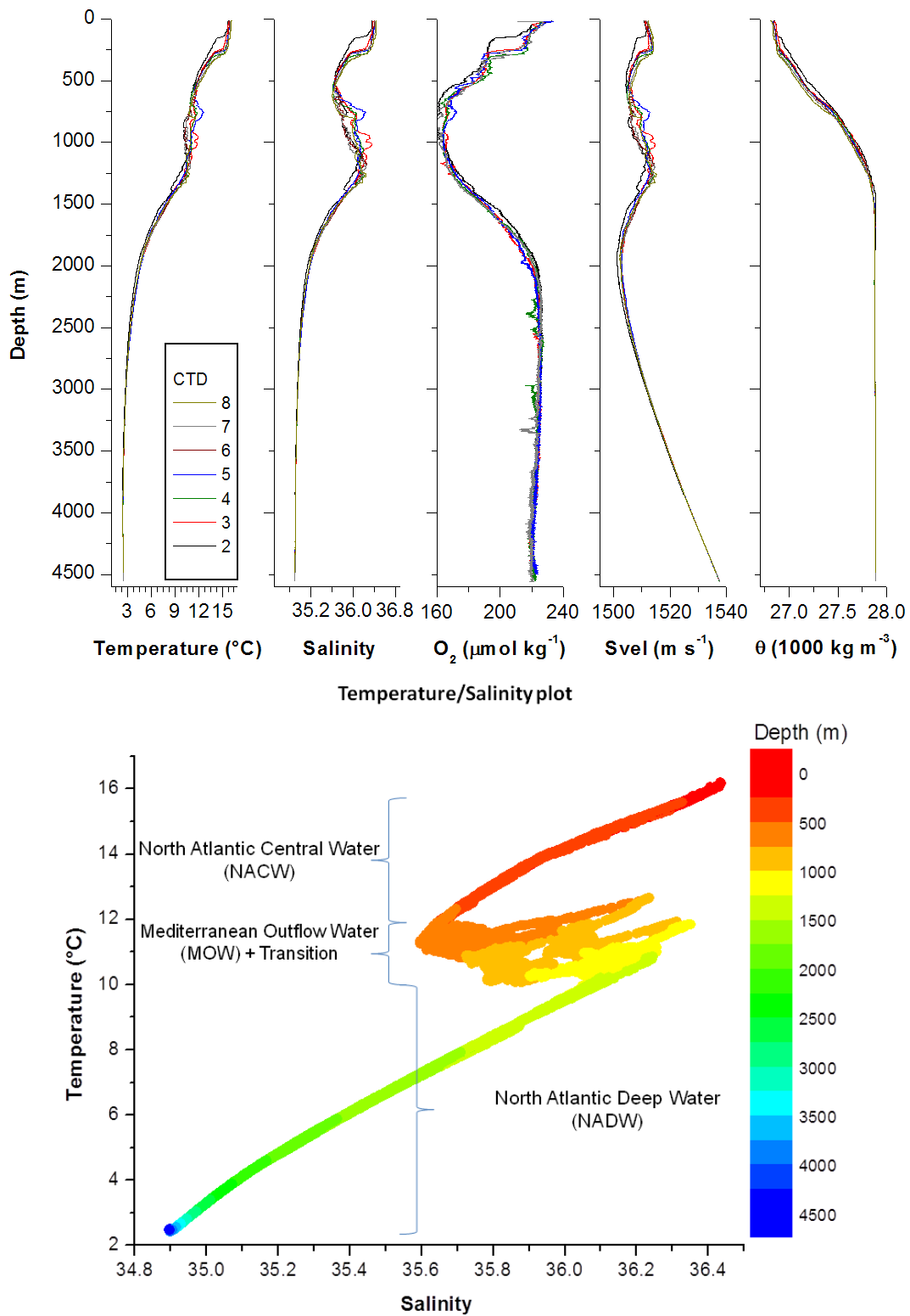


Fig. 4.3.2 Overview of CTD cast and water masses characterization. Top: Water column characterization. It shows from left to right temperature, salinity, dissolved oxygen, sound velocity, and potential density. While CTD 3-8 were taken within the same region (Tiamat, Abzu and M. Ivanov mud volcanos, respectively), CTD 2 was performed at the Porto mod volcano and thus displays slightly different physical properties. Note that no

dissolved oxygen profiles are shown for CTD 6 and 8 due to strong noise affecting the sensor. Bottom: Water masses characterization based on the temperature/salinity plot for CTD 2-8. The presence of the Mediterranean outflow water (MOW), carrying slightly warmer and saltier water is clearly evident in the 600 to 1200 m depth range.

Due to its relative proximity to Gibraltar and thus to the Mediterranean Sea, the Gulf of Cadiz is characterized by the confluence of both Atlantic and Mediterranean waters, that were investigated on previous cruises (i.e. M.S. Merian 1-3 cruise in 2006). In agreement with those investigations, the collected temperature and salinity profiles noticeably displayed both variable but consistently increased temperature (up to 12.5°C) and salinity (up to 36.1) in the depth range 600-1300 m. Interestingly, within that range, the dissolved oxygen concentration was found to be the lowest (160 $\mu\text{mol kg}^{-1}$ against the average 220 $\mu\text{mol kg}^{-1}$). A temperature versus salinity plot of CTD 2-8 (Figure 4.3.2) helped a further characterization of the water masses. Besides a weakly stratified first 240 m, the water column was characterized by 3 distinct regions:

- a stable thermo-halocline between ~240 to 600 m that corresponds to the North Atlantic Central Water (NACW),
- the Atlantic Deep Water (NADW) below ~1300 m depth,
- a region within ~600-1300 m where the salinity and temperature increased are consistent with the presence of the warmer and saltier Mediterranean Outflow Water (MOW) at its upper and lower end

These observations are in good agreement with previous studies in the Gulf of Cadiz (Criado-Aldeanueva et al. 2006 and references therein).

Independently from the different water masses and their physical properties, the density profiles were found to show an increase in density down to ~1800 m depth followed by a weakly stratified bottom water, and were found to vary little within the selected CTD locations. In contrast, the sound velocity profiles calculated from temperature and salinity based on the Del Grosso parameterization (Del Grosso, 1974) were strongly affected by the different water masses and displayed significant variability with the water column. The values ranged from 1502 m s^{-1} at 2000 m depth to 1538 m s^{-1} near the bottom.

Porto mud volcano

The Porto mud volcano was surveyed during CTD 2 using a conventional near bottom towed transect ~ 250 m long. The CTD was kept at 7 to 9 m from the bottom to maximize the chances of detection CH_4 sources at the seafloor while maintaining a safe distance from bottom to avoid collision with unforeseen emerging topographic features (e.g. the mud volcano rim). A total of 12 Niskin bottles were fired from the SE rim to the center of the mud volcano. The first gas chromatographic analysis revealed CH_4 concentrations near background values and no significant changes in the CH_4 concentrations were detected over the transect length.

M. Ivanov mud volcano

The M. Ivanov mud volcano was surveyed during CTD 3, 5 and 8. While CTD 3 was a conventional towed transect, with additional water column samples up to the surface, CTD 5 and 8 were 250 m long to-jo transects. With the exception of CTD 8 which was carried out based on the AUV sidescan sonar images, the other cast used ship based backscatter image previously collected as geographical reference. CTD 3 covered the NE-W region, while CTD 5 and 8

focused on the NW-SE transect. The first series of gas chromatographic results (CTD 3 and 5) provided little information on the spatial heterogeneity of the near bottom CH_4 concentration due to the lack of proper (high resolution) mud volcano images and issues with the gas chromatographer. As, however, around 60 Niskin bottles were fired near the bottom or within 100 m from the bottom, the results of shorebase analysis may be revealing.

Abzu mud volcano

The Abzu mud volcano was surveyed during CTD 6 using a to-jo approach. The CTD was towed near the bottom over 125 m long transect starting offsite and covering the whole SE-NW mud volcano diameter (Figure 4.3.3). Every 25 m, the transect was stopped and Niskin bottles were fired at preselected distances from bottom for a total of 23 samples (Figure 4.3.3). Other to-jo transects were not performed due to not favorable wind-wave directions and due to the presence of impracticable features revealed at the sidescan sonar images. The gas chromatographic analysis revealed higher CH_4 concentration in the first ~30 m from the bottom than above. The strongest increase in CH_4 was found 75 m, and in smaller extend 100m from the starting point which coincided with the presumed center of the mod volcano.

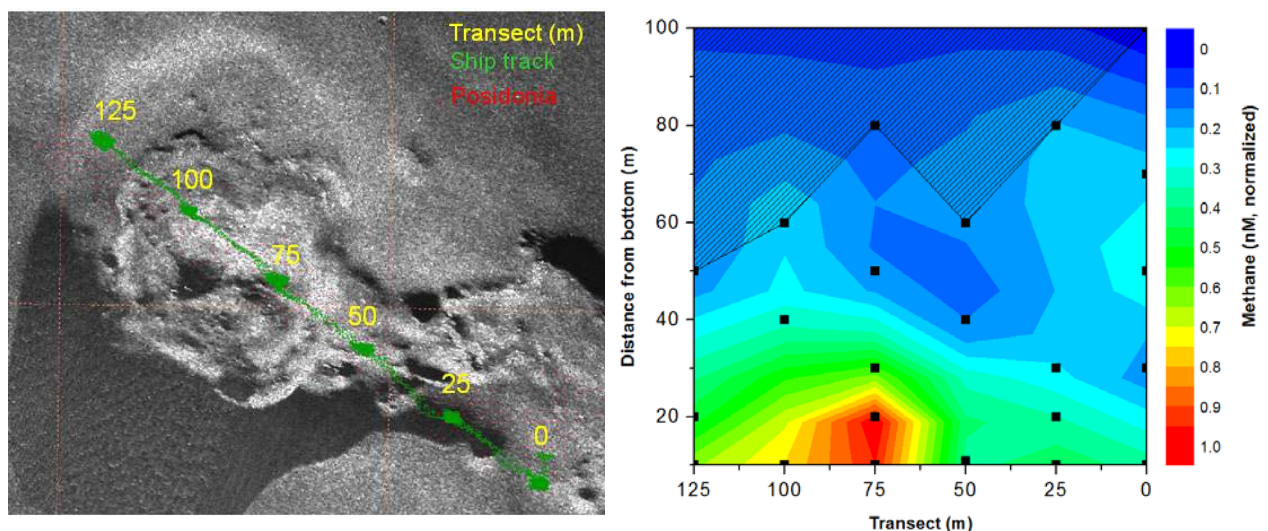


Fig. 4.3.3 CTD survey at the Abzu mud volcano. Left: AUV sidescan sonar image of the mud volcano with the to-jo transect over-layed. Distance from the starting point (yellow), ship position (green dots), and CTD position according to the Posidonia system (red dots) are also shown. Right: Contour plot of the normalized met CH_4 concentrations showing the place where Niskin bottles were fired. Note that the striped area marks an area where the data gridding is questionable due to the lack of samples.

Tiamat mud volcano

The Tiamat mud volcano was surveyed during CTD 4 and 7 using the same to-jo sampling grid used at Abzu. During CTD 4, 18 Niskin bottles were fired over the 250 m long SE-NW transect with 50 m stations. The gas chromatographic analysis was inconclusive as no clear CH_4 concentration increase was detected on the transect. CTD 7, in contrast, features a NS transect as during the deployment meteorological conditions very strongly limited the course. The starting point was also selected in order to avoid the supposedly steep rims of the NE region of the mud volcano (Figure 4.3.4). A total of 23 samples were taken during the transect (Figure 4.3.4). The gas chromatographic analysis revealed CH_4 concentration to be higher 200 m from the starting

point which coincided with the region of one of the most prominent topographic features of the mud volcano. Additional increase in near bottom concentration was detected 50 m from the start. A close look at the Posidonia location, current being performed, will help to better correlate topographic features and CH_4 concentration, better characterizing the site.

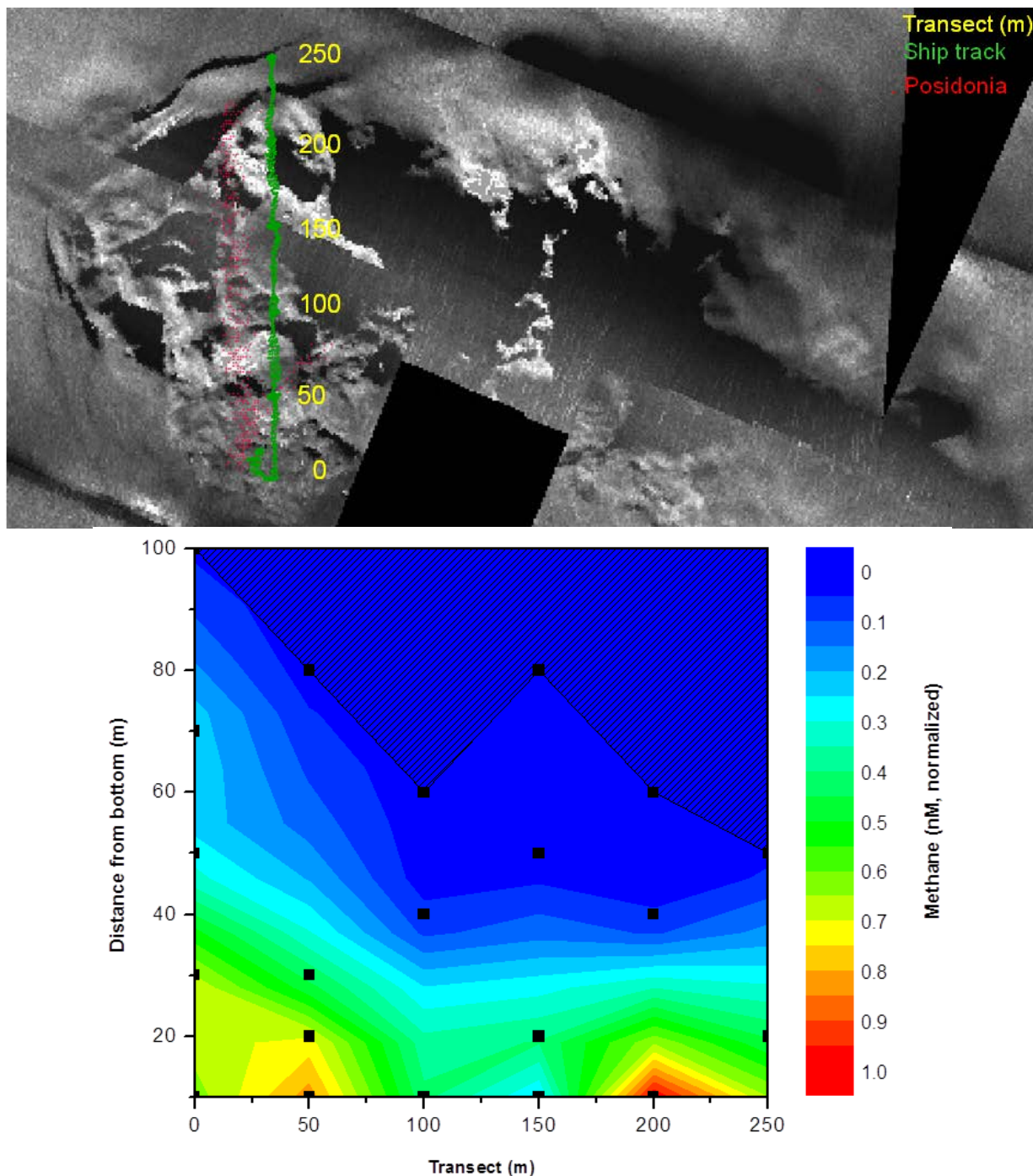


Fig. 4.3.4: CTD survey at the Tiamat mud volcano. Top: AUV sidescan sonar image of the mud volcano with the to-jo transect overlaid. Distance from the starting point (yellow), ship position (green dots), and CTD position according to the Posidonia system (red dots) are also shown. Bottom: Contour plot of the normalized CH_4 concentrations showing the place where Niskin bottles were fired. Note that the striped area marks an area where the data gridding is questionable due to the lack of samples.

Methane and carbon dioxide sensors

In total the instruments were used thirteen times during this expedition. The $p\text{CO}_2$ sensor and the CH_4 prototype were deployed during four sidescan or multibeam sonar exploration dives of the AUV. The HydroC CH_4 II was used during one video multicorer station and during eight CTD stations. The duration of the different stations varied between five and fifteen hours and the depth was between 4500 m and 4900 m. From all measurements data were received that will be post processed and analyzed once back in Kiel. Discrete water samples collected during the CTD casts that will be analyzed for their dissolved CH_4 concentration by means of gas chromatographic headspace analysis will allow for calibrated signal comparison or a field calibration of the instrument. Areas of increased CH_4 concentrations around mud volcanoes were identified. The CH_4 prototype sensed small concentration changes even during the dives onboard the fast moving AUV (appr. 3 kn) and $p\text{CO}_2$ profiles were obtained.

4.4 Sedimentology and Coring

(E. Pinero, V.H. Magalhaes, A. Petersen)

The Gulf of Cadiz hosts the present-day boundary between the African and the European plates. Recent multidisciplinary studies showed a number of active NE-SW folds and thrusts (e.g. Horseshoe fault), as well as WNW-ESE strike slip faults (e.g. SWIM lineaments; Zitellini et al., 2009; Gracia et al., 2003; Terrinha et al., 2009), which extend farther west of the accretionary prism and define the tectonic structure of the western Gulf of Cadiz.

During the M86/5 cruise, a total of 2 multicores (MUC), 8 box-corer (BC) and 25 gravity corers (GC) were deployed in order to recover sediment samples from the transition area between the accretionary prism and the Horseshoe Abyssal plain (HAP) in the Gulf of Cadiz (Table 4.4.1). A complete overview of all sampling stations is presented in Figure 4.4.1.

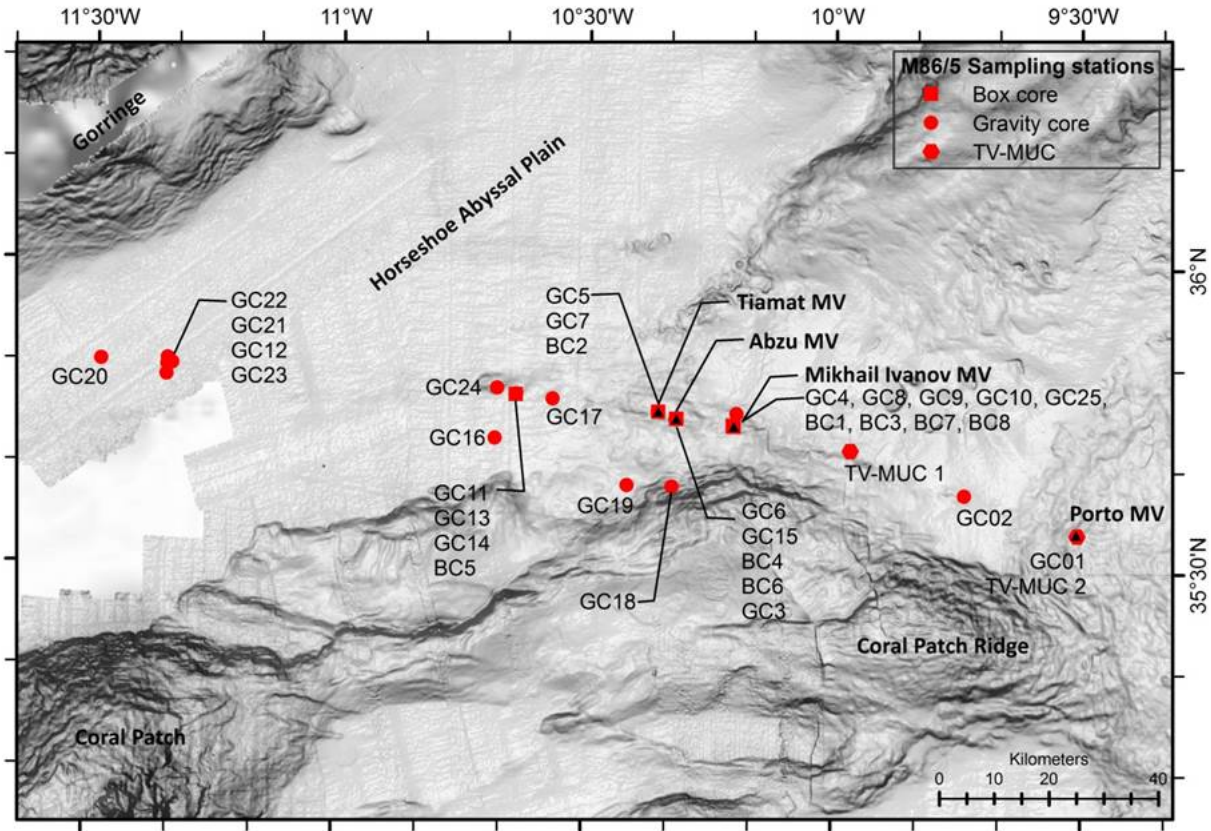


Fig. 4.4.1. Location of the sampling stations.

The main aim of this sediment sampling was to study the existence of mud volcanoes and areas of preferential fluid migration in relation to the SWIM lineaments and the Horseshoe Fault, farther west of the accretionary prism in the Gulf of Cadiz. With this purpose, the position of the sediment-sampling stations was carefully chosen based on the available information on MultiBeam, Parasound and Backscatter imaging of the study area. The box corers were sampled onboard for biological studies (see chapter 4.5), multi corers for pore water geochemistry (see chapter 4.6), organic geochemistry (see chapter 4.7) and biological studies, and gravity corers were sampled for pore water geochemistry.

Table 4.4.1: List of sediment sampling stations; t.p. = target point (as defined in the pre-cruise plan), HAP = Horseshoe Abyssal Plain, Ref. =Reference.

Sampling Station	Latitude (N)	Longitude (W)	Recovery (cm)	Thermal conductivity	Area
03TV-MUC-01	35.7001318	-9.9654501	up to 29	-	Topographic high (t.p. 16) on SWIM lineament
04TV-MUC-02	35.5617829	-9.5073501	up to 41	-	Porto M.V.
25BC-01	35.7389512	-10.2010668	yes	-	M. Ivanov M.V.
36BC-02	35.7618835	-10.3540665	yes	-	Tiamat M.V.
45BC-03	35.7403172	-10.2029665	yes	-	M. Ivanov M.V.
46BC-04	35.7508664	-10.31725	yes	-	Abzu M.V.
64BC-05	35.7875514	-10.6418164	yes	-	Topographic high (t.p. 2) at HAP
67BC-06	35.7505659	-10.3170170	yes	-	Abzu M.V.
83BC-07	35.738917	-10.2010335	yes	-	M. Ivanov M.V.
101BC-08	35.7389819	-10.2010497	yes	-	M. Ivanov M.V.
08GC-01	35.5618	-9.5073834	195	-	Porto M.V.
14GC-02	35.6274176	-9.7351164	420	-	Topographic high on SWIM lineament
18GC-03	35.749917	-10.3190336	480	-	Abzu M.V. (Ref.)
24GC-04	35.738917	-10.2010002	238	x	M. Ivanov M.V.
27GC-05	35.7620679	-10.3541501	454	x	Tiamat M.V.
28GC-06	35.7505318	-10.317233	475	x	Abzu M.V.
37GC-07	35.7619348	-10.3541834	475	x	Tiamat M.V.
40GC-08	35.7597491	-10.1955002	410	x	Ref. site for H.F. at M. Ivanov MV.
41GC-09	35.7390502	-10.2012837	no	-	M. Ivanov M.V.
42GC-10	35.7399825	-10.2030168	420	-	M. Ivanov M.V.
47GC-11	35.7883676	-10.6422834	468	x	Topographic high (t.p. 2) at HAP
54GC-12	35.8279349	-11.3462496	466	x	Topographic high at HAP
62GC-13	35.7885998	-10.6409003	211	x	Topographic high (t.p. 2) at HAP
63GC-14	35.7875343	-10.6419	428	x	Topographic high (t.p. 2) at HAP
68GC-15	35.7507674	-10.3169333	486	x	Abzu M.V.
69GC-16	35.7153333	-10.6826667	399	x	Background ref. HAP
73GC-17	35.7814828	-10.5673502	107	x	Topographic high at HAP
77GC-18	35.6391006	-10.3252004	72	x	N. flank Coral Patch Ridge
78GC-19	35.640535	-10.4153836	462	x	HAP N. of Coral Patch Ridge
92GC-20	35.8344509	-11.4800667	384	x	HAP
93GC-21	35.8299498	-11.336117	444	x	Topographic high at HAP
95GC-22	35.8379001	-11.3455999	304	x	Topographic high at HAP
96GC-23	35.8112316	-11.3476336	462	x	Topographic high at HAP
97GC-24	35.7979162	-10.6794003	482	x	Topographic high (t.p. 9) at HAP
100GC-25	35.7390161	-10.2010164	94	x	M. Ivanov M.V.

Methodology

Due to technical problems with the TV camera and with the coaxial cable that could not be solved, the MUC could only be operated 2 times (one without TV-camera). Therefore, the sediment sampling mainly focused on the deployment of GC and BC. For one station (GC-9), no sediment was recovered, resulting in 34 successful deployments and sediment sampling (including 25 GC's). As highlighted above, only GC's were described onboard for sedimentological purposes. The complete procedure followed onboard the M86/5 is described as follows. Right after recovery, the sediment core was labelled and cut in 1-meter-long sections. In

a number of cores, a specific sampling procedure for shore base He-isotope analyses was conducted in the deeper most section. Subsequently, cores were split onboard and their work half was sampled for different purposes such as pore water geochemistry, organic geochemistry, etc. Sedimentary description of the archive half sections included grain size, sedimentary fabric, colour, sedimentary structure, presence of fossils or fauna, disturbance and/or bioturbation, identification of paleo-redox fronts, presence of gas hydrates, authigenic minerals such as sulphides or carbonates, organic matter-rich sediments, etc. A special attention was made into the proxies for methane and hydrocarbons presence, such as H₂S smell, cracks and fluid migration pathways, distribution of carbonate concretions within the sediments, etc. After description and core photos taken, both archive and work sections were packed and stored at 4°C in order to preserve sediment moisture and other chemical properties. The work half of the only recovered section of GC M86/5-100GC-25, was totally sampled, and therefore, no work-half was stored for posterior studies.

In addition, measurements of thermal conductivity were carried out in the GC's by the heat flow group, with a minimum resolution of 10 cm. For more information, see chapter 4.9.



Fig. 4.4.2: Gravity corer retrieval and sampling.

Preliminary results

A number of sediment sampling stations were cored at the mud volcanoes Porto, M.Ivanov, Abzu and Tiamat, as well as at the Horseshoe Abyssal Plain (Figure 4.4.1), with a total recovery of up to 70 cm of MUC and a total of 88.36 m of GC sediment, which were sampled and described onboard.

In summary, the sediment recovered at the four mud volcanoes corresponds to a greenish gray mud-breccia with a hemiplegic coverage of variable-thickness in general composed of light olive brown to olive brown silty clay with forams. The sediments recovered at the Horseshoe Abyssal Plain are composed at the intercalation of turbidite deposits within an olive brown silty clay hemipellagite sequence that constitutes the normal background sediment. The main sedimentological results including photos and core-log descriptions of the GC's are attached in the appendix.

Mud Volcanoes: Porto, Abzu, Tiamat, and M. Ivanov:

Sediment stations on the four mud volcanoes include the high backscatter anomalies identified on the AUV side-scan and on the multibeam data, as well as a number of stations located in the mud volcano flanks, or in the nearby areas of the mud volcano rims.

The recovered sediment sequences correspond to a mud breccia, ranging from dark greenish gray to gray, with variable content in weak mud clasts of up to a few centimetres in diameter, mostly composed by claystones, and with a medium to strong H₂S smell. On top of the mud breccia, and depending on the position of the sediment station, sequences of hemipelagites of variable thicknesses are indicative of the heterogeneous activity or of changes over time in the directions of the mud flows within the mud volcanoes.

Gas hydrates were only recovered in the M. Ivanov mud volcano (M86/5-08GC-25).

Porto M.V.

A total of 2 sediment stations (M86/5-08GC-01 and M86/5-04MUC-02) were cored at the rim of the Porto M.V., with up to 195 cm of sediment recovered (Figure 4.4.3). The sediment sequence includes 7 cm of hemipelagic oxidized clay on top; while the intense H₂S smell as well as the presence of up to 7 mm in diameter claystone clasts characterizes the mud breccia extending to the bottom of the core. The breccia includes variable colour and organic-rich material, probably indicating the presence in the record of several episodes of mud flow. A number of paleo-oxidation fronts were also described (see Appendix).

Porto mud volcano

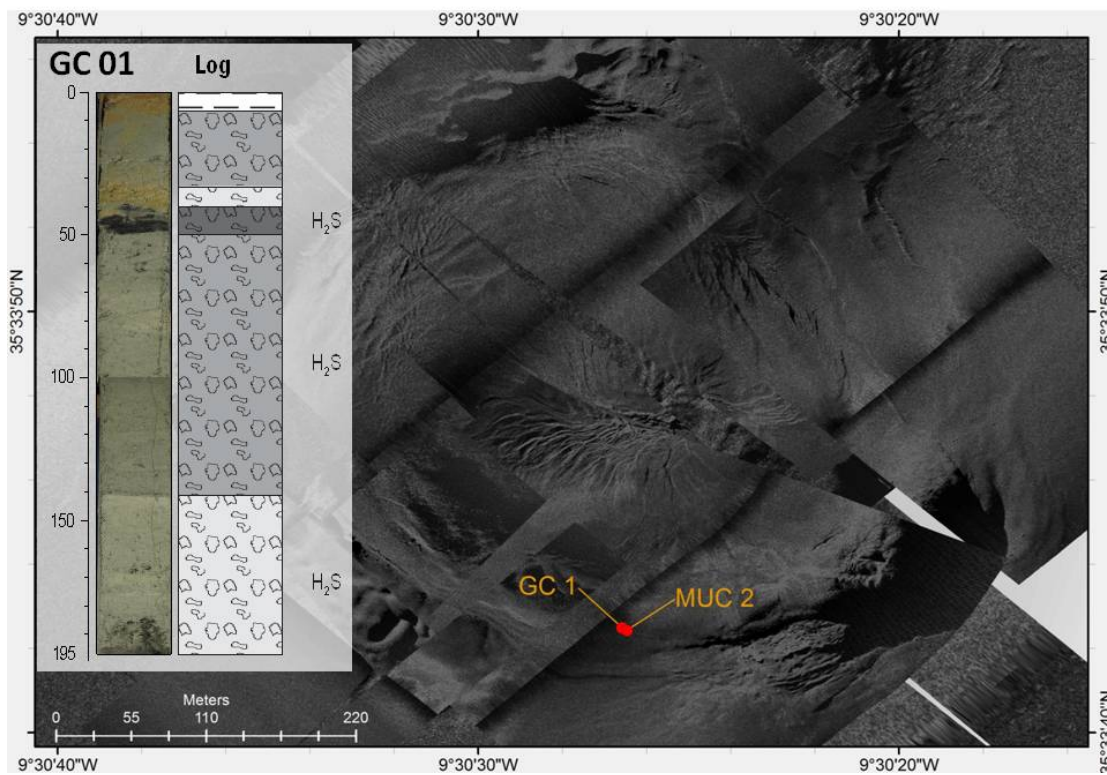


Fig. 4.4.3. Backscatter image showing the location of the 2 sediment-stations retrieved from the Porto M.V. Sediment core-log of the M86/5-8GC-1 is also shown (legend can be found in the appendix).

Abzu M.V.

Five sediment-sampling stations were conducted in the Abzu M.V. area, including two BC's and three GC's (Fig. 4.4.4). Two GC's and 2 BC's were recovered at different areas of the crater of the M.V., while GC M86/5-18GC-03 was collected 200 meters SW of the rim (Fig. 4.4.5).

The mud breccia with mainly claystone clasts and intense H₂S smell characterizes the sedimentary sequence from the crater of the M.V. (M86/5-28GC-06 and M86/5-68GC-15). The size of the claystone clasts do not exceed 1 cm in diameter, and their distribution is highly heterogeneous within the core, rare carbonate and sandstone clasts were also observed. At 251-265 cm and 290-298 cm depth (for M86/5-28GC-06 and M86/5-68GC-15, respectively) a transparent gel-like material occurs infilling several oblique surfaces. Although the nature of this material was discussed onboard, its composition and genesis is still unknown, but most probably corresponds to a bacterial mat, or a similar biological substance. On top of the mud breccia, both cores are covered by a hemipelagite, of 190 and 118 cm thick at M86/5-28GC-06 and M86/5-68GC-15, respectively, indicating the absence of recent activity or mud flows in the area. Moreover, the hemipelagite sequence includes in both cases a turbidite deposit at 109 and 118 cm respectively, with a few centimetres thick layer of medium sand at the bottom.

A black package of fine sediment is found at 430-454 cm depth in M86/5-28GC-06. This sediment has high content in forams and a rubber-like smell, probably indicating its high organic matter content.

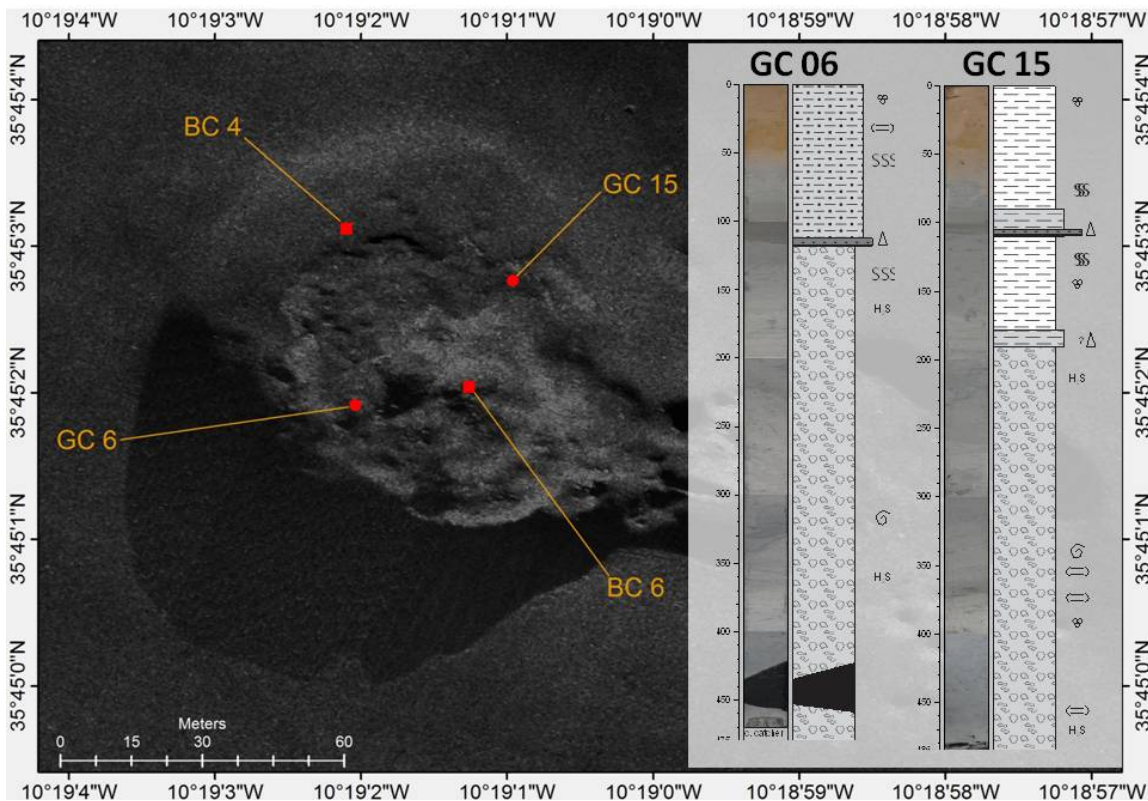
Abzu mud volcano

Fig. 4.4.4. Backscatter image of the Abzu M.V. with the location of the four sediment-stations. The sediment core-logs of M86/5-28GC-06 and M86/5-68GC-15 are also shown (legend can be found in the appendix).

The sediment recovered at core M86/5-18GC-03 away from the top of the mud volcano is a clayish hemipelagite, including a coarse sand turbidite at 105 cm depth. The bioturbation ranges from intense to medium, with a heterogeneous distribution of forams and bioturbation. Colour also shows a change at 67 cm depth, where it varies from light brown on top to greenish gray downwards, coinciding with the presence of an oxidation front.

Abzu mud volcano – reference Site

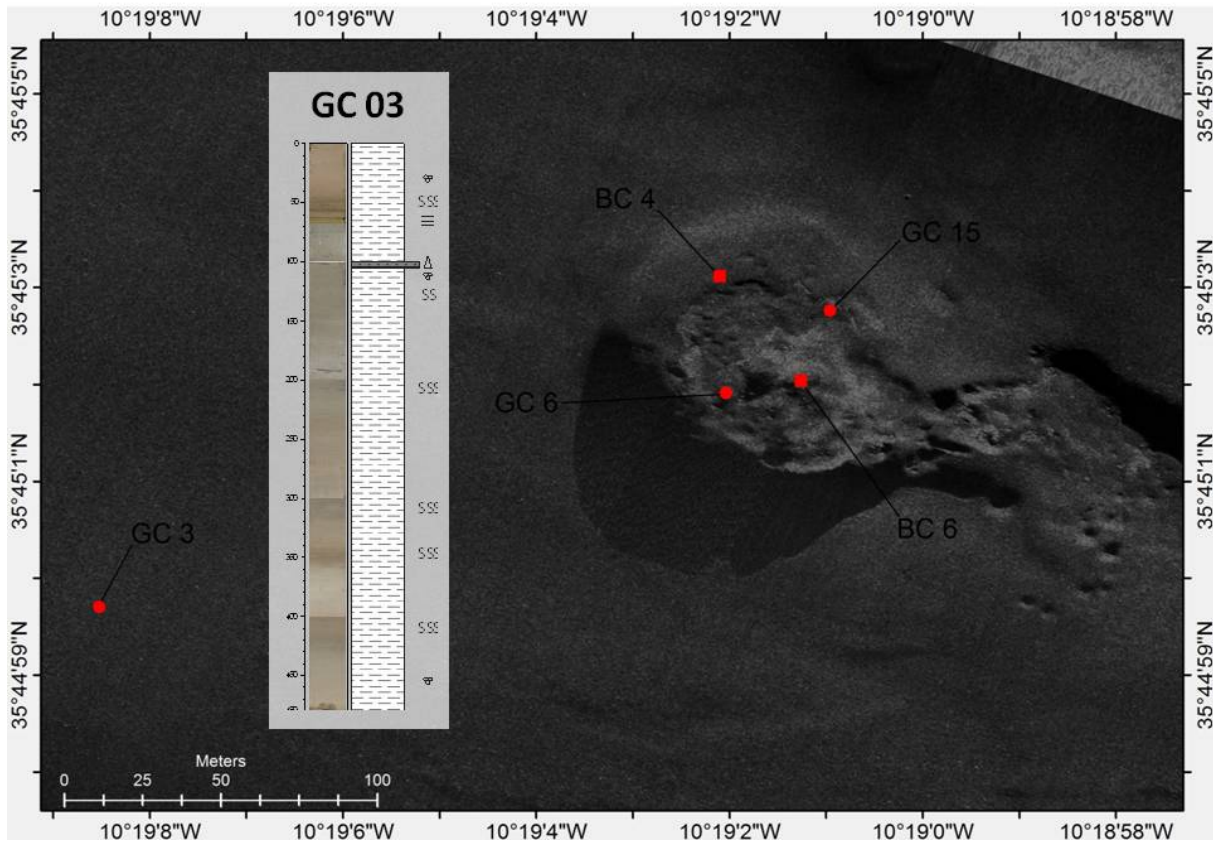


Fig. 4.4.5. Backscatter image of the Abzu M.V. showing the location of the sediment-stations. The sediment core-logs of M86/5-18GC-03, located near the M.V. is also shown (legend can be found in the appendix).

Tiamat M.V.

Two GC (M86/5-27GC-05 and M86/5-37GC-07) and one BC were recovered at the Tiamat M.V. (Fig. 4.4.6), with a recovery of up to 475 cm. The recovered sediment sequences include a hemipelagic silty-clay on top, of respectively 32 and 270 cm thickness, and a mud breccia below these depths. The transition between them is sharp at core M86/5-27GC-05, while it is gradual at core M86/5-37GC-07, where it was defined according to the presence of mud clasts, although it could occur shallower. Both GC's include the transparent gel-like material at 180-210 cm and 250-340 cm, respectively, and intense H₂S smell. Near the bottom of M86/5-27GC-05, several calcareous shells partially dissolved were found.

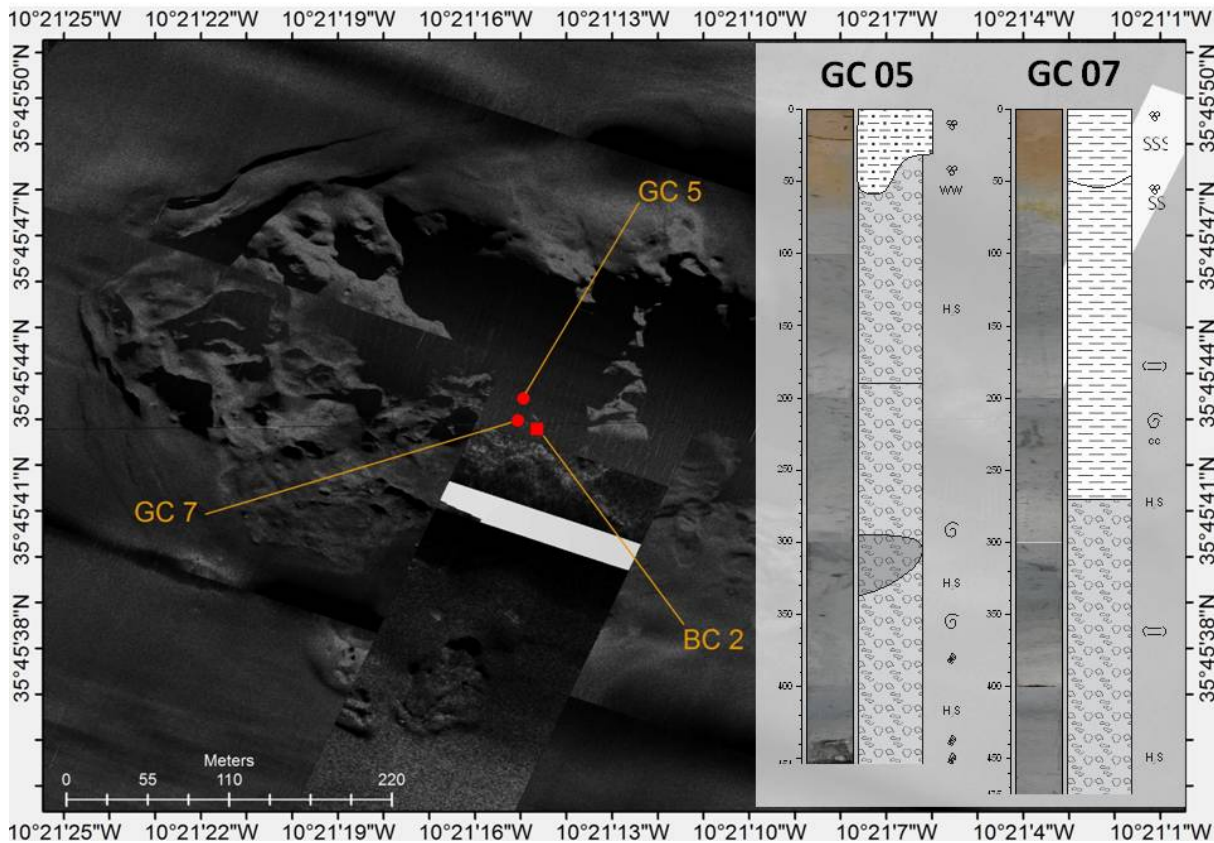
Tiamat mud volcano

Fig. 4.4.6. Backscatter image of the Tiamat M.V. showing the location of the sediment-stations. The core-logs of the M86/5-27GC-05 and M86/5-37GC-07 located at the top of the M.V. are also shown (legend can be found in the appendix).

Michael Ivanov M.V.

Two GC's and three BC's were recovered at the southern crater of the, apparently multi-crater, M. Ivanov M.V. (no recovery was obtained for M86/5-41GC-09), with a maximum corer length of 238 cm. M86/5-42GC-10 and M86/5-45BC-03 were recovered in the northern crater of the M.V. (Fig. 4.4.7.).

Sediments from the top of the M.V. are formed by mud breccias, with clasts up to 4 cm in diameter (M86/5-24GC-4), mainly of claystone but also including other lithologies, such as carbonate. They present intense H₂S smell. At M86/5-24GC-4, a hemipelagic sequence of 46 cm thickness covers the mud breccia, while at M86/5-100GC-25 this hemipelagic cover is not present, suggesting this is the most active area of the M.V., at present. This hypothesis is reinforced by the presence of a 10x4x6 cm size gas hydrate chunk at 65 to 76 cm depth in this GC. The gas hydrate chunk has a rounded shape, probably due to the melting of hydrate and subsequent formation of ice surrounding the hydrate, during the long time between recovery and sampling. During this time the He-sampling procedure was carried out, and the presence of high amounts of gas within the core were evidenced by several episodes of explosive degassing occurred during the He-sampling procedure. The gel-like transparent material already described at the sediment cores of Abzu and Timat M.V., was also found between 80 and 106 cm of core M86/5-24GC-4, while it was not found at core M86/5-100GC-25, that did not reach this depth.

420 cm of sediment were recovered at the northern M.V. crater (core M86/5-42GC-10), showing a sequence of silty clays and clays ranging from light olive brown at the top to greenish gray colour below 63 cm depth. The presence of mud breccias in the record is restricted to the interval between 225 and 290 cm, including rare clasts of claystone very weak and partially dissolved into the matrix. The gel-like material occurs in patches within the mud breccia sequence. Several intervals of high authigenic carbonate content occur, with a carbonate concretion of 12 cm in diameter at 370-380 cm depth. This carbonate concretion was sampled for further onshore analyses.

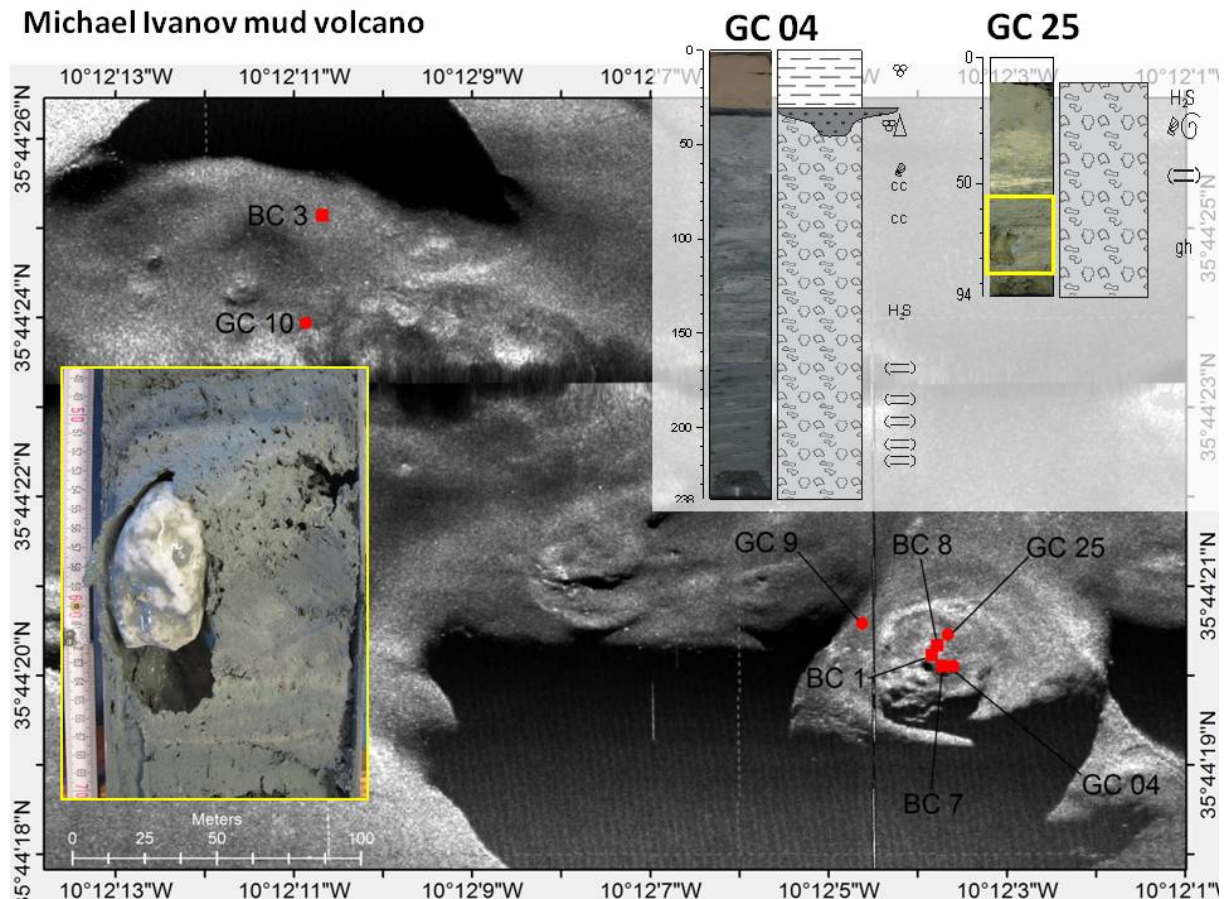


Fig. 4.4.7. Backscatter image of the M. Ivanov M.V., showing the location of the sediment-stations. The core-logs of the M86/5-24GC-04 and M86/5-100GC-25 are also shown (legend can be found in the appendix). A picture of the gas hydrate chunk (white) inside the sediment (grey) recovered at M86/5-100GC-25 is also shown.

Horseshoe Abyssal plain

A total of 16 GC's and 1 BC were collected in several areas in the Horseshoe Abyssal Plain, especially in the vicinity of the SWIM lineament, and including several topographic highs or areas of high reflectivity on the multibeam, previously defined as target points (see Fig. 4.1.2). Sediment recovery was very good, up to 482 cm at M86/5-97GC-24, only three GC recovered less than three meters, and only one recovered less than 1 meter (72 cm at core M86/5-77GC18, located at the North flank of the Coral Patch Ridge).

The sediments collected in the Horseshoe Abyssal Plain consisted of a sequence of hemipelagic silty clay with forams, with intercalation of up to 16 turbidite deposits recorded in core M86/5-54GC-12. The turbidite deposits range from several cm to dm thickness and its coarse layer at the base ranges from several mm to cm thickness, with a grain size of fine to coarse sand. Most of them show similar mineralogical composition, although a distinct turbidite rich in foraminifera shells was recorded at 73-134 cm at M86/5-69GC-16. At 162-219 cm depth of core M86/5-96GC-23 a turbidite rich in shell fragments was found. Although these organic-rich turbidites were only recognized in a few cores, they can probably be used to correlate levels with patches of forams-rich contents over the cores. A number of pyrite crystals were found during the sediment description of the turbidites. Pyrite exists as isolated crystals or as concretions at the sandy-base layer of several turbidites (e.g. 59-157 cm at M86/5-62GC-13). A tabular concretion of 5cmx3cmx3mm size was found at 99-121 cm in M86/5-62GC-13 (Fig. 4.4.8). At site M86/5-54GC-12 crystals of pyrite are found mixed with sandy components infilling a fracture. The presence of this authigenic mineral within the turbidite layers suggests that turbidites act as preferential conduits for fluids in the abyssal plain, enabling geochemical reactions taking place within the high permeability coarse layers.

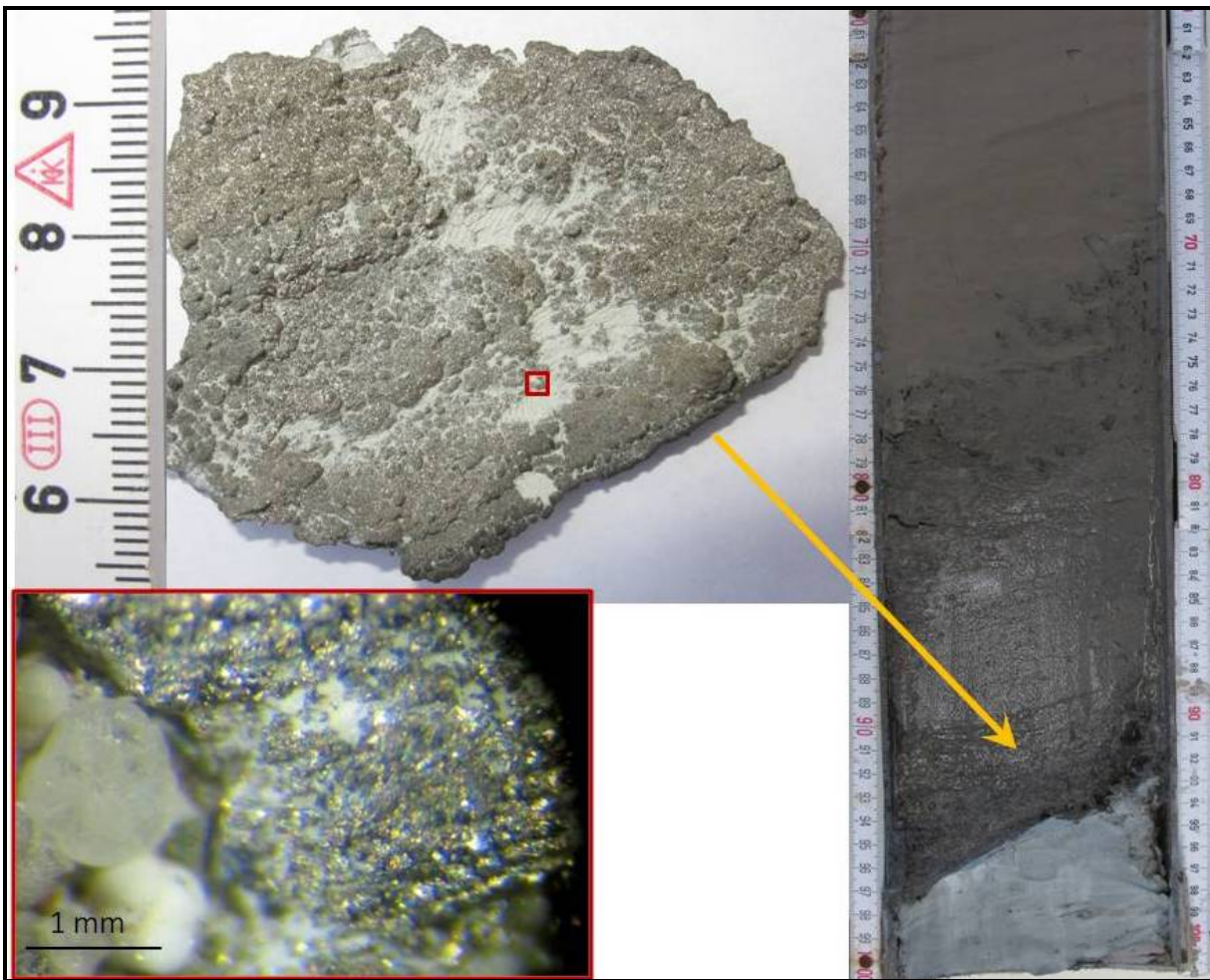


Fig. 4.4.8. Turbidite deposit in core M86/5-62GC-13 with details of the pyrite tabular concretion collected from the sandy layer at the base of the turbidite.

4.5 Biology

M.R. Cunha, A. Hilário

As a biogeographic crossroad where the oceanographic circulation establishes pathways for organism dispersal and favours the links to the Mediterranean, African equatorial and European boreal regions the Gulf of Cadiz is crucial for the interpretation of phylogeographical patterns and evolutionary history of marine organisms in the Atlantic Ocean. Its strategic central location in relation to other known seeps and vents makes the Gulf of Cadiz it a key-site for understanding dispersal of chemosynthetic organisms and the connectivity among cold seeps, and between cold seep and vent habitats (Génio et al. 2008). Previous studies have shown the high degree of novelty in the fauna associated to the numerous mud volcanoes that pierce the accretionary prism between the Iberian and Moroccan margins (e.g. Dworshack & Cunha 2007, Błażewicz-Paszkowycz et al. 2011) and the high diversity of chemotrophic species particularly in the deeper studied sites (Hilário & Cunha 2008; Hilário et al. 2010; Oliver et al. 2011). Ongoing simulations using oceanographic modelling of the transport of particles released in the Gulf of Cadiz show that: i) the direction and pathways of dispersal are highly variable (spatially and temporally); ii) there are oceanographic retention mechanisms which may limit the demographic connectivity of chemosynthetic organisms with planktotrophic larvae; iii) demersal transport is mostly restricted within the boundaries of the Gulf of Cadiz (Génio et al. in preparation). These results support the hypothesis that chemosynthetic-based ecosystems are probably more common than previously suspected and that our knowledge on their distribution is probably far from complete. In this context, our main goal during the Transflux cruise was to investigate the occurrence of chemosynthetic-based assemblages associated with eventual fluid seepage along the SWIM fault. This goal will certainly benefit from a multidisciplinary approach that provides information on the environmental setting of the biological assemblages and is therefore perfectly embedded in the objectives of the cruise.

The biological material collected during the cruise will contribute to attain the following specific objectives:

- 1) to gain more information on the biodiversity and distributional ecology of different compartments of the biological assemblages (microbial, meiofaunal and macrofaunal) associated to chemosynthesis-based environments.
- 2) to investigate reproductive and trophic ecology aspects (including symbiosis) of chemotrophic metazoan invertebrates.

Sub-sampling

Biological samples were taken from multi-core (MUC) and box-core (BC) sampling. MUC samples were taken from site 16 (M86-5-307 st.03, only partially successful – a few cm of surficial sediments could be collected from 3 replicates) and from Porto MV (M86-5-308 st.04; 4 replicate cores 10 cm Ø). One replicate was used for meiofauna and three replicates for microbiology sub-samples and macrofauna.

BC samples were taken from M. Ivanov MV (M86-5-329 st.25, M86-5-348 st.45, M86-5-388 st.83; M86-5-407 st.101), Tiamat MV (M86-5-339 st.36), Abzu MV (M86-5-349 st.46, M86-5-369 st.67) and site 2 (M86-5-366 st.64). After removal of any conspicuous organisms at the surface the BC samples were sliced at 0-1, 1-3, 3-5, 5-10 and 10-20cm bsf and sub-sampled for

microbiology (three sub-samples) and for meiofauna (one sub-sample); the remaining sediments (down to 20cm bsf) were collected for macrofauna (Fig. 4.5.1).

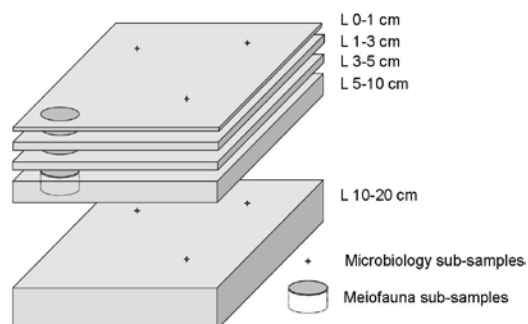


Fig. 4.5.1: Sub-sampling of the sediments collected with the box-core.

A thick layer of hemipelagic sediments, rich in foraminifera ooze was collected in most samples; in two cases, the MUC in Porto MV (st.04) and two BCs from M. Ivanov MV (st.25 and st.83)) an additional layer of mud breccia with very few clasts was recovered at approximately 30-50 cm bsf. The last boxcore recovered from M. Ivanov (st.101) showed a surficial layer of irregular thickness (20-50 cm bsf) with brown sediments and abundant small clasts (up to a few mm in diameter) covering an additional layer of mud breccia. Frenulate tubes and burrows could be observed at the surface of some samples (Fig. 4.5.2)



Fig. 4.5.2: Aspect of the surficial sediments collected with the box-core.

Microbiology

Sub-samples of 0.5-1g of surficial sediments (0-1 cm and 10-11 cm bsf) were collected and deep-frozen (-80°C) for 16S rRNA-based sediment microbial (bacterial and archaeal) community analysis (metagenomic approach). Additional sub-samples of 0.5-1g of sediments were collected from the surface layer (0-1 cm bsf), homogenised with 1 ml glycerol and stored at -80°C for further isolation of deep-sea bacterial guilds.

Meiofauna:

Each meiofaunal subsample (10 cm Ø, sliced in layers 0-1, 1-3, 3-5 and 5-10cm bsf) was preserved in 10% formalin solution for the morphological identification of the organisms, ¼ of the first layer was preserved in 96% ethanol for molecular taxonomy. The biodiversity, abundance and vertical distribution of nematodes, modern “live” foraminifera (soft-shelled, agglutinated and calcareous species stained with rose Bengal) and fossil (calcareous species) foraminifera will be described, interpreted in relation to the environmental setting and compared to cognate assemblages from other cold seep and vent areas.

Macrofauna

Sediment samples sliced in layers 0-1, 1-3, 3-5, 5-10 and 10-20cm bsf were washed through 1, 0.5 and 0.25 mm mesh sieves. The fauna removed from the surface and the different fractions of the washed sediments were kept in 96% ethanol to be sorted later under a stereoscopic microscope. Preliminary results consist on lists of macrofaunal organisms compiled in Table 4.5.1.

Table 4.5.1: Preliminary list of the fauna observed onboard.

St.	Phylum Class	CNI		NEM	ANN		MOL		ARTH		ECH		Biological debris	
		Scy	Ant		Polychaeta		Bivalvia		Malacost.		Echi	Hol	For	Pte
					Fre	Oth.	Ach	Oth	Amp	Tan				
Porto MV	M86-5-307/004		+		+	+				+				
M. Ivanov MV	M86-5-329/025				+			+	+	+			+	
Tiamat MV	M86-5-339/036				+			+		+			+	
M. Ivanov MV	M86-5-348/045				t					+	+	+	+	
Abzu MV	M86-5-349/046				t	+		+		+	+		+	+
Site 2	M86-5-366/064							+		+			++	+
Abzu MV	M86-5-369/067				t	+		+		+			+	+
M. Ivanov MV	M86-5-388/083	+		+	t	+	+	+	+	+		+	+	+
M. Ivanov MV	M86-5-407/101			+	t	+	+			+	+			

CNI: Cnidaria; NEM: Nematoda; ANN: Annelida; MOL: Mollusca; ARTHR: Arthropoda; ECH: Echinodermata; Scy: Scyphozoa; Ant: Anthozoa; Malac: Malacostraca; Echi: Echinoidea; Hol: Holothuroidea; Fre: Frenulata; Oth: other; Ach: *Acharax* sp.; Amp: Amphipoda; Tan: Tanaidacea; For: Foraminifera; Pte: Pteropoda. t: tubes.

Some samples yielded bivalves (shells and/or living specimens) and frenulates (Figs. 4.5.3 and 4.5.4) known to harbour chemoautotrophic endosymbionts. The bivalves found in M. Ivanov MV (st.25; st.83) were ascribed to *Acharax* sp.. The Frenulata examined on board were ascribed to the genera *Lamellisabella* sp. (Porto MV st.04), *Spirobrachia* sp. (M. Ivanov MV st.25) and *Polybrachia* sp. (Tiamat MV, st.36). Other examples of the fauna collected are pictured in Fig. 4.5.5. In most samples there were numerous small tubes built with aggregated foraminiferan shells probably inhabited by polychaetes. The conspicuous organisms more frequently observed were small unidentified bivalves (Nuculanidae?) and tanaids (apseudomorph and tanaidomorph; Crustacea:Tanaidacea). Also observed onboard were specimens of Limopsidae and Arcidae (Bivalvia); Amphipoda (Crustacea); Capitellidae and Spionidae (Polychaeta), *Brissopsis lyrifera*? (Echinoidea). Numerous large nematods (>1cm long) were found in M. Ivanov M (st.83 and st.101) in the layer 10-20 cm bsf. The samples will be processed in the lab for a complete inventory. The specimens collected will be curated and deposited in the Biological Research

Collection of the University of Aveiro (Department of Biology) for further ecologic, taxonomic, morphologic and genetic studies.



Fig. 4.5.3: *Acharax* sp. from M.Ivanov MV.



Fig. 4.5.4: Frenulata specimens collected during the cruise: A) *Spirobrachia* sp. (M. Ivanov MV), B) *Polybrachia* sp. (Tiamat MV), C) *Lamelisabella* tube with anthozoans (Porto MV).

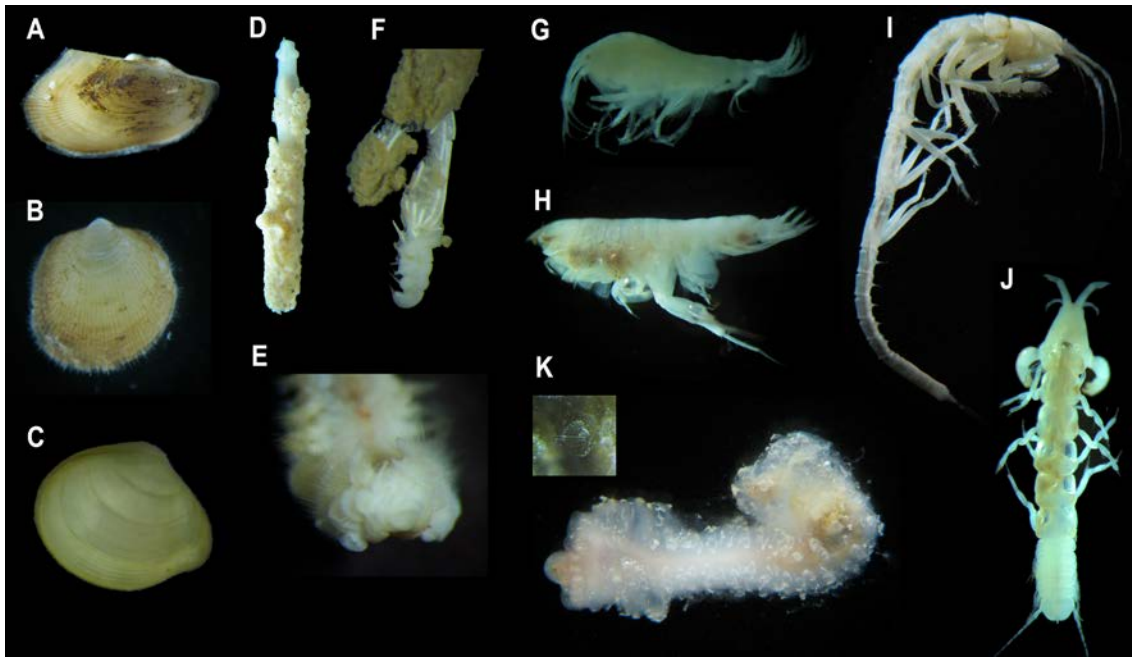


Fig. 4.5.5: Examples of macrofaunal organisms collected during the cruise. A: Arcidae (Bivalvia); B: *Limopsis* sp. (Bivalvia); C: Bivalvia; D and E: Polychaeta; G: Amphipoda; H: Phoxocephalidae (Amphipoda); I: Apeudomorpha (Tanaidacea); J: Tanaidomorpha (Tanaidacea); K: Holothurian (Echinodermata). Pictures not to scale.

The abundance, taxonomic composition and distribution of the macrofauna found in the study area will be described, interpreted in relation to the environmental setting and compared with the assemblages known from other mud volcanoes in the Gulf of Cadiz and other cold seep locations in the Atlantic Ocean and Mediterranean Sea. The preservation in ethanol will enable sequencing of commonly used genes (e.g. COI, 18S rRNA, 28 rRNA) for an integrative taxonomical approach.

Specimens of Frenulata tubeworms and Solemydae bivalves (*Acharax* sp.) known to harbour chemoautotrophic endosymbionts, as well as an unidentified species of bivalves were selected and prepared onboard for different purposes. While the specimens of the unidentified bivalves were preserved whole, in the Solemydae and Frenulata the organs that harbour the endosymbionts, the ctenidium and the trophosome, respectively, were dissected out (Table 4.5.2). Some specimens were preserved in 4% formaldehyde for histological examination of the gonad tissue, others were prepared for analyses of the natural stable isotopic composition ($\delta^{13}\text{C}$, $\delta^{15}\text{N}$, $\delta^{34}\text{S}$) of tissues and for the study of prokaryotic endosymbionts, including phylogenetic relationships based on 16S rRNA sequence analysis and DGGE community profiling, and characterization of symbiont distribution using FISH (Fluorescence in situ hybridization). In the case of frenulate tubeworms samples of trophosome and tube of the same specimens preserved for FISH were also preserved in 100% ethanol for molecular and phylogenetic studies of the symbiotic bacteria. Some bivalve shells will also be used for elemental fingerprinting (e.g. ^{48}Ca , ^{55}Mn , ^{59}Co , ^{88}Sr , ^{138}Ba , ^{208}Pb , and ^{238}U) using LA-ICPMS (inductively coupled plasma-mass spectrometry with laser ablation).

Tissues for stable isotopes and 16S rRNA analyses were carefully washed in cold seawater and deep-frozen (-80°C). Tissues for FISH were fixed during 3-6 hours at 4°C in formaldehyde (4%),

rinsed 2-3 times in sterile seawater, dehydrated in a gradient of 30%, 50%, 80% and 100% ethanol (15 minutes each) and stored at 100% ethanol at 4°C.

Table 4.5.2: List of species prepared for reproduction (Rep), stable isotope (SI), genetic (Gen) and prokaryotic endosymbiont (Sym) studies.

Station	Species	Tissue	Rep	SI	Gen	Sym
M86-5-329 st.25 (M. Ivanov MV)	<i>Acharax</i> sp.	Ctenidia				+
		Foot		+		
		All	+		+	
	<i>Bivalvia</i> und.	All	+		+	+
	<i>Spirobrachia</i> sp.	Trophosoma				
All				+	+	
M86-5-339 st.36 (Tiamat MV)	<i>Polybrachia</i> sp	Trophosoma				+
		Tube				+
		All	+		+	
M86-5-349 st.46 (Abzu MV)	<i>Bivalvia</i> und.	All	+		+	+
M86-5-369 st.67 (Abzu MV)	<i>Bivalvia</i> und.	All	+		+	+
M86-5-388 st.83 (M.Ivanov MV)	<i>Acharax</i> sp.	Foot		+		
		All	+		+	
	<i>Bivalvia</i> und.	All	+			
M86-5-407 st.101 (M. Ivanov MV)	<i>Acharax</i> sp.	All	+		+	

4.6 Pore Water Geochemistry

(*F. Scholz, B. Domeyer, U. Lomnitz, V. Thoenissen, A. Voelsch*)

Sampling pore water recovery

Sediment samples were taken from the gravity cores (GCs) at depth intervals of 10 to 40 cm. The MUCs were stepwise extruded from the core liners and cut into 1 – 5 cm thick discs. Pore water recovery was realized in a cold room at 5 °C using a sediment squeezer at a pressure of 1 to 7 bar. The extruded pore water was filtered through 0.2 µm cellulose membrane filters. In addition to the squeezing method, some cores were treated with rhizons (purchased from Rhizosphere, The Netherlands) in order to minimize contamination with atmospheric oxygen during pore water extraction. About 5 cm³ of wet sediment sample were stored for the determination of water content and porosity. Sediments remaining after pressure filtration (squeeze cakes) were stored for potential solid phase analyses in shore-based laboratories.

For selected methane-rich GCs sediment samples were taken for the analysis of He isotopes (³He/⁴He) and other noble gases. To this end, sediments inside the core liner were squeezed using a horizontal press in the on-board laboratory at ambient temperature. Prior to squeezing, air-tight fittings were inserted into pre-drilled and threaded fittings in the core liner (previously sealed with tape before coring) into which 3/8" diameter copper tubes were attached. The tubes were then flushed with sediment by squeezing the 1-m core section from both ends and then sealed with stainless steel clamps. Preferentially, two sediment samples from the deepest section of the core were taken.

Geochemical analyses

Analyses for ammonium (NH_4^+), phosphate (PO_4^{3-}), silicate (SiO_4^{4-}) and dissolved sulfide (H_2S) were carried out onboard using a Hitachi U2800A spectrophotometer. The respective chemical analytics follow standard procedures and are described in detail in Grasshoff et al. (1999) and on the GEOMAR webpage (www.geomar.de), respectively. Aliquots for NH_4^+ analyses were partly diluted prior to measurements in order to avoid interferences with HS^- . For the same purpose, aliquots for PO_4^{3-} and SiO_4^{4-} analyses were acidified and bubbled with argon for at least one hour. The total alkalinity (TA) of the pore water was determined by titration with 0.02 N HCl using the Tashiro indicator, a mixture of methyl red and methylene blue. The titration vessel was bubbled with argon to strip any CO_2 and H_2S produced during the titration. The pore water contents of chloride (Cl^-), bromide (Br^-) and sulfate (SO_4^{2-}) were determined by ion-chromatography (IC, Metrohm 761 Compact). The IAPSO seawater standard was used to check the reproducibility and accuracy of all chemical analyses.

In addition to the shipboard analyses, sub-samples were taken for shore-based analyses of major and minor cations (acidified with HNO_3), iodide (IC), oxygen isotopes, carbon isotopes (poisoned using mercury chloride) as well as acetate (see organic geochemistry group).

Preliminary results

Table 4.6.1 gives an overview about the number of sub-samples taken and analyses realized at each station. In the following sections, three aspects of the resulting data set will be discussed in more detail.

Pore water chemistry at the M. Ivanov, Abzu and Tiamat MVs

Three new MVs were discovered along a major strike-slip fault (so called SWIM lineament) during the research cruise M86-5. Figure 4.6.1 shows exemplary pore water profiles of Cl^- , TA, SO_4^{2-} and H_2S for sediment cores from M. Ivanov MV, Abzu MV and Tiamat MV. The pore water profiles of Cl^- and SO_4^{2-} decrease downcore whereas the TA and H_2S profiles are characterized by peaks in the zone of sulfate depletion.

The distribution of sulfur species and TA in pore water is best explained with anaerobe methane oxidation (AMO), a microbially mediated process that is commonly observed in shallow MV and cold seep deposits (Wallmann et al., 2004). In brief, deep-sourced methane is oxidized and converted to bicarbonate through simultaneous reduction of seawater sulfate to sulfide thus maintaining a downward-directed flux of seawater sulfate into the sediment.

In contrast to most other MVs in the Gulf of Cadiz (Hensen et al., 2007), TA at the M. Ivanov, Abzu and Tiamat MVs decreases again below the zone of AMO, thus indicating precipitation of authigenic carbonate minerals below this depth. Oversaturation with respect to carbonates requires high concentrations of bicarbonate and/or dissolved calcium (Ca) in pore water. The downward decrease in TA observed at the deep-sea mud volcanoes in the Gulf of Cadiz suggests that calcium carbonate precipitation is mediated by a deep-sourced Ca flux. Such a Ca flux from deeper sediment strata has previously been observed in settings where plagioclase minerals in the underlying oceanic crust or ash particles of related composition are altered to smectite and other authigenic clay minerals, respectively (Kastner et al., 1991). Ca release from volcanogenic sediments can be excluded since this kind of deposit does not occur in the Gulf of Cadiz. The

other alternative, i.e. release of Ca from oceanic basement rocks beneath the sedimentary cover is in agreement with previous geochemical investigations in the Gulf of Cadiz. These suggested based on a suite of isotopic tracers that some of the MVs here (e.g. Porto MV) discharge deep-sourced fluids that have partly been generated in the oceanic crust (Scholz et al., 2009, 2010). Pore water Ca profiles from previously studied MVs in the Gulf of Cadiz did not imply a deep-sourced flux suggesting that any hydraulic connection to the basement would be even more pronounced at the newly discovered MVs in the westernmost reaches of the Gulf of Cadiz. Major and trace element as well as isotopic analyses in shore-based laboratories will show if this hypothesis is correct.

Additional evidence for upward transport of fluids from greater depth and possibly from shortly above the oceanic basement is provided by the pore water Cl⁻ profiles at the M. Ivanov, Abzu and Tiamat MVs. The downcore Cl⁻ decrease (Fig. 4.6.1) is a commonly observed feature in active MVs (Hensen et al., 2007; Scholz et al., 2009) and usually attributed to upward advection of fluids that have been altered by clay mineral dehydration processes such as the transformation of smectite to illite (Kastner et al., 1991). This process does take place at temperatures between 60 and 150 °C which, assuming a background geothermal gradient of 44°C/km (see result of the heat flow group), corresponds to a sediment depth of 1.3 to 3.4 km below seafloor. The sediment thickness beneath M. Ivanov, Abzu and Tiamat MV likely ranges between 2 and 4 km which is in reasonable agreement with this estimate.

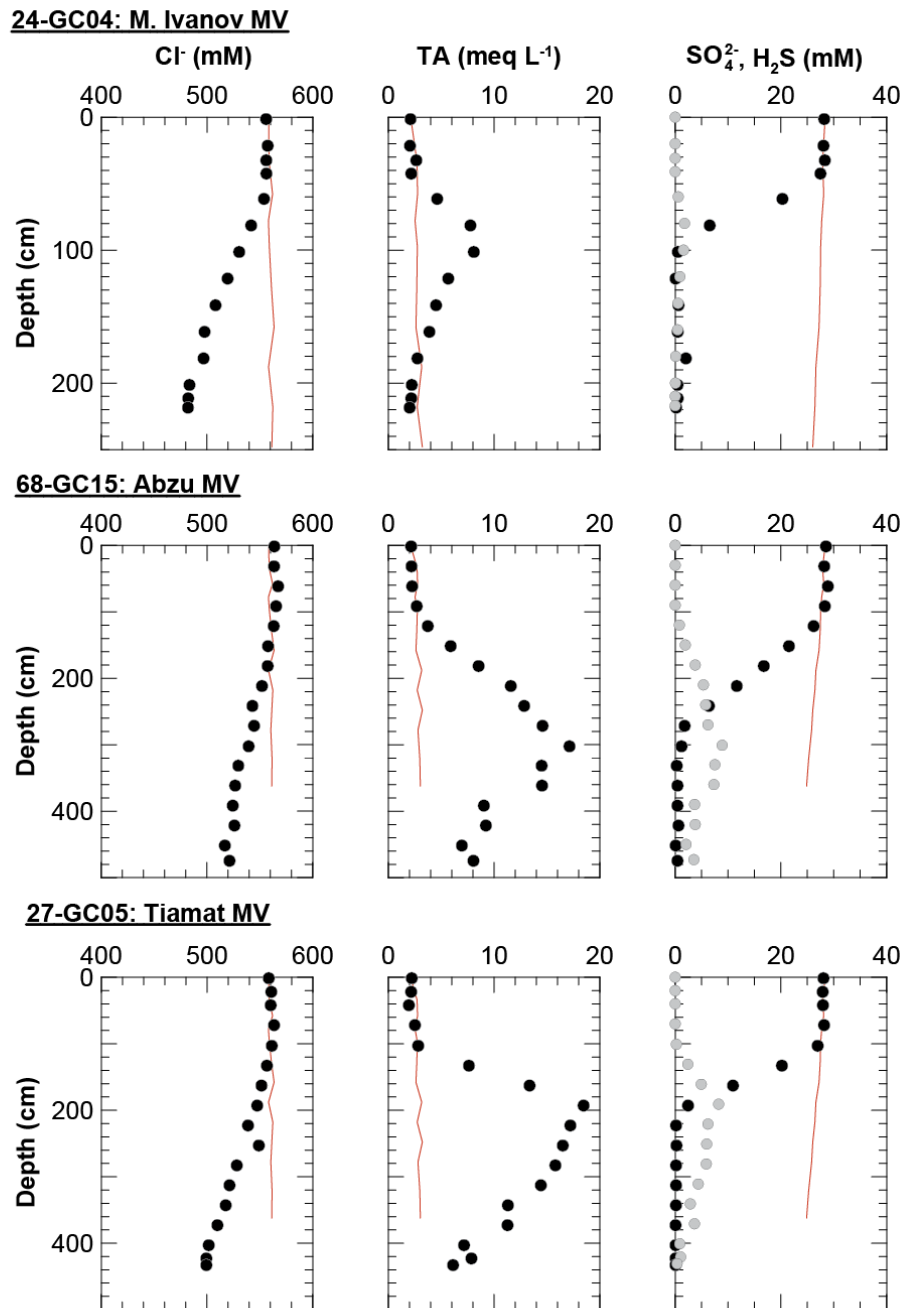


Fig. 4.6.1: Pore water profiles of Cl^- , TA, SO_4^{2-} (black dots) and H_2S (gray dots) at the M. Ivanov, Abzu and Tiamat MVs. The pore water profiles of a reference core (40-GC08; pore water sulfide was below the detection limit), representing the regional background sedimentation and diagenesis, are shown as red lines.

Gas hydrates at M. Ivanov MV

A fist-sized gas hydrate chunk was recovered from one core retrieved at M. Ivanov MV. The pore water Cl^- , SO_4^{2-} and H_2S profiles are shown in figure 4.6.2.

The Cl^- profiles decrease downcore, which likely results from upward advection of freshened pore fluids as described in the previous section. The hydrate chunk was situated at a sediment depth of about 65 to 75 cm. Pore water Cl^- concentrations are quite variable at this depth which could be the result of rapid gas hydrate formation, gas hydrate dissolution or both. Shore-based

analyses of the oxygen and hydrogen isotope composition of pore water and hydrate water samples will help to decipher hydrate dynamics at M. Ivanov MV.

100-GC25: M. Ivanov MV

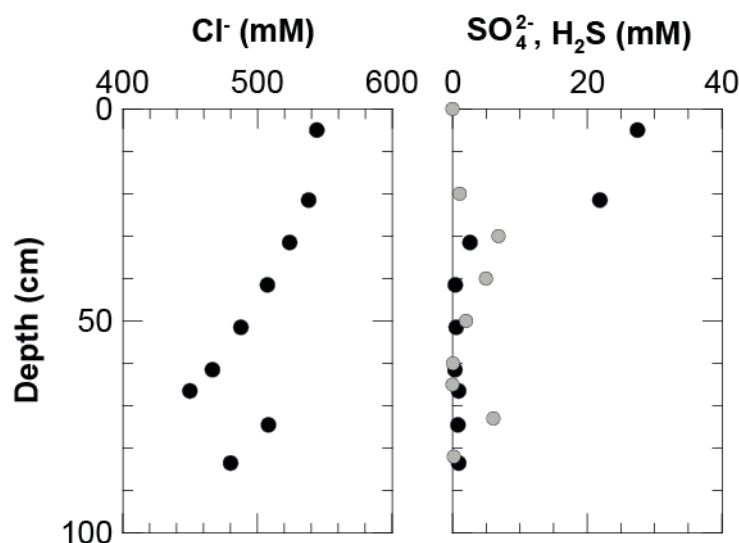


Fig. 4.6.2: Pore water profiles of Cl⁻, SO₄²⁻ (black dots) and H₂S (gray dots) in 100-GC25 from M. Ivanov MV. A fist-sized gas hydrate chunk was recovered at a sediment depth 65-75 cm.

Pore water chemistry of sediment cores in the Horseshoe Abyssal Plain

The second major working area besides the newly discovered MVs was the Horseshoe Abyssal Plain where sediment cores were retrieved along the SWIM lineament. Figure 4.6.3 shows the SO₄²⁻ and TA profiles of three GCs that were taken on a seafloor high on the E-W trending fault (GC12) as well as further south (GC23) and further north (GC22) of the fault.

In general, SO₄²⁻ decreases and TA increases with depth, which is most likely the result of AMO below the cored sediment interval (see above). As a consequence, the steepness of the sulfate gradient can be considered a first-order estimate of the methane flux at the different sites. The steepest sulfate gradient is observed in GC12 that was retrieved on the fault. As organic matter accumulation rates are likely to be rather uniform throughout the deep-sea plain, it may be anticipated that increases sulfate consumption at GC12 is maintained by a higher methane flux from deeper sediment strata. This flux is not rapid or focused enough to cause total SO₄²⁻ depletion at shallow depth or Cl⁻ anomalies in pore water like those observed at the MVs further east. However, the difference in sulfate gradient between GCs on the fault and away from the fault is a clear indication that the SWIM strike-slip fault serves as a pathway for gas and fluids, even in the deep-sea plain west of the three MVs.

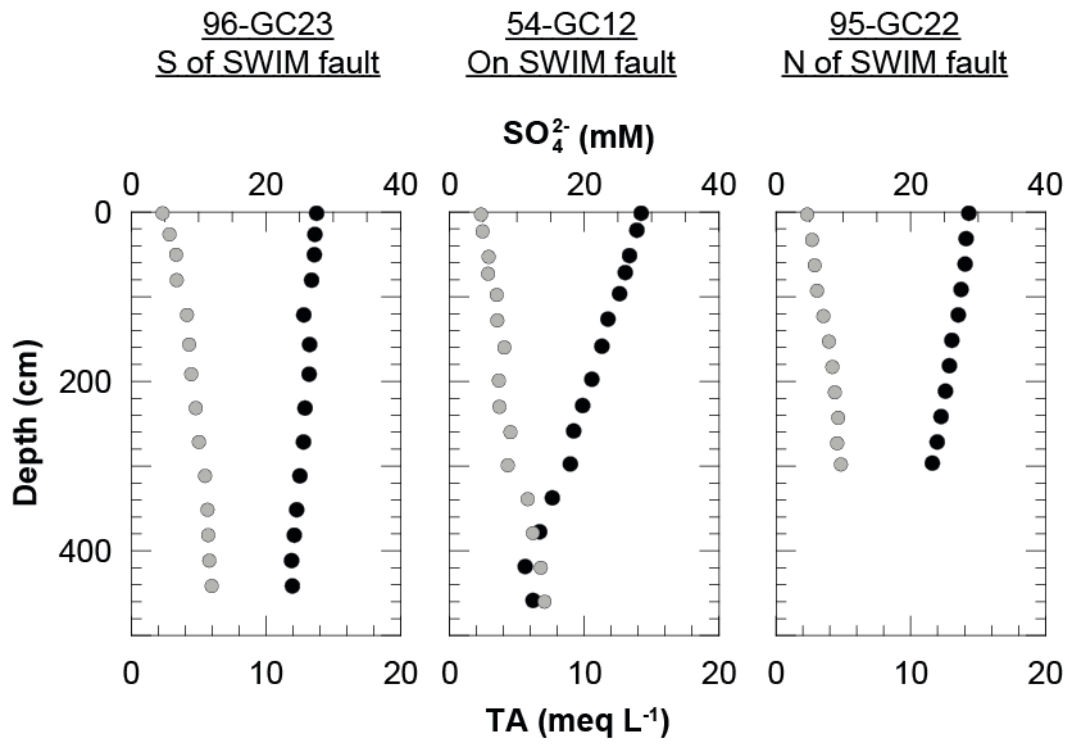


Fig. 4.6.3: Pore water profiles of SO_4^{2-} (black dots) and TA (gray dots) in GCs that were taken on a transect across the SWIM strike-slip fault in the Horseshoe Abyssal Plain.

Table 4.6.1. Overview about samples taken and analyses done by the pore water chemistry group during M86-5.

Station	Device	#	Samples	Noble gas samples	Parameter measured onboard								Subsamples						Squeeze cakes	Physical properties
					H ₂ S	PO ₄ ³⁻	H ₄ SiO ₄	NH ₄ ⁺	TA	Cl ⁻	SO ₄ ²⁻	Br ⁻	δ ¹³ C	δ ¹⁸ O/δD	ICP-OES/MS	DIC	IC	Acetate		
3	MUC	1	14	-	-	x	x	x	x	x	x	x	x	x	x	x	x	-	x	x
4	MUC	2	15	-	x	x	x	x	x	x	x	x	x	x	x	x	x	-	x	x
8	GC	1	12	-	x	x	x	x	x	x	x	x	x	x	x	-	x	x	x	x
14	GC	2	14	-	-	x	x	x	x	x	x	x	x	x	x	x	x	-	x	x
18	GC	3	13/5 ¹	-	-	x	x	x	x	x	x	x	x	x	x	x	x	-	x	x
24	GC	4	14	-	x	x	x	x	x	x	x	x	x	x	x	-	x	-	x	x
27	GC	5	17	-	x	x	x	x	x	x	x	x	x	x	x	x	x	x	x	x
28	GC	6	16	-	x	x	x	x	x	x	x	x	x	x	x	x	x	x	x	x
37	GC	7	17	2	x	x	x	x	x	x	x	x	x	x	x	x	x	-	x	x
40	GC	8	14	-	-	x	x	x	x	x	x	x	x	x	x	x	x	x	x	x
42	GC	10	16	1	x	x	x	x	x	x	x	x	x	x	x	x	x	x	x	x
47	GC	11	17	-	-	x	x	x	x	x	x	x	x	x	x	x	x	x	x	x
54	GC	12	15	-	-	x	x	x	x	x	x	x	x	x	x	x	x	x	x	x
62	GC	13	10	-	-	x	x	x	x	x	x	-	x	x	-	x	x	x	x	x
63	GC	14	14	-	-	x	x	x	x	x	x	x	x	x	x	x	x	x	x	x
68	GC	15	15	2	x	x	x	x	x	x	x	x	x	x	x	x	x	x	x	x
69	GC	16	17	-	-	x	x	x	x	x	x	-	x	x	x	x	x	x	x	x
73	GC	17	7	-	-	x	x	x	x	x	x	-	x	x	x	x	x	-	x	x
78	GC	19	14	-	-	x	x	x	x	x	x	-	x	x	-	x	x	x	x	x
92	GC	20	13	-	-	x	x	x	x	x	x	x	x	x	x	-	x	-	x	x
93	GC	21	14	-	-	x	x	x	x	x	x	x	x	x	x	-	x	-	x	x
95	GC	22	11	-	-	x	x	x	x	x	x	x	x	x	x	-	x	-	x	x
96	GC	23	14	-	-	x	x	x	x	x	x	x	x	x	x	-	x	-	x	x
97	GC	24	14	-	-	x	x	x	x	x	x	x	x	x	x	-	x	-	x	x
100	GC	25	9/1 ²	1	x	x	x	x	x	x	x	x	x	x	x	-	x	-	x	x

¹Additional five samples were taken from the topmost section by the aid of rhizons²One sample represents dissociated gas hydrate.

4.7 Organic Geochemistry

(M. Nuzzo, E. dos Santos Godinho)

Introduction

One of the main objective of the organic geochemistry studies includes the determination of concentrations in light volatile hydrocarbon gases (methane: CH₄ to pentanes C₅H₁₂) at the novel seep sites investigated. The composition in stable carbon isotopes of CH₄ ($\delta^{13}\text{C-CH}_4$) and heavier homologues will be performed to assess their origin (microbial versus thermogenic; Whiticar et al., 1986)). Along a West-East transect across Gulf of Cadiz MVs in the accretionary wedge, a transition has been reported in which the thermal maturity of the thermogenic hydrocarbon gases vented at the MVs decrease westward. At the westernmost Porto MV, the gas is composed mainly of CH₄ of microbial origin (acetate fermentation), which suggests microbes use acetate produced by hydrothermal leaching of the basement (Scholz et al., 2009; Seewald et al. 2001) rather than from the organic-lean mud breccia sediments which cannot sustain a quantitatively significant production (Nuzzo et al., 2009). This is consistent with the finding of high acetate levels at some Gulf of Cadiz MVs (Nuzzo et al., 2008). The organic geochemistry of fluids (acetate and other organic acids) and of sediment lipids will be analyzed comparatively to that of the gases to investigate the possible involvement of microbes in hydrocarbon gases production and degradation, including the near-surface Anaerobic Oxidation of Methane at the four MVs sampled.

Sediment sampling

Sediment samples were taken from the gravity cores (GCs) at depth intervals of about 20 cm for sampling of porewater hydrocarbon gases and at depths varying for 1 to 40 cm for lipid biomarker analyses (Table 4.7.1). Porewater samples were collected from selected GCs to measure concentrations in Volatile Fatty Acids (VFAs). The MUCs were stepwise extruded from the core liners and cut into 1 – 2 cm thick intervals for sampling. Pore water recovery was realized in a cold room at 5 °C using a sediment squeezer at a pressure of 1 to 7 bar. The extruded pore water was filtered through 0.2 µm cellulose membrane filters. In addition to the squeezing method, some cores were treated with rhizons (purchased from Rhizosphere, The Netherlands).

Sub-sampling and sample preservation

Porewater light volatile hydrocarbon gases were stripped from the sediments following the method of McAullife (1971). The sediment plugs sampled from the GC sections on deck were immediately injected into 30 ml glass vials filled with 10 ml of 10 % KCl to poison the bacteria. The vials were sealed and vigorously shaken to disaggregate the mud and to stop all bacterial activity. The samples were stored upside-down to minimize the potential gas exchange with the atmosphere and were allowed to equilibrate with the vial headspace for 24h. The gas was extracted in a syringe by injecting an equivalent amount of 10% KCl solution into the vials. The headspace gas was later transferred into a 20 ml sterile serum vial filled (bubble-free) with 10 % KCl solution at pH 1 by displacement of an equivalent amount of solution. The vials were again stored upside-down to minimize the potential for gas exchange with air through the septum.

Sediments were also collected in pre-furnaced glass vials and immediately stored at -20 °C for the analysis of lipid biomarkers at the on-shore laboratory of the LNEG and Faculty of Science of the University of Lisbon (Portugal). Aliquots (2 to 4 ml) of porewater were filtered using acetate-free regenerated cellulose filters (0.2 µm; Wheaton®) and placed into pre-furnaced glass chromatography vials. The samples were immediately frozen at -20°C.

Analyses at onshore laboratories

The concentrations in methane (CH₄) and heavier homologues will be determined at the onshore-based Laboratory at GEOMAR by Gas Chromatography-Flame Ionization Detection (GC-FID) using a Shimadzu GC14A instrument fitted with a Restek Rt® Alumina Bond/KCl capillary column (50m, 0.53mm ID). The stable carbon isotope composition of CH₄ will be measured by GC- combustion-isotope ratio Mass Spectrometry (GC-irMS) at GEOMAR.

Lipids will be extracted from the sediments using a modified Blye and Dyer method and separated into fractions of increasing chemical polarity by column chromatography at the laboratory of the LNEG (Portugal). The identification and quantification of biomarker compounds will be performed by GC-MS and GC-FID, respectively, at the LNEG and at the Faculty of Sciences of the University of Lisbon (Portugal). Compound-specific isotope analyses will also be performed on selected samples by GC-irMS at the Organic Geochemistry laboratory at MARUM (University of Bremen). All methods are described in Elvert et al. (2003).

The identification and quantification of organic acids by Gas Chromatography-Mass Spectrometry will be performed at the onshore laboratory of the Faculty of Science of the University of Lisbon.

Table 4.7.1: Overview about samples collected by the organic geochemistry group during M86-5.

Station	Device	#	Number of samples collected			
			CH ₄ -C ₅ H ₁₂	d ¹³ C-CH ₄	Lipid Biomarkers	Volatile Fatty Acids
3	MUC	1	12	12	12	-
4	MUC	2	35	35	35	-
8	GC	1	10	10	12	7
14	GC	2	12	12	8	-
18	GC	3	15	15	6	-
24	GC	4	13	13	10	-
27	GC	5	20	20	15	11
28	GC	6	25	25	19	7
37	GC	7	20	20	12	-
40	GC	8	19	19	12	14
42	GC	10	22	22	17	16
47	GC	11	22	22	20	17
54	GC	12	25	25	18	-
62	GC	13	13	13	12	10
63	GC	14	22	22	22	15
68	GC	15	23	23	21	9

Station	Device	#	Number of samples collected			
			CH ₄ -C ₅ H ₁₂	d ¹³ C-CH ₄	Lipid Biomarkers	Volatile Fatty Acids
69	GC	16	26	26	26	10
73	GC	17	5	5	10	-
78	GC	19	25	25	17	10
92	GC	20	20	20	62	-
93	GC	21	23	23	42	10
95	GC	22	15	15	52	-
96	GC	23	22	22	24	-
97	GC	24	25	25	21	-
100	GC	25	5	5	12	-

4.8 Heat flow measurements

(N. Kaul, B. Heesemann, T. Kulgemeyer)

Rationale of heat flow measurements

Mud volcanoes (MV) are sources of mass and energy, transported from deeper levels of the sediment pile to the surface. Together with fluid and gas, thermal energy is emitted through these structures. Therefore heat flow determination is a sensible tool to detect and quantify the amount of convective flow. In the Gulf of Cadiz several mud volcanoes can be found along major tectonic lines (SWIM faults). We employ geothermal measurements to observe the activity of mud volcanoes and possible leakage at the faults apart from pronounced structures.

Heat probe and shipboard operation

On cruise M86/5 the heat flow probe, a Lister type violin bow design (Fig. 4.8.1), from the University of Bremen, *Meerestechnik und Sensorik* was used to obtain temperature gradients and *in-situ* thermal conductivities. The active length of sensor string is 6 m, with 21 thermistors spaced every 0.26 m. The probe is rated at 6000 m water depth. Four 8-channel 22 bit A/D converters are used to record the digital data into solid state memory. Additionally the instrument is used in conjunction with an online FSK data transmission while a conducting cable is available.



Fig. 4.8.1: Six meter heat flow probe during M86/5.

On this cruise, following instruments and parameters were in service:

Parameters of Lister-type heat probe:

Probe(s): #487 and #488

Stings: 1-10, (2-10), 3-10

Pulse duration: 20 sec

Online data transmission: 2400 Baud net via coax wire

Wire: 8000 m 18 mm deep sea cable (W12), coaxial; W10, 18 mm cable

Measurements are made in so called ‘pogo-style’, performing several penetrations in a row at small distances. Each penetration consists of raising the probe some hundred meters above the sea floor from the previous penetration, slowly moving the ship to the next penetration site and letting the wire angle become nearly vertical before dropping the probe into the sediment for the next penetration. Once the probe is in the bottom, it is left undisturbed for 8 minutes for the equilibrium temperature measurements and another 8 minutes, if a thermal conductivity measurement is made. For the penetration spacing used in this survey, transit between penetration points lasts about 30 – 75 minutes, a recording cycle in the sea floor is either 8 or 16 minutes, yielding a rate of about one hour per penetration. Transit speed is governed by the trade-off between keeping the wire angle small and minimizing the time between penetration points.

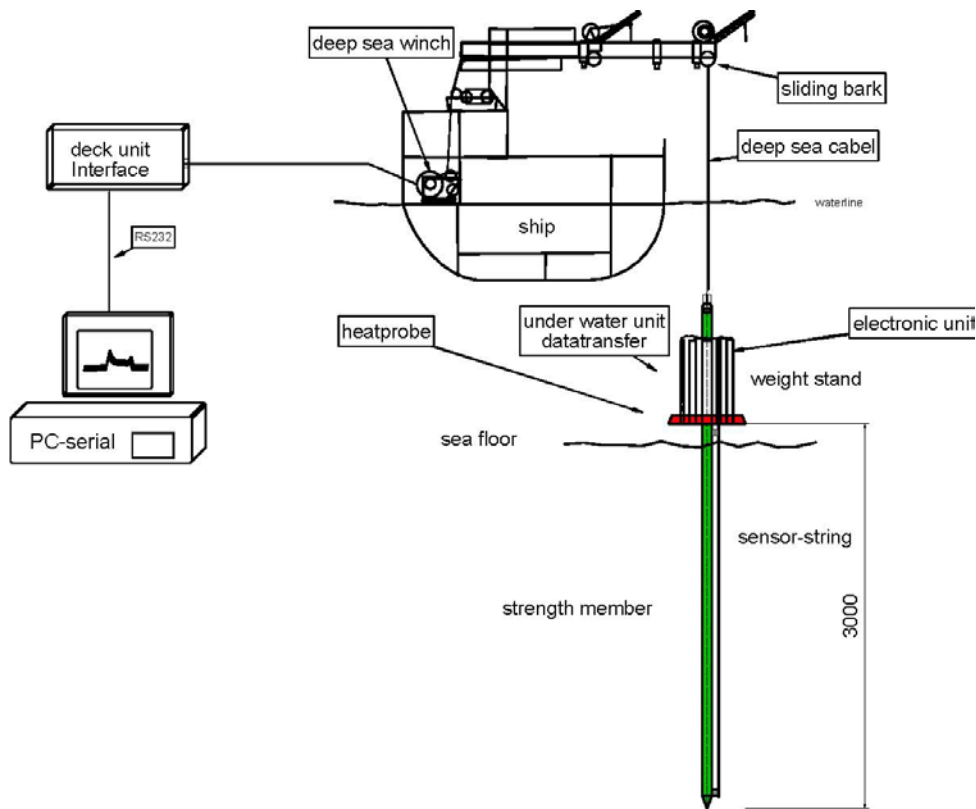


Fig. 4.8.2: Schematic view of heat flow probe operation

Winch speed during payout and retrieval of wire is 1-1.1 m/s. The initial penetration velocity is generally 1.0 m/s. Deployment of the instrument is amid ship on the starboard side (Fig. 4.8.2), employing a beam crane and assistance crane. This procedure ensures safe operation even during medium sea state and minimum interference due to the ships vertical movement during station work. An IXSEA® transponder/releaser type “OCEANO 2500 Universal” is mounted 50 m above the instrument. The IXSEA Oceanos Abyss® positioning system is used to track the subsea target up to the full working depth of 4900 m with good results. To achieve spatially high resolution of heat flow determinations, penetrations were positioned between 300 (on top of mud volcanoes) and 700 m apart.

Heat flow data reduction

Processing temperature data includes calibration of thermistor sensors, calculation of sediment temperatures and temperature gradients, correction for probe tilt during penetration, and calculation of thermal conductivities. While the 8 minute wait is not long enough for the sediment temperatures to return to equilibrium after the frictional disturbance of penetration, it is long enough to extrapolate to an equilibrium temperature with a high degree of precision. Each temperature-time series is extrapolated to equilibrium temperature by the program MHFRED according to Villinger (Villinger et al., 1987). Because the calibration of each thermistor by the manufacturer is only good to 0.1°C, a secondary calibration is applied. This is usually done in deep marine environment (> 3000 m water depth) where negligible thermal gradients exist

within the limits of observation. For this calibration the heat flow probe is allowed to equilibrate at a certain depth for 5 minutes (usually 200 m above seafloor).

Fourier's law of heat conduction in one-dimension shows that heat flow (Q) is the product of the thermal gradient (dT/dz) and thermal conductivity (k). If these terms are constant over the depth of the measurements then the calculation of heat flow is trivial. However if these values are changing proportionately to each other, as is the case for a constant basal heat flux, then heat flow can be derived from Bullard's (1939) relation given by,

$$\Delta T = Q \sum \Delta z_i \cdot k_i,$$

where Δz_i is the thickness and k_i is the thermal conductivity over the i -th interval. In this case heat flow can easily be calculated as the slope of the line given by the summation. To properly calculate the temperature gradient a correction for the penetration tilt angle is applied. In most cases the tilt angle is less than 10° and the tilt correction is modest. Determination of thermal conductivity requires the knowledge of the amount of heat, dissipated into the sediment. Therefore a pulsed heat source is used (approximated by 20 seconds of electrical heating of known current and voltage), producing a set of 21 thermal conductivities. Because thermal conductivities are sensitive to the sediment porosity over the depth range of the measurements, these measurements can reflect the reduction of porosity within the upper meters of sediment.

Preliminary results of heat flow determinations

All sites for heat flow determinations are located on or near the SWIM-1 fault and mud volcanoes, residing on the fault (figure 4.8.3). The bulk of values is from 20 – 45 mW/m² with some exceptions to higher values up to 58 mW/m². The expected value for a 130 - 140 Ma old crust would be about 42 mW/m². A closer look at the data shows, that higher values are obtained in mud volcanoes, especially Porto MV. At M. Ivanov MV, there is a clear tendency of decreasing heat flow with increasing distance from the centre. However, values off the centre are much too low compared to the regional background. Measurements directly on the fault or nearby show heat flow values of 42 – 46 mW/m², which is undistinguishable from the expected age related value.

Gulf of Cadiz Heatflow

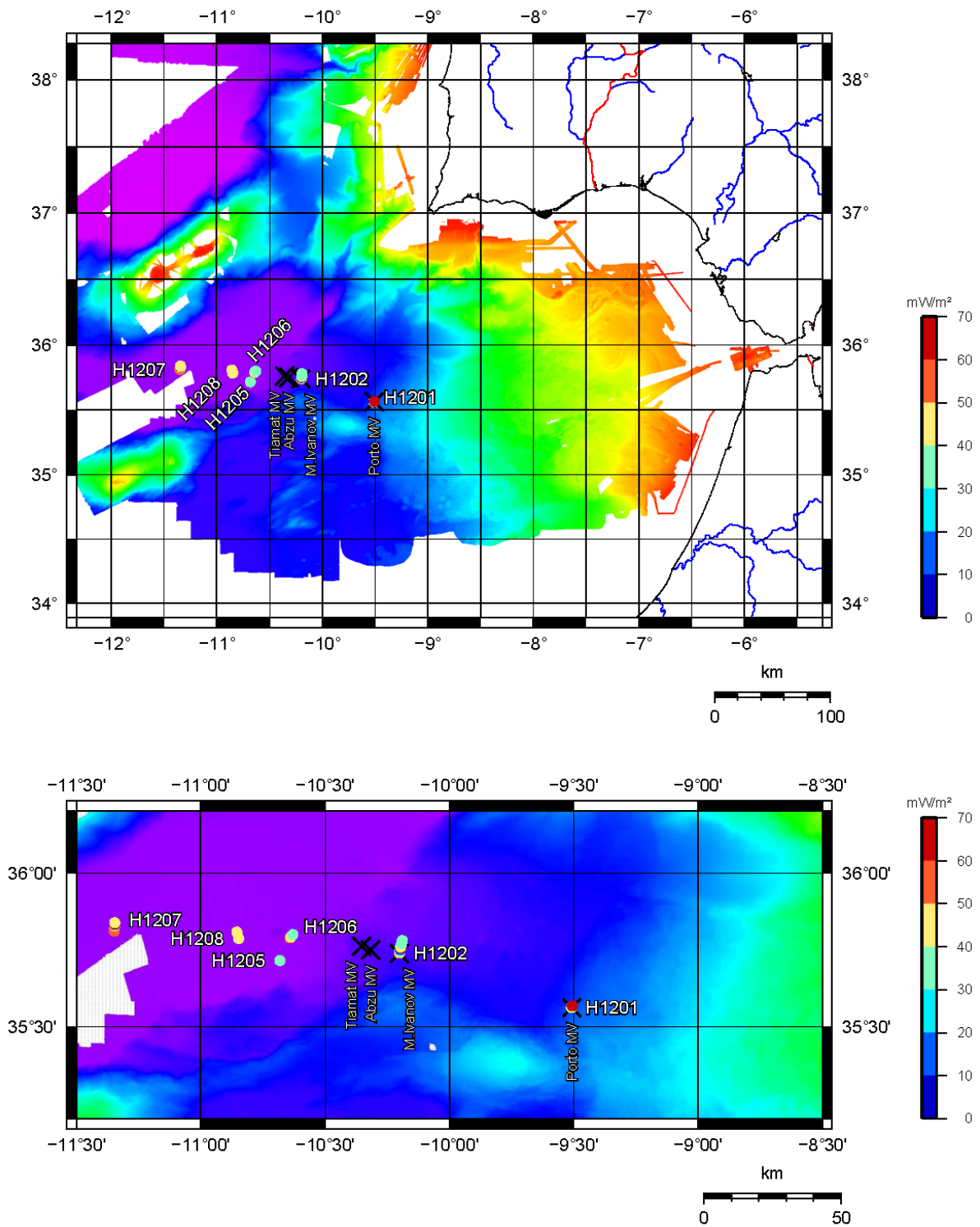


Fig. 4.8.3: Heat flow sites along SWIM-1 fault with named mud volcanoes.

4.9 Measurement of thermal conductivity on sediment cores

T. Kulgemeyer, N. Kaul

Additional to the *in situ* measurement the thermal conductivity of local sediments was measured on sediment cores. A total number of 20 sediment cores (GC4 – 8 and GC 11 – 25) was sampled at a minimum spacing of 5 to 10 cm. When necessary, additional measurements were taken.

The instrument used for these measurements is a Decagon Devices KD2 Pro Thermal Properties Analyzer. This device consists of a handheld controller and a number of different needle probes. On all measurements a probe with a single needle 6 cm length was used. In this configuration it is possible to measure thermal conductivity in a range of 0.02 to 2 W/mK with an accuracy of 5%. When inserted into the sediment the instrument first measures the starting temperature and its drift. After that a heat pulse is generated. A new temperature measurement is done after about a minute and thermal conductivity calculated by the temperature decay.

Thermal conductivity measured in the sediment cores ranges from 0.82 W/mK to 1.58 W/mK with a mean thermal conductivity of 1.03 W/mK for the entire region. Lower values generally appear in water saturated clay whereas higher values are correlated to basal sand layers of turbidites. An example of a typical measurement is shown in figure 4.9.1.

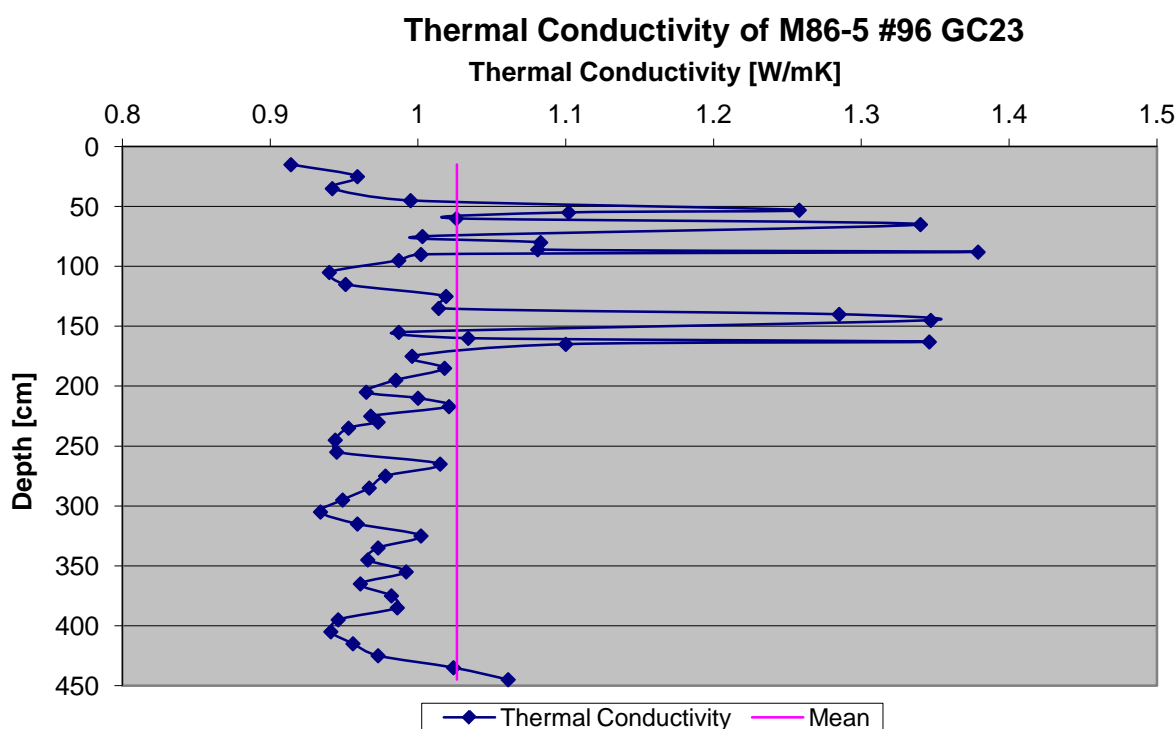


Fig. 4.9.1: Thermal conductivity values measured on core GC23

Table 4.9.1: Geothermal gradients

Cruise No.	Ship	HF	Lon	Lat	Depth[m]	Gradient [mK/m]
M86-5-5-1	#309	H1201P01	35° 33.783'N	009° 30.515'W	3868	27
M86-5-5-2		H1201P02	35° 33.845'N	009° 30.476'W	3871	38
M86-5-5-3		H1201P03	35° 34.065'N	009° 30.355'W	3920	55
M86-5-26-1	#330	H1202P01	35° 44.333'N	010° 12.053'W	4494	44
M86-5-26-2		H1202P02	35° 44.440'N	010° 12.027'W	4493	45
M86-5-26-3		H1202P03	35° 44.548'N	010° 11.998'W	4493	34
M86-5-26-4		H1202P04	35° 44.743'N	010° 11.947'W	4500	27
M86-5-26-5		H1202P05	35° 45.005'N	010° 11.871'W	4517	14
M86-5-26-6		H1202P06	35° 45.211'N	010° 11.800'W	4567	47
M86-5-26-7		H1202P07	35° 45.584'N	010° 11.723'W	4581	32
M86-5-26-8		H1202P08	35° 45.842'N	010° 11.655'W	4593	32
M86-5-26-9		H1202P09	35° 46.152'N	010° 11.578'W	4622	24
M86-5-26-10		H1202P10	35° 46.478'N	010° 11.491'W	4641	27
M86-5-26-11		H1202P11	35° 46.801'N	010° 11.406'W	4643	23
M86-5-38-1	#341	H1203P01	35° 47.503'N	010° 37.971'W	4825	NAN
M86-5-38-2	#341	H1203P02	35° 47.257'N	010° 37.844'W	4869	NAN
M86-5-38-3	#341	H1203P03	35° 47.012'N	010° 37.727'W	4869	NAN
M86-5-38-4	#341	H1203P04	35° 46.756'N	010° 37.591'W	4873	NAN
M86-5-38-5	#341	H1203P05	35° 46.505'N	010° 37.450'W	4869	NAN
M86-5-55-1	#357	H1204P01	35° 49.684'N	011° 20.790'W	4818	NAN
M86-5-55-2	#357	H1204P02	35° 49.882'N	011° 20.787'W	4837	NAN
M86-5-55-3	#357	H1204P03	35° 50.084'N	011° 20.780'W	4844	NAN
M86-5-55-4	#357	H1204P04	35° 50.284'N	011° 20.785'W	4847	NAN
M86-5-55-5	#357	H1204P05	35° 50.484'N	011° 20.777'W	4848	NAN
M86-5-55-6	#357	H1204P06	35° 50.884'N	011° 20.778'W	4848	NAN
M86-5-55-7	#357	H1204P07	35° 51.331'N	011° 20.790'W	4848	NAN
M86-5-55-8	#357	H1204P08	35° 51.725'N	011° 20.780'W	4849	NAN
M86-5-71-1	#373	H1205P01	35° 42.931'N	010° 40.962'W	4866	44
M86-5-71-2	#373	H1205P02	35° 42.932'N	010° 40.964'W	4866	44
M86-5-81-1	#386	H1206P01	35° 47.307'N	10° 38.506'W	4862	56
M86-5-81-2	#386	H1206P02	35° 47.517'N	10° 38.258'W	4862	46
M86-5-81-3	#386	H1206P03	35° 47.730'N	10° 38.992'W	4862	NAN
M86-5-81-4	#386	H1206P04	35° 47.941'N	10° 37.732'W	4862	33
M86-5-94-1	#399	H1207P01	35° 48.665'N	11° 20.851'W	4864	55
M86-5-94-2	#399	H1207P02	35° 48.980'N	11° 20.824'W	4855	58
M86-5-94-3	#399	H1207P03	35° 49.276'N	11° 20.798'W	4842	NAN
M86-5-94-4	#400	H1207P04	35° 49.685'N	11° 20.762'W	4822	35
M86-5-94-5	#400	H1207P05	35° 49.979'N	11° 20.743'W	4842	66
M86-5-94-6	#400	H1207P06	35° 50.274'N	11° 20.717'W	4845	47
M86-5-103	#409	H1208P01	35° 47.192'N	11° 50.909'W	4865	42
M86-5-104	#410	H1208P02	35° 48.467'N	11° 51.332'W	4863	46

5. Cruise and weather report M86/5

(Hempelt, Raeke, Knobelsdorf)

On the 24th of February FS METEOR left the port of Palma de Mallorca. The vessel experienced mostly cloudy conditions within a W'ly wind of 1 to 2 Bft. The working area was confined to the western Gulf of Cadiz within the coordinates 36°N and 10°W. The main focus of this expedition was in principal to collect data from potential fluid dewatering sites located in the deep-sea region. At the beginning of the expedition the area was under the influence of an almost stationary high to the west of Brittany. On the transit down to the working area there was a brief stop over in the harbour of Cadiz due to a personal incident. On the way down to the working area FS METEOR experienced weak north to westerly winds, at times variable with a sea/swell of 0.5 m. On the evening of the 25th close to the Strait of Gibraltar, the W'ly wind increased temporarily to a force of Bft 5. During the night the wind decreased quickly and weakened to 3 to 4 Beaufort.

After mostly cloudy conditions in the harbour of Palma, clouds cleared quite quickly. From noon on the day mostly sunny conditions prevailed. Late on the 26th the N'ly winds slightly increased to wind speeds of 3 to 4 Bft, at times 5 Bft was measured. During the 27th the sea state climbed to 1 to 2 m. The sea/swell persisted with a major elongated swell with a period of 11 seconds.

On the 29th a trough of a low close to Svalbard reached the sea area of the Azores. The next following day in the early hours the trough crossed the local area with W'ly winds picking up to a strength of Bft 5 and a sea/swell of up to 3 m. Showers and thunderstorms were experienced. In the early hours of the 3th of March the wind calmed down to a strength of 2 to 3 Bft, at times even less. The sea/swell dropped for a while before increasing again to about 3 m from the NW. On the 4th isolated waves of 4 m of height were observed. This sea state lasted until the 7th before weakening later to 1 to 2 m. On the evening of the 5th a weak low (1005 hPa) was located close to the Azores. An associated trough crossed the local area with winds picking up again. On the 6th the METEOR experienced N'ly winds with strength of 5 to 6 Bft. On the 8th the wind weakened and dropped down to 4 Bft. On the 7th of March a hurricane force low (945 hPa) was located close to Iceland while a strong high was situated over the Azores (1038 hPa). This brought a rise in swell of about 4 m from the NNW. Additionally there was a flat low (1025 hPa) in the Strait of Gibraltar, which filled rapidly. However, the wind from the east to northeast picked up to a strength of 5 to 6 Bft. The swell was the major part of the sea state with a significant period of 18 seconds. The peak was reached during the day with calming conditions towards the evening. On the 13th the sea/swell dropped down to 1 to 2m.

During the 14th FS METEOR was in the vicinity of another flat low (1019 hPa). This brought weak and variable winds. Sheet lightning was observed on the morning of the 15th.

On the transit to Lisbon the vessel experienced northerly winds with 3 to 4 Bft and a sea/well about 2 m. In the morning hours of the 16th FS METEOR reached the port of Lisbon with winds of strength 3 Bft from northern directions. For most parts of the research cruise M 86/5 the METEOR was under the influence of a high pressure zone.

6. List of Stations

Hyperlink					Time (UTC)					Begin / on seafloor		End / off seafloor		Water depth (m)	Comment	Recovery	Area
	Date (UTC)	St. No. M86-5	St. No. METEOR	Gear	Begin	Start Sci. Prog.	End Sci. Prog.	End	Duration hh:mm	Latitude N°	Longitude W°	Latitude N°	Longitude W°				
detail	26.02.2012	1-1	305	HA	23:58	23:58	00:20	-	00:22	35°49.77'	9°49.13'	35°47.99'	9°50.96'	4591			Target point 14
detail	27.02.2012	1-2	305	HA	-	01:00	01:32	-	00:32	35°42.80'	9°57.67'	35°40.18'	9°59.06'	4623			Target point 14-15
detail	27.02.2012	1-3	305	HA	-	01:39	02:17	02:17	00:38	35°39.90'	9°58.56'	35°42.87'	9°56.83'	4462			Target point 15-16
details	27.02.2012	2	306	CTD+CH 4	03:36	03:36	08:25	08:27	04:51	35°42.01'	9°57.94'	35°42.30'	9°57.92'	4586	CH4 sensor failure at 3700 m includes a mini-transect.		Target point 16
details	27.02.2012	3	307	TV-MUC-01	08:57	09:18	11:18	13:04	03:46	35°42.003'	9°57.925'	35°42.003'	9°57.926'	4585.5	TV camera failed at 1600 m WD	up to 29 cm	Target point 16
details	27.02.2012	4	308	MUC-02	15:42	17:03	18:25	18:30	02:43	35°33.73'	9°30.46'	35°33.714'	9°30.443'	3909	MUC without TV camera, Posidonia failed.	up to 41 cm	Porto MV
details	27.02.2012	5-1	309	HF	19:15	20:29	20:45	-	-	35°33.783'	9°30.515'	-	-	3868	3 measurements/transect /Posidonia failed		Porto MV
detail	27.02.2012	5-2	309	HF	-	21:14	21:24	-	-	35°33.845'	9°30.476'	-	-	3871			Porto MV
detail	28.02.2012	5-3	309	HF	-	00:52	01:10	03:04	08:11	35°34.065'	9°30.355'	-	-	3918.7			Porto MV
detail	28.02.2012	6	310	TP-AUV	03:45	03:45	06:57	06:57	03:12	35°33.72'	9°31.74'	35° 34,09'	9° 30,08'	3955	Drop and calibration of the transponder		Porto MV
detail	28.02.2012	7-1	311	AUV	07:55	08:22	-	-	-	35°33.32'	9°29.35'	-	-	3866	AUV#82 launched		Porto MV
detail	28.02.2012	7-2	311	AUV	-	-	15:40	17:42	09:47	-	-	35°33.28'	9°34.93'	3800	AUV#82 recovered		Porto MV
detail	28.02.2012	8	312	GC-1	17:59	19:17	19:20	21:00	03:01	35°33.71'	9°30.45'	35°33.71'	9°30.45'	3865.7		1.95 m	Porto MV
detail	28.02.2012	9	313	TP-AUV	19:45	19:45	20:22	20:22	00:37	35°33.71'	9°30.44'	35° 32,71'	9° 30,80'	3886	Recovery of the transponder		Porto MV
detail	28.02.2012	10	314	CTD+CH 4	23:00	01:18	01:42	03:10	04:10	35°33.71'	9°30.449'	35°33.79'	9°30.47'	3871	No posidonia >3200 m WD		Porto MV
detail	29.02.2012	11	315	HA	03:29	03:32	04:07	-	00:38	35°33.75'	9°31.07'	35°35.91'	9°29.46'	3913			Various Target points
detail	29.02.2012	12	316	HA	-	05:05	05:20	-	00:15	35°36.74'	9°42.41'	35°37.47'	9°44.15'	4339			Various Target points

Hyperlink					Time (UTC)					Begin / on seafloor		End / off seafloor		Water depth (m)	Comment	Recovery	Area
	Date (UTC)	St. No. M86-5	St. No. METEOR	Gear	Begin	Start Sci. Prog.	End Sci. Prog.	End	Duration hh:mm	Latitude N°	Longitude W°	Latitude N°	Longitude W°				
detail	29.02.2012	13	317	HA	-	06:06	06:30	06:30	00:24	35°38.20'	9°43.65'	35°87.87'	9°44.95'	4343			Various Target points
detail	29.02.2012	14	318	GC-2	06:49	08:13	08:14	09:36	02:47	35°37.658'	9°44.129'	35°37.652'	9°44.115'	4277	Posidonia failed at 1500 m	4.20 m	New MVs
detail	29.02.2012	15	319	HA	12:10	12:10	12:53	12:53	00:43	35°44.76'	10°18.37'	35°45.96'	10°22.28'	4514			New MVs
detail	29.02.2012	16-1	320	TP-AUV	13:22	13:22	14:30	14:30	01:08	35°45.296'	10°16.322'	35° 45,50'	10° 16,33'	4559,3	Transponder only dropped, calibration carried out AUV#83/84		Abzu MV
detail	29.02.2012	17	321	HA	14:45	14:45	15:11	15:11	00:26	35°43.65'	10°18.55'	35°45.55'	10°18.54'	4581			New MVs
detail	29.02.2012	18	322	GC-3	15:35	17:05	17:06	18:45	03:06	35°44.974'	10°19.162'	35°44,995'	10°19.143'	4546.5		4.80 m	Abzu MV
detail	29.02.2012	16-2	320	TP-AUV	19:05	19:05	20:54	20:54	01:49	35° 42,98'	10° 17,46'	35° 43,12'	10° 17,51'	4578,2	Transponder calibration for AUV#83 and AUV# 84		Abzu and Tiamat MV
detail	29.02.2012	19-1	323	AUV	21:45	21:45	-	-		35°44.89'	10°18.10'	-	-	4505	AUV#83 launched		Abzu and Tiamat MV
detail	01.03.2012	19-2	323	AUV	-	-	18:13	18:13	20:28	-	-	35°46.89'	10°21.44'	-	AUV#83 recovered		Abzu and Tiamat MV
detail	01.03.2012	20	324	HA	00:00	00:11	01:11	-	00:39	35°43.01'	10°12.31'	35°47.11'	10°11.30'	4453			New MVs
detail	01.03.2012	21	325	HA	-	01:19	02:13	-	00:54	35°47.18'	10°10.260'	35°43.35'	10°10.27'	4610			New MVs
detail	01.03.2012	22	326	HA	-	02:32	03:50	03:50	01:18	35°45.035'	10°7.85'	35°43.70'	10°15.80'	4575			New MVs
detail	01.03.2012	23	327	CTD+CH 4	04:18	04:18	08:40	08:44	04:26	35°44.35'	10°12.06'	35°44.31'	10°12.14'	4489			M Ivanov MV
detail	01.03.2012	24	328	GC-4	08:55	10:26	10:26	12:20	03:25	35°44.335'	10°12.055'	35°44.337'	10°12.057'	4488		2.38 m	M Ivanov MV
detail	01.03.2012	25	329	BC-1	12:56	14:33	14:33	16:20	03:24	35°44.338'	10°12.057'	35°44.338'	10°12.056'	4492			M Ivanov MV
detail	01.03.2012	26-1	330	HF	19:23	20:56	21:12	-	-	35°44.355'	10°12.03'	-	-	4493			Profile from M.Ivanov M.V. to the north
detail	01.03.2012	26-2	330	HF	-	21:42	21:53	-	-	35°44.44'	10°12.027'	-	-	4496			M Ivanov MV -> N
detail	01.03.2012	26-3	330	HF	-	22:20	22:38	-	-	35°44.551'	10°11.999'	-	-	4492			M Ivanov MV -> N
detail	01.03.2012	26-4	330	HF	-	23:17	23:25	-	-	35°44.743'	10°11.947'	-	-	4499.5			M Ivanov MV -> N

Hyperlink					Time (UTC)					Begin / on seafloor		End / off seafloor		Water depth (m)	Comment	Recovery	Area
	Date (UTC)	St. No. M86-5	St. No. METEOR	Gear	Begin	Start Sci. Prog.	End Sci. Prog.	End	Duration hh:mm	Latitude N°	Longitude W°	Latitude N°	Longitude W°				
detail	02.03.2012	26-5	330	HF	-	00:08	00:31	-	-	35°45.005'	10°11.871'	-	-	4517			M Ivanov MV -> N
detail	02.03.2012	26-6	330	HF	-	01:09	01:32	-	-	35°45.291'	10°11.800'	-	-	4567			M Ivanov MV -> N
detail	02.03.2012	26-7	330	HF	-	02:09	02:42	-	-	35°45.211'	10°11.723'	-	-	4581			M Ivanov MV -> N
detail	02.03.2012	26-8	330	HF	-	03:14	03:34	-	-	35°45.842'	10°11.655'	-	-	4593			M Ivanov MV -> N
detail	02.03.2012	26-9	330	HF	-	04:10	04:39	-	-	35°46.152'	10°11.578'	-	-	4622			M Ivanov MV -> N
detail	02.03.2012	26-10	330	HF	-	05:18	05:34	-	-	35°46.478'	10°11.491'	-	-	4641			M Ivanov MV -> N
detail	02.03.2012	26-11	330	HF	-	06:19	06:45	09:00	13:37	35°46.801'	10°11.406'	-	-	4644	Coax cable damaged		M Ivanov MV -> N
detail	02.03.2012	27	331	GC-5	10:40	12:07	12:10	13:53	03:13	35°45.713'	10°21.236'	35°45.727'	10°21.246'	4564		4.54 m	Tiamat MV
detail	02.03.2012	28	332	GC-6	14:28	15:57	15:59	17:34	03:06	35°45.020'	10°19.000'	35°45.038'	10°19.033'	4558		4.75 m	Abzu MV
detail	02.03.2012	29	333	AUV	17:37	17:37	-	-	-	35°44.22'	10°17.77'	-	-	4558	ship on 2000m circle, AUV#84 launched		M Ivanov MV
detail	03.03.2012	29	333	AUV	-	-	12:40	12:40	17:03	-	-	35° 45,02'	10° 18,93'	-	AUV#84 recovered		M Ivanov MV
detail	02.03.2012	30	334	CTD+CH 4	20:43	20:43	02:17	02:17	05:34	35°45.72'	10°21.28'	35°45.79'	10°21.39'	4568			Tiamat MV
detail	03.03.2012	31	335	HA	02:53	02:53	03:49	03:49	00:56	35°47.39'	10°24.53'	35°46.42'	10°31.62'	4685			HAP
detail	03.03.2012	32	336	HA	-	04:11	05:08	-	00:57	35°48.48'	10°35.58'	35°45.82'	10°42.136'	4871			HAP
detail	03.03.2012	33	337	HA	-	05:20	06:16	-	00:56	35°45.77'	10°40.88'	35°51.48'	10°42.95'	4878			HAP
detail	03.03.2012	34	338	HA	-	06:35	07:30	07:30	00:55	35°50.76'	10°39.69'	35°45.27'	10°36.77'	4866			HAP
	missing	35	-	-	-	-	-	-	-	-	-	-	-	-	-	-	-
detail	03.03.2012	36	339	BC-2	08:44	10:06	10:08	11:35	02:51	35°45.782'	10°21.330'	35°45.712'	10°21.248'	4551			Tiamat MV
detail	03.03.2012	37	340	GC-7	13:53	15:24	15:25	17:09	03:16	35°45.712'	10°21.204'	35°45.711'	10°21.249'	4547		4.75 m	Tiamat MV
detail	03.03.2012	38-1	341	HF	18:45	20:23	20:45	-	-	35°47.503'	10°37.971'	-	-	4825			HAP, Target point 2
detail	03.03.2012	38-2	341	HF	-	21:54	22:06	-	-	35°47.257'	10°37.844'	-	-	4869			HAP, Target point 2
detail	03.03.2012	38-3	341	HF	-	23:00	23:10	-	-	35°47.012'	10°37,727'	-	-	4869			HAP, Target point 2
detail	04.03.2012	38-4	341	HF	-	00:06	00:25	-	-	35°46.756'	10°37.591'	-	-	4873			HAP, Target point 2
detail	04.03.2012	38-5	341	HF	-	01:26	01:38	01:38	06:53	35°46.505'	10°37.450'	-	-	4869			HAP, Target point 2

Hyperlink					Time (UTC)					Begin / on seafloor		End / off seafloor		Water depth (m)	Comment	Recovery	Area
	Date (UTC)	St. No. M86-5	St. No. METEOR	Gear	Begin	Start Sci. Prog.	End Sci. Prog.	End	Duration hh:mm	Latitude N°	Longitude W°	Latitude N°	Longitude W°				
detail	04.03.2012	39	342	AUV	05:45	05:45	-	-	-	35°43.82'	10°14.28'	-	-	4511	AUV#85 launched		M Ivanov, Tiamat, Abzu MVs
detail	04.03.2012	39	342	AUV	-	-	22:55	22:55	17:10	-	-	35°45.28'	10°22.15'	4576	AUV#85 recovered		M Ivanov, Tiamat, Abzu MVs
detail	04.03.2012	40	343	GC-8	08:58	10:25	10:26	12:01	03:03	35°45.591'	10°11.758'	35°45,719'	10°12.099'	4584		4.10 m	Reference site, Heat flow
detail	04.03.2012	41	344	GC-9	12:29	13:59	14:00	15:41	03:12	35°44.321'	10°12.078'	35°44.34'	10°12.07'	4494		No recovery	M Ivanov MV
detail	04.03.2012	42	345	GC-10	16:10	17:33	17:34	19:00	2:50	35°44.341'	10°12.073'	35°44.403'	10°12.174'	4481		4.20 m	M Ivanov MV
detail	04.03.2012	43	346	TP-AUV	19:34	19:34	21:22	21:22	01:52	35°45.06'	10°14.70'	35°42.93'	10°17.67'	4537	Transponders recovered		M Ivanov, Tiamat, Abzu MVs
detail	05.03.2012	44	347	CTD-CH4	00:22	02:30	04:03	05:57	05:35	35°44.31'	10°12.15'	35°44.35'	10°12.14'	4502			M Ivanov MV
detail	05.03.2012	45	348	BC-3	06:25	07:54	07:56	09:30	03:05	35°44.410'	10°12.186'	35°44.410'	10°12.179'	4497			M Ivanov MV
detail	05.03.2012	46	349	BC-4	10:15	11:41	11:42	13:24	03:09	35°45.058'	10°19.042'	35°45.046'	10°19.026'	4560			Abzu MV
detail	05.03.2012	47	351	GC-11	16:34	18:07	18:08	19:54	03:20	35°47.302'	10°38.532'	35°47.308'	10°38.525'	4864		4.68 m	HAP, Target point 2
detail	05.03.2012	48-A	350	TP-AUV	15:17	15:17	16:08	16:08	00:51	35°50,84'	10°38.29'	35° 48,56'	10° 37,64'	4848	Drop transponders		HAP, Target point 1,2,9
detail	05.03.2012	48-B	350	TP-AUV	20:20	20:20	22:02	22:02	01:42	35° 50,78'	10° 38,17'	35°49.61"	10°39.04'	4846	Calibration transponders		HAP, Target point 1,2,9
detail	05.03.2012	49	(350)	AUV	22:15	-	-	23:15	00:55	35°49.61"	10°39.04'			4840	AUV#86 cancelled due to ADCP failure; AUV recovered		HAP, Target point 1,2,9
detail	06.03.2012	50	352	HA	01:20	01:20	01:52	-	00:32	35°48.019'	11°1.11'	35°50.815'	11°3.323'	4871			Western HAP
detail	06.03.2012	51	353	HA	-	03:07	04:07	-	01:00	35°48.226'	11°20.200'	35°53.578'	11°20.17'	4870			Western HAP
detail	06.03.2012	52	354	HA	-	04:23	05:34	-	01:11	35°53.72'	11°16.78'	35°48.008'	11°21.735'	4860			Western HAP
detail	06.03.2012	53	355	HA	-	05:34	06:12	-	00:38	35°48.008'	11°21.735'	35°51.38'	11°20.731'	4866			Western HAP
detail	06.03.2012	54	356	GC-12	06:30	08:03	08:04	09:46	03:16	35°49.677'	11°20.789'	35°49.68'	11°20.79'	4823		4.66 m	Western HAP
detail	06.03.2012	55-1	357	HF	10:15	11:45	12:08	-	-	35°49.684'	11°20.790'	-	-	4818			HAP, west of Target Point 1
detail	06.03.2012	55-2	357	HF	-	12:45	12:58	-	-	35°49.882'	11°20.787'	-	-	4837			Western HAP

Hyperlink					Time (UTC)					Begin / on seafloor		End / off seafloor		Water depth (m)	Comment	Recovery	Area
	Date (UTC)	St. No. M86-5	St. No. METEOR	Gear	Begin	Start Sci. Prog.	End Sci. Prog.	End	Duration hh:mm	Latitude N°	Longitude W°	Latitude N°	Longitude W°				
detail	06.03.2012	55-3	357	HF	-	13:36	13:49	-	-	35°50.084'	11°20.78'	-	-	4844			Western HAP
detail	06.03.2012	55-4	357	HF	-	13:29	14:48	-	-	35°50.284'	11°20.785'	-	-	4847			Western HAP
detail	06.03.2012	55-5	357	HF	-	15:28	15:41	-	-	35°50.484'	11°20.777'	-	-	4848			Western HAP
detail	06.03.2012	55-6	357	HF	-	16:52	17:01	-	-	35°50.884'	11°20.778'	-	-	4848			Western HAP
detail	06.03.2012	55-7	357	HF	-	18:22	18:42	-	-	35°51.331'	11°20.790'	-	-	4848			Western HAP
detail	06.03.2012	55-8	357	HF	-	19:52	20:02	21:53	11:38	35°51.725'	11°20.780'	-	-	4849			Western HAP
detail	07.03.2012	56	358	HA	00:29	00:29	01:05	-	00:36	35°59.305'	10°52.60'	36°01.514'	10°49.778'	4870			Western HAP
detail	07.03.2012	57	359	HA	-	01:22	01:57	-	00:35	36°14.28'	10°52.572'	35°58.597'	10°50.798'	4865			Western HAP
detail	07.03.2012	58	360	HA	-	03:40	03:56	-	00:16	35°53.87'	10°28.448'	35°52.725'	10°27.413'	4827			Western HAP
detail	07.03.2012	59	361	HA	-	04:19	04:49	-	00:30	35°54.455'	10°24.785'	35°52.224'	10°22.52'	4820			Western HAP
detail	07.03.2012	60	362	HA	-	05:28	06:02	-	00:30	35°56.009'	10°20.366'	35°53.311'	10°17.702'	4848			Western HAP
detail	07.03.2012	61	363	HA	-	06:16	06:57	06:57	00:41	35°54.280'	10°16.328'	35°54.280'	10°19.199'	4717			Western HAP
detail	07.03.2012	62	364	GC-13	08:40	10:12	10:13	12:33	03:53	35°47.471'	10°38.436'	35°47.317'	10°38.453'	4843	2.11 m		HAP, Target point 2
detail	07.03.2012	63	365	GC-14	13:15	15:00	15:01	17:00	03:45	35°47.315'	10°38.450'	35°47.257'	10°38.506'	4865	4.28 m		HAP, Target point 2
detail	07.03.2012	64	366	BC-5	17:32	19:05	19:07	20:38	03:06	35°47.257'	10°38.507'	35°47.265'	10°38.499'	4864			HAP, Target point 2
detail	07.03.2012	65	367	HA	21:06	21:06	22:42	22:42	01:36	35°47.265'	10°38.499'	35°40.475'	10°40.255'	4863			Survey, reference station
detail	08.03.2012	66	368	CTD-CH4	00:43	02:38	04:04	06:10	05:27	35°45.05'	10°19.04'	35°45.05'	10°19.04'	4555			Abzu MV
detail	08.03.2012	67	369	BC-6	06:23	07:54	07:56	09:24	03:01	35°45.048'	10°19.032'	35°45.045'	10°19.018'	4550			Abzu MV
detail	08.03.2012	68	370	GC-15	09:56	11:20	11:21	12:59	03:03	35°45.045'	10°19.017'	35°45.04'	10°19.02'	4549	486 cm		Abzu MV
detail	08.03.2012	69	371	GC-16	14:56	16:25	16:27	18:08	03:12	35°42.923'	10°40.940'	35°42.925'	10°40.963'	4864	399 cm		Referece station
detail	08.03.2012	70-1	372	AUV	18:59	18:59	-	-	-	35°49.00'	10°38.33'	35°49.67'	10°38.25'	4835	AUV#86 launched		HAP, Target point 1,2,9
detail	09.03.2012	70-2	372	AUV	-	-	10:48	10:48	15:49	-	-	35° 49,67'	10° 38,25'	-	AUV#86 recovered		HAP, Target point 1,2,10
detail	08.03.2012	71-1	373	HF	21:15	23:10	23:20	-	2:45	35°42.931'	10°40.962'	-	-	4866			Referece station
detail	08.03.2012	71-2	373	HF	-	23:33	23:45	01:28	01:28	35°42.932'	10°40.964'	-	-	4866			Referece station

Hyperlink					Time (UTC)					Begin / on seafloor		End / off seafloor		Water depth (m)	Comment	Recovery	Area
	Date (UTC)	St. No. M86-5	St. No. METEOR	Gear	Begin	Start Sci. Prog.	End Sci. Prog.	End	Duration hh:mm	Latitude N°	Longitude W°	Latitude N°	Longitude W°				
detail	09.03.2012	72	374	CTD-CH4	03:18	05:04	06:51	08:50	05:32	35°45.71'	10°21.25'	35°45.81'	10°21.32'	4562			Tiamat MV
detail	09.03.2012	73	375	GC-17	11:54	13:31	13:34	15:27	03:33	35°46.889'	10°34.040'	35°46.768'	10°34.545'	4853		107 cm	V structure
detail	09.03.2012	48-C	376	TP-AUV	16:00	16:00	18:59	18:59	02:59	35°49.45'	10°38.85'	35°50.81'	10°38.76'	4839	Transponder recovered		HAP, Target point 1,2,9
detail	09.03.2012	74	377	TP-AUV	20:55	20:55	21:42	21:42	00:47	35° 39,35'	10° 27,00'	35° 37,36'	10° 26,96'	4684,6	Transponder launched		NW flank, CPR
detail	09.03.2012	75-1	378	HA	22:06	22:06	22:38	-	00:32	35°39.943'	10°25.106'	35°37.046'	10°24.900'	4669			NW flank, CPR
detail	09.03.2012	75-2	378	HA	-	23:03	23:27	23:27	00:24	35°38.286'	10°26.402'	35°38.619'	10°23.634'	4669			NW flank, CPR
detail	10.03.2012	76-1	379	AUV	02:15	02:15	-	-	-	35° 38,10'	10° 27,41'	-	-	4655	AUV#87 launched		NW flank, CPR
detail	10.03.2012	76-2	379	AUV	-	-	18:56	18:56	21:11	-	-	35° 38,27'	10° 21,04'	-	AUV#87 recovered		NW flank, CPR
detail	10.03.2012	75-3	380	HA	04:46	04:46	05:17	-	00:31	35°39.624'	10°20.502'	35°37.125'	10°18.614'	4600			NW flank, CPR
detail	10.03.2012	75-4	380	HA	-	05:35	05:59	05:59	00:24	35°37.742'	10°20.696'	35°39.115'	10°17.95'	4371			NW flank, CPR
detail	10.03.2012	77	381	GC-18	06:58	08:24	08:26	09:53	02:55	35°38.349'	10°19.551'			4553,4		72 m	NW flank, CPR
detail	10.03.2012	78	382	GC-19	10:58	12:23	12:26	14:17	03:19	35°38.426'	10°24.956'	35°38.430'	10°24.915'	4642		4.62 m	NW flank, CPR
detail	10.03.2012	79-1	383	HA	15:14	15:14	15:32	15:32	00:18	35°40.744'	10°31.383'	35°39.222'	10°32.735'	4812			NW flank, CPR
detail	10.03.2012	80	384	TP-AUV	16:00	16:00	18:15	18:15	02:15	35°39.03'	10°27.47'	35°37.32'	10°27.19'	4679	Transponder recovered		NW flank, CPR
detail	10.03.2012	79-2	385	HA	16:09	16:09	16:19	16:19	00:10	35°38.850'	10°25.960'	35°38.39'	10°25.03'	4687			NW flank, CPR
detail	10.03.2012	81-1	386-1	HF	22:10	23:45	23:57	-	-	35°47.307'	10°38.506'	-	-	4862			HAP, Target point 2
detail	11.03.2012	81-2	386-2	HF	-	00:52	01:04	-	-	35°47.517'	10°38.253'	-	-	4837			HAP, Target point 2
detail	11.03.2012	81-3	386-3	HF	-	02:01	02:13	-	-	35°47.730'	10°37.992'	-	-	4850			HAP, Target point 2
detail	11.03.2012	81-4	386-4	HF	-	03:03	03:15	05:02	-	35°47.941'	10°37.732'	-	-	4848			HAP, Target point 2
detail	11.03.2012	82	387	TP-AUV	07:12	07:12	14:14	14:14	07:02	35°45.04'	10°15.69'	35°44.66'	10°18.43'	4525	Drop transponder, transponder calibration		M Ivanov MV
detail	11.03.2012	83	388	BC-7	08:44	10:10	10:12	11:49	03:05	35°44.336'	10°12.075'	35°44.327'	10°11.965'	4485			M Ivanov MV
detail	11.03.2012	84	389	AUV	14:28	-	-	16:00	1:32	35°43.33'	10°17.62'	35°44.04'	10°14.34'	4572	Launch and		M Ivanov MV

Hyperlink					Time (UTC)					Begin / on seafloor		End / off seafloor		Water depth (m)	Comment	Recovery	Area
	Date (UTC)	St. No. M86-5	St. No. METEOR	Gear	Begin	Start Sci. Prog.	End Sci. Prog.	End	Duration hh:mm	Latitude N°	Longitude W°	Latitude N°	Longitude W°				
															recovery AUV#88; cancelled due to leak		
detail	11.03.2012	85	390	HA	23:52	23:52	01:13	-	1:21	35°54.49'	11°12.17'	36°08.125'	11°16.891'	4865			Western HAP
detail	12.03.2012	86	391	HA	-	01:52	03:02	-	02:10	36°03.387'	11°24.087'	35°51.098'	11°20.135'	4591			Western HAP
detail	12.03.2012	87	392	HA	-	03:38	04:55	-	01:17	35°47.557'	11°27.557'	36°0.674'	11°34.300'	4864			Western HAP
detail	12.03.2012	88	393	HA	-	05:31	05:53	-	00:22	35°56.699'	11°39.426'	35°55.29'	11°37.811'	4787			Western HAP
detail	12.03.2012	89	394	HA	-	06:05	06:14	-	00:09	35°55.822'	11°38.972'	35°56.44'	11°38.58'	4838			Western HAP
detail	12.03.2012	90	395	HA	-	06:22	06:31	-	00:09	35°56.719'	11°38.872'	35°56.067'	11°39.368'	4785			Western HAP
detail	12.03.2012	91	396	HA	-	08:19	08:06	08:06	00:47	35°49.28'	11°29.68'	35°50.5932'	11°28.6596'	4858			Western HAP
detail	12.03.2012	92	397	GC-20	09:26	10:54	10:56	12:38	03:12	35°50.083'	11°28.837'	35°50.073'	11°28.736'	4848		3.84 m	Western HAP
detail	12.03.2012	93	398	GC-21	13:48	15:24	15:27	17:17	03:29	35°49.850'	11°20.197'	35°49.790'	11°20.172'	4824		4.44 m	Western HAP
detail	12.03.2012	94-1	399	HF	17:55	19:28	19:39	-	-	35°48.665'	11°20.851'	-	-	4864			Western HAP
detail	12.03.2012	94-2	399	HF	-	20:36	20:48	-	-	35°48.980'	11°20.824'	-	-	4855			Western HAP
detail	12.03.2012	94-3	399	HF	-	21:48	21:54	-	-	35°49.276'	11°20.798'	-	-	4842			Western HAP
detail	13.03.2012	94-4	400	HF	-	01:54	02:05	-	-	35°49.685'	11°20.762'	-	-	4822			Western HAP
detail	13.03.2012	94-5	400	HF	-	02:59	03:11	-	-	35°49.979'	11°20.743'	-	-	4842			Western HAP
detail	13.03.2012	94-6	400	HF	-	04:04	04:15	-	10:20	35°50.274'	11°20.717'	-	-	4845			Western HAP
detail	13.03.2012	95	401	GC-22	06:44	08:15	08:17	09:54	03:10	35°50.273'	11°20.717'	35°50.274'	11°20.734'	4847		3.04 m	Western HAP
detail	13.03.2012	96	402	GC-23	10:21	11:48	11:50	13:42	03:21	35°48.659'	11°20.839'	35°48.675'	11°20.850'	4859		4.62 m	Western HAP
detail	13.03.2012	97	403	GC-24	16:55	18:27	18:28	20:08	03:13	35°47.876'	10°40.762'	35°47.873'	10°40.765'	4814		4.82 m	HAP, close target point 9
detail	13.03.2012	98	404	CTD-CH4	22:27	00:19	01:50	04:40	06:13	35°44.33'	10°12.08'	35°44.50'	10°12.07'	4485			M Ivanov MV
detail	14.03.2012	99-1	405	HA	05:18	05:18	06:03	-	00:45	35°44.852'	10°4.491'	35°40.156'	10°1.667'	4593			New MVs
detail	14.03.2012	99-2	405	HA	-	06:03	06:27	-	00:24	35°40.156'	10°1.667'	35°40.893'	10°6.187'	4404			New MVs
detail	14.03.2012	99-3	405	HA	-	06:27	06:47	06:47	00:20	35°40.893'	10°6.187'	35°43.801'	10°7.303'	4425			New MVs

Hyperlink					Time (UTC)					Begin / on seafloor		End / off seafloor		Water depth (m)	Comment	Recovery	Area
	Date (UTC)	St. No. M86-5	St. No. METEOR	Gear	Begin	Start Sci. Prog.	End Sci. Prog.	End	Duration hh:mm	Latitude N°	Longitude W°	Latitude N°	Longitude W°				
detail	14.03.2012	100	406	GC-25	07:13	08:36	08:38	10:19	03:06	35°44.340'	10°12.059'	35°44.341'	10°12.056'	4497		0.94 m	M Ivanov MV
detail	14.03.2012	101	407	BC-8	10:45	12:09	12:11	13:48	03:03	35°44.341'	10°12.057'	35°44.342'	10°12.056'	4507			M Ivanov MV
detail	14.03.2012	102-1	408	AUV	14:49	14:49	-	16:26	-	35° 44,74'	10° 15,95'	-	-	4515,1	AUV#89 launched		M Ivanov MV
detail	15.03.2012	102-2	408	AUV	-	-	09:36	09:36	18:47	-	-	35° 44,54'	10° 12,04'	-	AUV#89 recovered		M Ivanov MV
detail	14.03.2012	103	409	HF	19:10	20:41	20:53	-	-	35°47.192'	10°50.909'	-	-	4865			HAP
detail	15.03.2012	104	410	HF	-	00:36	00:48	00:48	04:29	35°48.476'	10°51.332'	-	-	4863			HAP
detail	15.03.2012	105	411	TP-AUV	05:27	05:27	07:57	07:57	02:00	35° 45,41'	10° 16,41'	35° 42,99'	10° 17,76'	4522,7	Transponder recovered		M Ivanov MV

Abbreviations:

AUV: Autonomous underwater vehicle; TP: Transponders; TV–MUC: TV–Multicorer; GC: Gravity Corer; BC: Box Corer; HF: Heat Flow; CTD: Conductivity Temperature Density
 PS: Parasound; EM122: Multibeam; HA: HydroAcustics; EM122 + PS: Posidonia; Contros Sensors: CO2 = CO₂; CH4 = Methane;
 HAP: Horseshoe Abyssal Plain, CPR: Coral Patch Ridge

7. Acknowledgments

We thank Captain Stefan Schwarze and the entire crew of RV METEOR for their excellent support during the cruise. Cruise M86/5 was funded by the “Deutsche Forschungsgemeinschaft” (DFG) through the grant “TRANSFLUX”. Pedro Terrinha, Marianne Nuzzo and Vasco Valadares acknowledge the support of the Fundação para a Ciência e a Tecnologia through the SWIMGLO and TOPOMED projects (TOPOMED – “Plate re-organization in the western Mediterranean: lithospheric causes and topographic consequences”, TOPOEUROPE/0001/2007; SWIMGLO- The Gloria-SWIM plate boundary Faults connection and its importance on the propagation of tectonic deformation and deep water ecosystems along the Azores-Gibraltar Plate Boundary PTDC/MAR/100522/2008).

8. Data and sample storage and availability

The data were collected within the project TRANSFLUX, which is related on long-term activities and collaborations to Portuguese and Spanish partners in the working area. In Kiel a joint data management team of GEOMAR and Kiel University organises and supervises data storage and publication by marine science projects in a webbased multi-user system. In a first phase data are only available to the project user groups. After a three year proprietary time the data management team will publish these data by dissemination to national and international data archives, i.e. the data will be submitted to PANGAEA no later than March, 2016. Digital object identifiers (DOIs) are automatically assigned to data sets archived in the PANGAEA Open Access library making them publically retrievable, citeable and reusable for the future. All metadata are available publically via the following link pointing at the GEOMAR portal (<https://portal.geomar.de/metadata/leg/show/314694>). Core descriptions and geochemical data of sediments and pore waters are already available at the data portal.

In addition the portal provides a single downloadable KML formatted file (<https://portal.geomar.de/metadata/leg/kmlexport/314694>) which retrieves and combines up-to-date cruise (M86/5) related information, links to restricted data and to published data for visualisation e.g. in GoogleEarth.

9. References

- Błażewicz-Paszkowycz M, Bamber RN, Cunha MR (2011) New tanaidomorph Tanaidacea (Crustacea: Peracarida) from submarine mud-volcanoes in the Gulf of Cadiz (North-east Atlantic). *Zootaxa* 2769, 1-53.
- Bullard, E.C., 1939, Heat flow in South Africa, Proc. R. Soc. London Series A, 173, 474-503.
- Criado-Aldenueva, F., J. Garcia-Lafuente, J. M. Vargas, J. Del Rio, A. Vazquez, A. Reul, and A. Sanchez. 2006. Distribution and circulation of water masses in the Gulf of Cadiz from in situ observations. *Deep Sea Res. II* 53: 1144-1160, doi:10.1016/j.dsr2.2006.04.012.
- Dan obeitia, J., Masson, D.G., Mulder, T., Ramella, R., Somoza, L., Diez, S., 2009. The Quest for the Africa–Eurasia plate boundary west of the Strait of Gibraltar. *Earth and Planetary Science Letters* 280, 13–50.
- Del Grosso, V. A. 1974. New equation for speed of sound in natural waters (with comparisons to other equations). *J. Acoustical Society of America* 56 (4): 1084–1091. doi:10.1121/1.1903388.
- Duarte, J.C., Terrinha, P., Rosas, F.M., Valadares, V., Pinheiro, L.M., Matias, L., Magalhães, V., Roque, C., 2010. Crescent-shaped morphotectonic features in the Gulf of Cadiz (offshore SW Iberia). *Marine Geology* 27, 236-249.
- Dworschak P, Cunha MR (2007) A new subfamily, Vulcanocalliacinae n. subfam., for *Vulcanocalliax arutyunovi* n.gen., n.sp. from a mud volcano in the Gulf of Cadiz (Crustacea, Decapoda, Callianassidae). *Zootaxa* 1460, 35-46.





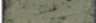



- Elvert, M., Boetius, A., Knittel, K., and Jørgensen, B. B., 2003. Characterization of specific membrane fatty acids as chemotaxonomic markers for sulphate reducing bacteria involved in anaerobic oxidation of methane. *Geomicrobiology Journal* 20, 403-419.
- Fonseca, Luciano; Calder, Brian (2005) *Geocoder: An Efficient Backscatter Map Constructor*. Center for Coastal and Ocean Mapping, University of New Hampshire, 2005.
- Génio L, Johnson SB, Vrijenhoek RC, Cunha MR, Tyler PA, Kiel S, Little CTS (2008) New record of "*Bathymodiolus*" *mauritanicus* Cosel from Gulf of Cadiz (NE Atlantic) mud volcanoes. *Journal of Shellfish Research* 27 (1), 53-61.
- Gràcia, E, A Vizcaino, C Escutia, A Asioli, A Rode, R Pallàs, J Garcia-Orellana e, S Lebreiro, C Goldfinger. Holocene earthquake record offshore Portugal (SW Iberia): testing turbidite paleoseismology in a slow-convergence margin. *Quaternary Science Reviews* 29 (2010) 1156–1172
- Gracia, E., Danobeitia, J.J., Verges, J., PARSIFAL Team, 2003a. Mapping active faults offshore Portugal (36_N–38_N): implications for seismic hazard assessment along the southwest Iberian margin. *Geology* 31 (1), 83–86.
- Grasshoff K., Erhardt M. and Kremling K. (2002) *Methods of Seawater Analysis*. Wiley VCH, Weinheim.
- Gutscher, M-A., Malod, J., Rechault, J-P., Contrucci, I., Klingelhoefer, F., Mendes-Victor, L., Spakman, W., 2002. Evidence for active subduction beneath Gibraltar. *Geology* 30, 1071-1074.
- Hensen C., Nuzzo M., Hornibrook E., Pinheiro L. M., Bock B., Magalhaes V. H. and Brückmann W. (2007) Sources of mud volcano fluids in the Gulf of Cadiz - indications for hydrothermal imprint. *Geochimica et Cosmochimica Acta* 71, 1232–1248.
- Hernández-Molina, F.J., Llave, E., Somoza, L., Fernández-Puga, M.C., Maestro, A., León, R., Medialdea, T., Barnolas, A., García, M., Díaz del Río, V., Fernández-Salas, L.M., Vázquez, J.T., Lobo, F., Alveirinho Dias, J.M., Rodero, J., Gardner, J., 2003. Looking for clues to paleoceanographic imprints: a diagnosis of the Gulf of Cadiz contourite depositional system. *Geology* 31, 19-22.
- Hilário A, Cunha MR (2008) On some frenulate species (Annelida: Polychaeta: Siboglinidae) from mud volcanoes in the Gulf of Cadiz (Northeast Atlantic). *Scientia Marina* 72, 361-371.
- Hilário A, Johnson SB, Vrijenhoek RC, Cunha MR (2010) High diversity of frenulates (Polychaeta: Siboglinidae) in the Gulf of Cadiz mud volcanoes: a DNA taxonomy analysis. *Deep Sea Research I* 57, 143-150.
- Iribarren, L., Vergés, J., Camurri, F., Fulla, J., Fernández, M., 2007. The structure of the Atlantic–Mediterranean transition zone from the Alboran Sea to the Horseshoe Abyssal Plain (Iberia–Africa plate boundary). *Marine Geology* 243, 97–119.
- Kastner, M., Elderfield, H. and Martin J. B. (1991) Fluids in convergent margins - What do we know about their composition, origin, role in diagenesis and importance for oceanic chemical fluxes, *Philosophical Transactions of the Royal Society of London A*, 335(1638), 243-259.
- Keir, R. S., O. Schmale, M. Walter, J. Silltenfuss, R. Seifert, and M. Rhein. 2008. Flux and dispersion of gases from the "Drachenschlund" hydrothermal vent at 8 degrees 18'S, 13 degrees 30'W on the Mid-Atlantic Ridge. *Earth Planet. Sc. Lett.* 270: 338-348, doi:10.1016/j.epsl.2008.03.054.
- Lurton, X (2002). *An introduction to underwater acoustics: principles and applications*. Springer Berlin-Heidelberg, 2002.
- McAulliffe, C. 1971. GC determination of solutes by multiple phase equilibration. *Chemical Technology*, 1, 46–51.
- Nuzzo M., Hornibrook E. R. C., Gill F., Hensen C., Pancost R., Haeckel M., Reitz A., Scholz F., Magalhães V. H., Brückmann W., and Pinheiro L. M. 2009. Origin of light volatile hydrocarbon gases in mud volcano fluids, Gulf of Cadiz - Evidence for multiple sources and transport mechanisms in active sedimentary wedges. *Chemical Geology* 266, 359-372.
- Nuzzo M., Hornibrook E. R. C., Hensen C., Parkes R. J., Cragg B. A., Rinna J., von Deimling J. S., Sommer S., Magalhães V. H., Reitz A., Brückmann W., and Pinheiro L. M. (2008) Shallow microbial recycling of deep-sourced carbon in Gulf of Cadiz mud volcanoes. *Geomicrobiology Journal* 25, 283-295.
- Oliver PG, Rodrigues CF, Cunha MR (2011) Chemosymbiotic bivalves from the mud volcanoes of the Gulf of Cadiz, with descriptions of new species of Solemyidae, Lucinidae and Vesicomidae. *Zookeys* 113, 1-38.
- Roque, C., Duarte, H., Terrinha, P., Valadares, V., Noiva, J., Cachão, M., Ferreira, J., Legoinha, P., Zitellini, N., Pliocene and Quaternary depositional model of the Algarve margin contourite drifts (Gulf of Cadiz, SW Iberia): Seismic architecture, tectonic control and paleoceanographic insights, *Marine Geology* (2011), doi: 10.1016/j.margeo.2011.11.001.
- Scholz F., Hensen C., Lu Z., and Fehn U. (2010) Controls on the 129I/I ratio of deep-seated marine interstitial fluids: 'Old' organic versus fissiogenic 129-iodine. *Earth and Planetary Science Letters* 294(1-2), 27-36.
- Scholz F., Hensen C., Reitz A., Romer R. L., Liebetau V., Meixner A., Weise S. M., and Haeckel M. (2009) Isotopic evidence ($^{87}\text{Sr}/^{86}\text{Sr}$, $\delta^7\text{Li}$) for alteration of the oceanic crust at deep-rooted mud volcanoes in the Gulf of Cadiz, NE Atlantic Ocean. *Geochimica et Cosmochimica Acta* 73(18), 5444-5459.

- Scholz F., Hensen C., Reitz A., Romer R. L., Liebetau V., Meixner A., Weise S. M., and Haeckel M. (2009) Isotopic evidence ($^{87}\text{Sr}/^{86}\text{Sr}$, $\delta^7\text{Li}$) for alteration of the oceanic crust at deep-rooted mud volcanoes in the Gulf of Cadiz, NE Atlantic Ocean. *Geochimica et Cosmochimica Acta* 73(18), 5444-5459.
- Seewald J. S. (2001) Aqueous geochemistry of low molecular weight hydrocarbons at elevated temperatures and pressures: constraints from mineral buffered laboratory experiments. *Geochimica et Cosmochimica Acta* 65(10), 1641-1664.
- Terrinha, P., Matias, L., Vicente, J., Duarte, J., Luis, J., Pinheiro, L., Lourenço, N., Diez, S., Rosas, F., Magalhaes, V., Valadares, V., Zitellini, N., Roque, C., Mendes Victor, L., MATESPRO Team, 2009. Morphotectonics and strain partitioning at the Iberia–Africa plate boundary from multibeam and seismic reflection data. *Marine Geology* 267, 156–174.
- Terrinha, P., Matias, L., Vicente, J., Duarte, J., Luís, J., Pinheiro, L., Lourenço, N., Diez, S., Rosas, F., Magalhães, V., Valadares, V., Zitellini, N., Roque, C., Mendes Víctor, L., MATESPRO Team, 2009. Morphotectonics and strain partitioning at the Iberia–Africa plate boundary from multibeam and seismic reflection data. *Marine Geology* 267, 156-174.
- Villinger, H., Davis, E. E., 1987, A new reduction algorithm for marine heat flow measurements, *Journal of Geophysical Research*, 92 (B12), 846-856.
- Wallmann K., Drews M., Aloisi G., and Bohrmann G. (2006) Methane discharge into the Black Sea and the global ocean via fluid flow through submarine mud volcanoes. *Earth and Planetary Science Letters* 248(1-2), 545-560.
- Zitellini, N., Gràcia, E., Matias, L., Terrinha, P., Abreu, M.A., DeAlteriis, G., Henriot, J.P., Dañobeitia, J.J., Masson, D.G., Mulder, T., Ramella, R., Somoza, L., Diez, S., 2009. The quest for the Africa-Eurasia plate boundary west of the Strait of Gibraltar. *Earth and Planetary Science Letters* 280, 13-50.

Appendix:

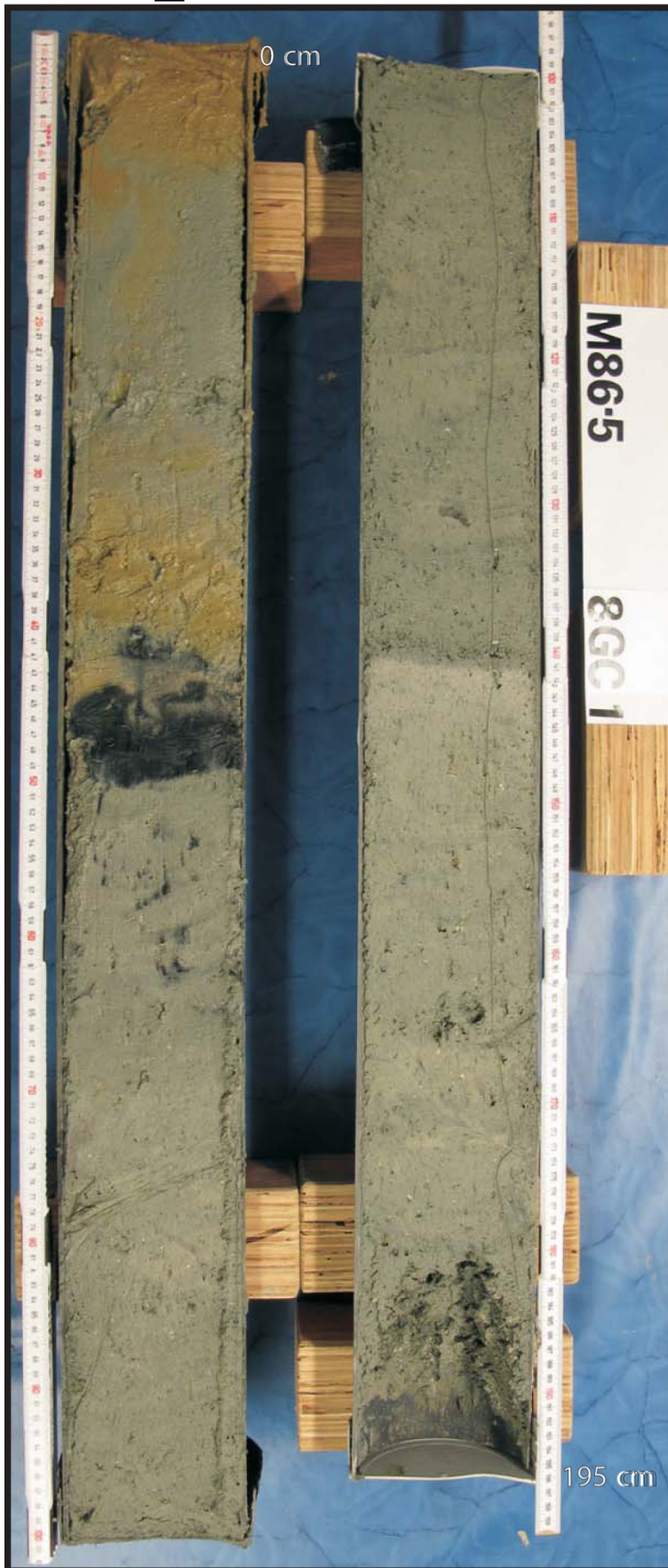
Core descriptions and core photos:

R/V METEOR M86/5	Station: M86/5 - 08 GC01
Location: Gulf of Cadiz, Porto mud volcano	M86/5_312
Latitude: 35°33.706' N	Date: 28.02.2012, 19:16 (UTC)
Longitude: 09°30.444' W	Recovery: 195 cm
Water depth: 3865 m	

Depth (cmbsf)	LITHOLOGY					Thermal conductivity					
	Photo	Color	Section	Grain size						Description	
				Log	Cl		Slt	FS	MS		CS
0		2.5Y 6/6	1							0-7 cm: water saturated, oxidized, olive yellow clay.	not measured
		2.5Y 6/0								7-33 cm: homogeneous mud breccia, gray color, with clasts of claystone up to 6-7 mm in diameter;	
		2.5Y 6/6								23-24 cm: a level of water-saturated mud breccia.	
50		2.5Y 2/0								33-40 cm: oxidized, olive yellow mud breccia, with a gradual top contact.	
		5G 4/1							40-49 cm: mud breccia with high organic content, of black color and with a sharp contact at the bottom.		
100			2							49-142 cm: dark greenish gray mud breccia with claystone clasts of up to 7 mm in diameter, fragments of frenalata tubes; 49-59, occurrence of black patches of 0.5 up to 1 cm in diameter.	
150		5B 7/1									
195		5BG 5/1								142-195 cm: mud breccia with a sharp contact at the top, the color gradually changes from light blue gray at top to greenish gray at 150 cm; claystone clasts of up to 1 cm in diameter.	

M86/5-08 GC-01

M86/5_312

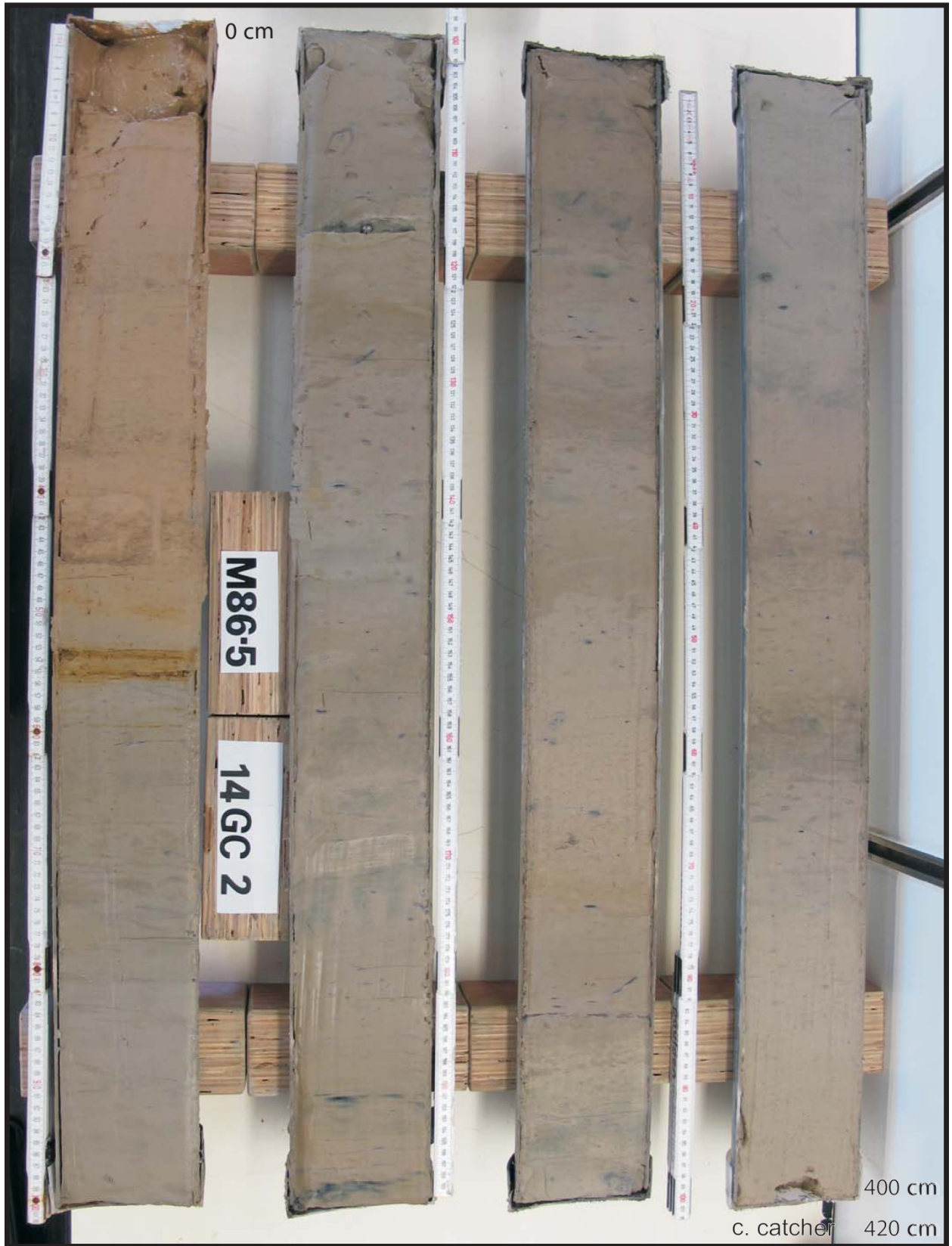


R/V METEOR M86/5 Location: Gulf of Cadiz, topographic high on SWIM lineament Latitude: 35°37.653' N Longitude: 09°44.114' W Water depth: 4271 m	Station: M86/5 - 14 GC02 M86/5_318 Date: 29.02.2012, 08:13 (UTC) Recovery: 420 cm
--	--

Depth (cmbssf)	LITHOLOGY						Thermal conductivity
	Photo	Color	Section	Log	Grain size	Description	
					Cl		
0		2.5Y 6/8	1		☉	0-8 cm: water saturated, homogeneous olive yellow silty clay, with forams.	not measured
		2.5Y 5/4				8-53 cm: silty clay with forams, gradual color change from light olive brown at top to olive brown at 53 cm.	
50		2.5Y 4/2				46 cm: 0.5 cm dark grayish brown layer, diffuse contact at the top, sharp contact at the base.	
		2.5Y 4/4 2.5Y 6/8 2.5Y 5/2			(=)	53-55 cm: olive yellow clay with forams; sub-millimeter lamination at the bottom.	
100		5Y 4/1	2		SS	55-114 cm: homogeneous clay with forams of grayish brown color: 59 cm: lamination, patches of intense bioturbation; black patches of organic-rich material, up to 1 cm in diameter.	
150						117 cm: base of the turbidite, fine sand with a sandstone clast of 7 mm in diameter; sharp erosive contact at the bottom; dark gray color.	
200		2.5Y 6/2				117-400 cm: grayish brown clay with patches of organic-rich sediment forming layering; 160-180 cm: black vertical dendritic pathways (probably fluid migration);	
					SS	284 cm: 5 mm thick layer of bioturbated clay; intense bioturbation at several intervals: 225-250, 270-285, 340-347, and 355-368.	
250		2.5Y 4/2	3		SSS		
					SS		
300		2.5Y 4/2			SSS		
					SS		
350		2.5Y 4/2	4		SSS		
		2.5Y 4/2			SSS		
400					SS		
420	corer catcher						

M86/5-14 GC-02

M86/5_318



R/V METEOR M86/5 Location: Gulf of Cadiz, reference station close to the Abzu mud volcano Latitude: 35°44.334' N Longitude: 10°19.145' W Water depth: 4557 m	Station: M86/5 - 18 GC03 M86/5_322 Date: 29.02.2012, 17:05 (UTC) Recovery: 480 cm
---	--

Depth (cmbsf)	LITHOLOGY						Thermal conductivity
	Photo	Color	Section	Log	Grain size	Description	
					Cl Slt FS MS CS Gr		
0						0-63 cm: homogeneous light yellowish brown clay with forams; 48-59 cm: intense bioturbation.	not measured
50		2.5Y 6/4	1		⊗ SSS		
		2.5Y 5/6 5Y 5/2			≡	63-67 cm: laminated light olive brown clay (oxidation front?).	
100		5Y 6/4	2		△ ⊗ SS	67-105 cm: olive gray clay, highly bioturbated, grain size increases to coarse sand (grains up to 1 mm in diameter) at the base of a turbidite that has an erosive and very irregular contact.	
150						105-420 cm: clay with forams, highly bioturbated, with darker patches of organic-rich material, especially from 170 to 208 cm; the forams content increases to the bottom; intense bioturbation at: 208-220, 295-328, 345-364 and 402-429 cm.	
200			3		SSS		
250							
300			4		SSS		
350							
400			5		SSS		
450		2.5Y 5/2			⊗		
480							

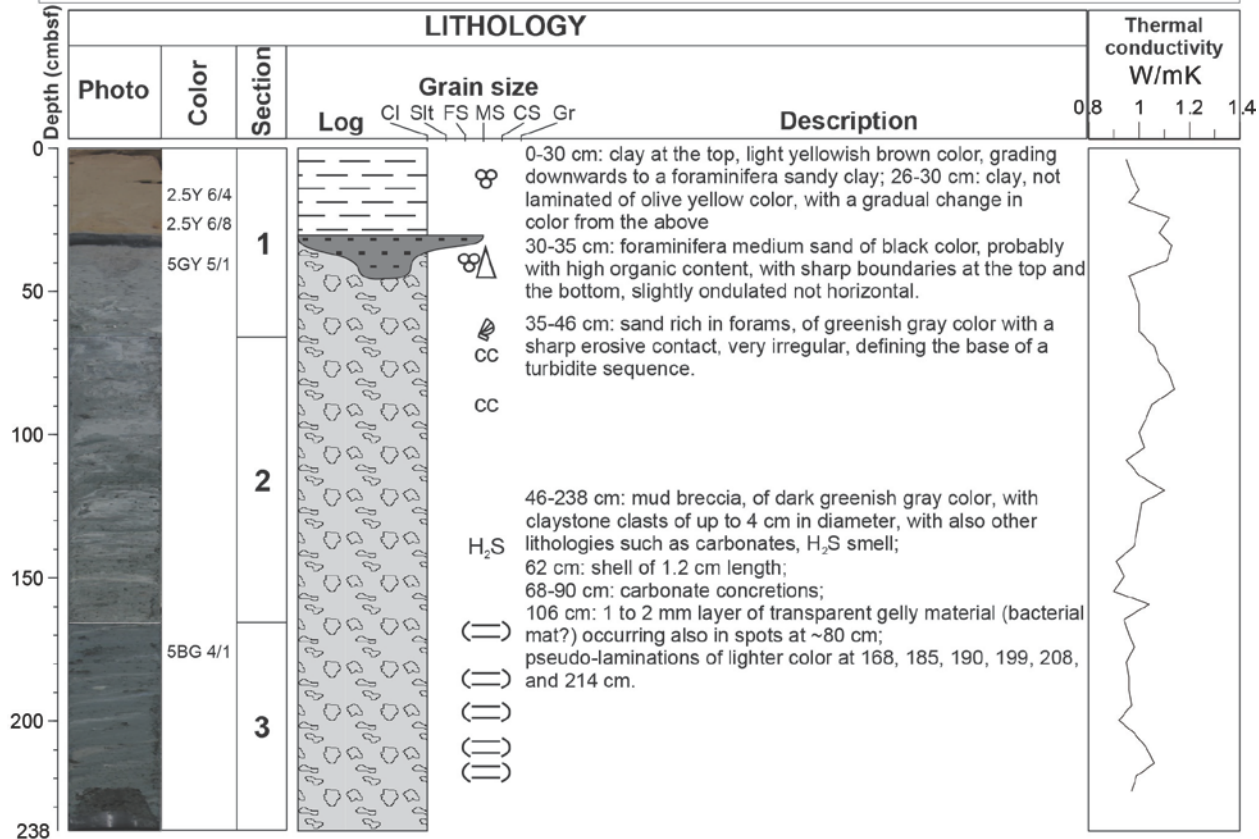
M86/5-18 GC-03

M86/5_322



480 cm

R/V METEOR M86/5 Location: Gulf of Cadiz, Michael Ivanov MV Latitude: 35°44.335' N Longitude: 10°12.067' W Water depth: 4490 m	Station: M86/5 - 24 GC04 M86/5_328 Date: 01.03.2012, 10:26 (UTC) Recovery: 238 cm
---	--



M86/5-24 GC-04

M86/5_328



R/V METEOR M86/5

Station: M86/5 - 27 GC05

Location: Gulf of Cadiz, Tiamat MV

M86/5_331

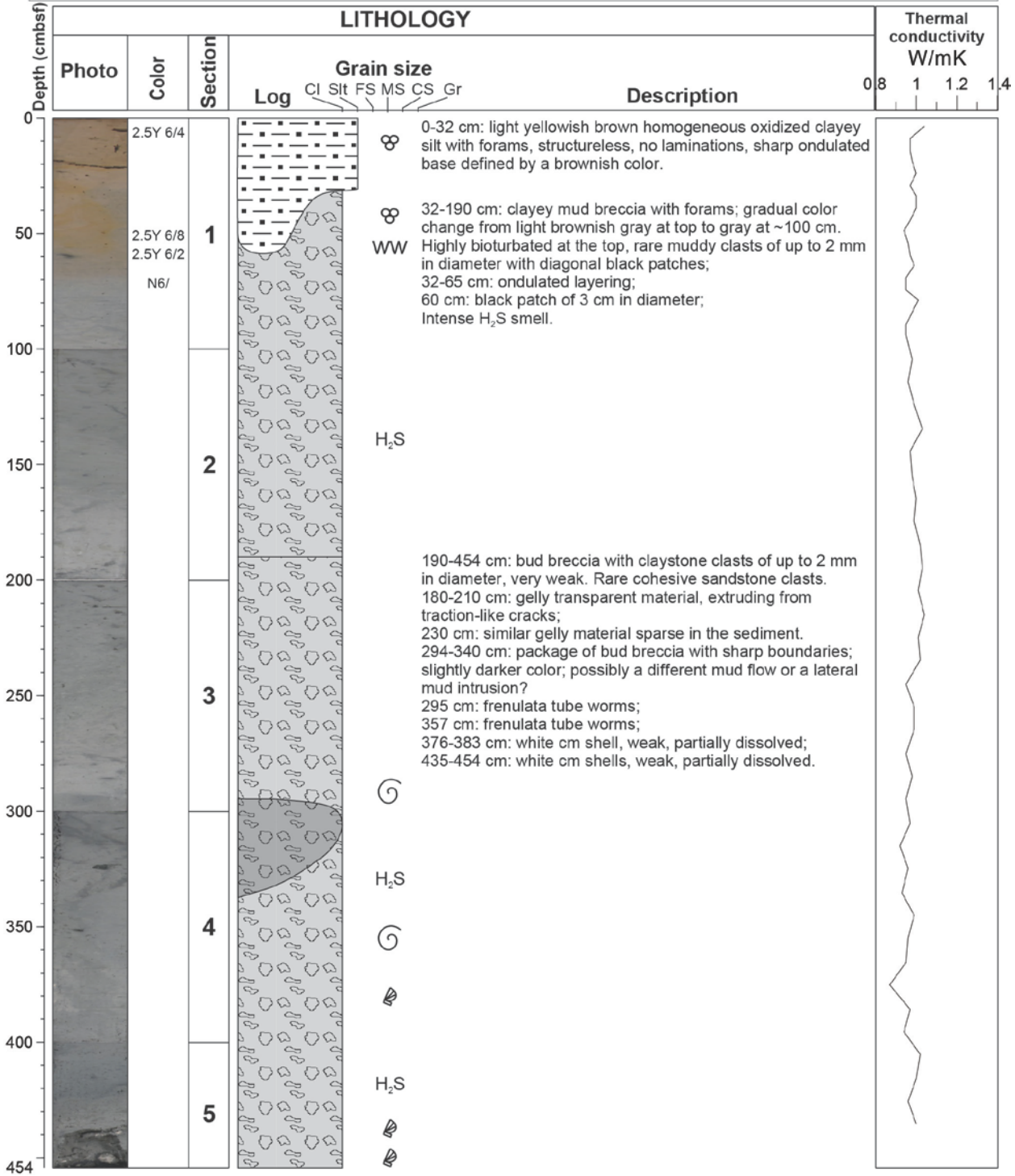
Latitude: 35°45.727' N

Date: 03.03.2012, 12:08 (UTC)

Longitude: 10°21.248' W

Water depth: 4564 m

Recovery: 454 cm



M86/5-27 GC-05

M86/5_331



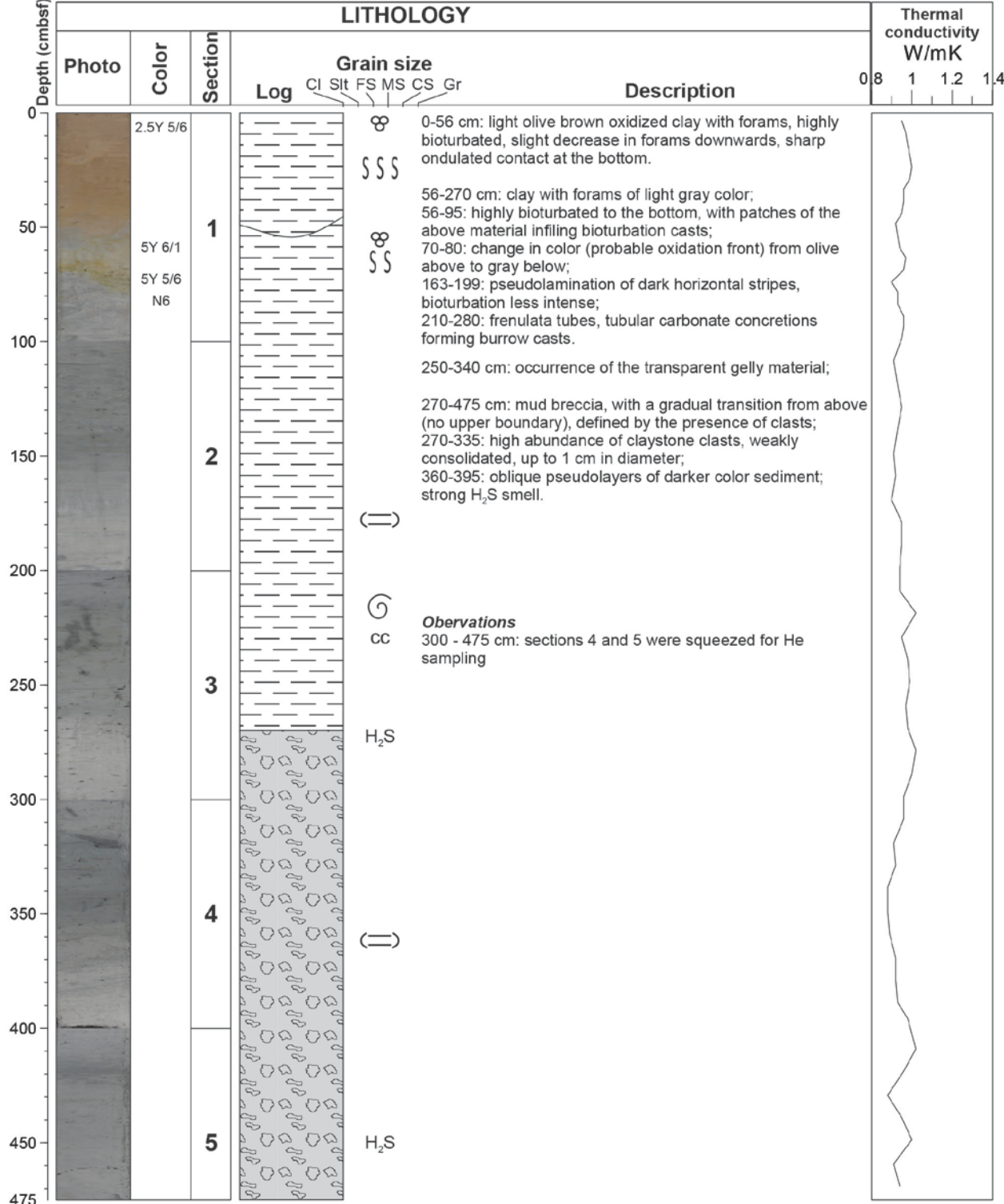
M86/5-28 GC-06

M86_332



475 cm

R/V METEOR M86/5	Station: M86/5 - 37 GC07
Location: Gulf of Cadiz, Tiamat mud volcano	M86/5_340
Latitude: 35°45.708' N	Date: 03.03.2012, 15:24 (UTC)
Longitude: 10°21.253' W	
Water depth: 4547 m	Recovery: 475 cm



0-56 cm: light olive brown oxidized clay with forams, highly bioturbated, slight decrease in forams downwards, sharp undulated contact at the bottom.

56-270 cm: clay with forams of light gray color; 56-95: highly bioturbated to the bottom, with patches of the above material infilling bioturbation casts; 70-80: change in color (probable oxidation front) from olive above to gray below; 163-199: pseudolamination of dark horizontal stripes, bioturbation less intense; 210-280: frenulata tubes, tubular carbonate concretions forming burrow casts.

250-340 cm: occurrence of the transparent gelly material;

270-475 cm: mud breccia, with a gradual transition from above (no upper boundary), defined by the presence of clasts; 270-335: high abundance of claystone clasts, weakly consolidated, up to 1 cm in diameter; 360-395: oblique pseudolayers of darker color sediment; strong H₂S smell.

Observations
300 - 475 cm: sections 4 and 5 were squeezed for He sampling

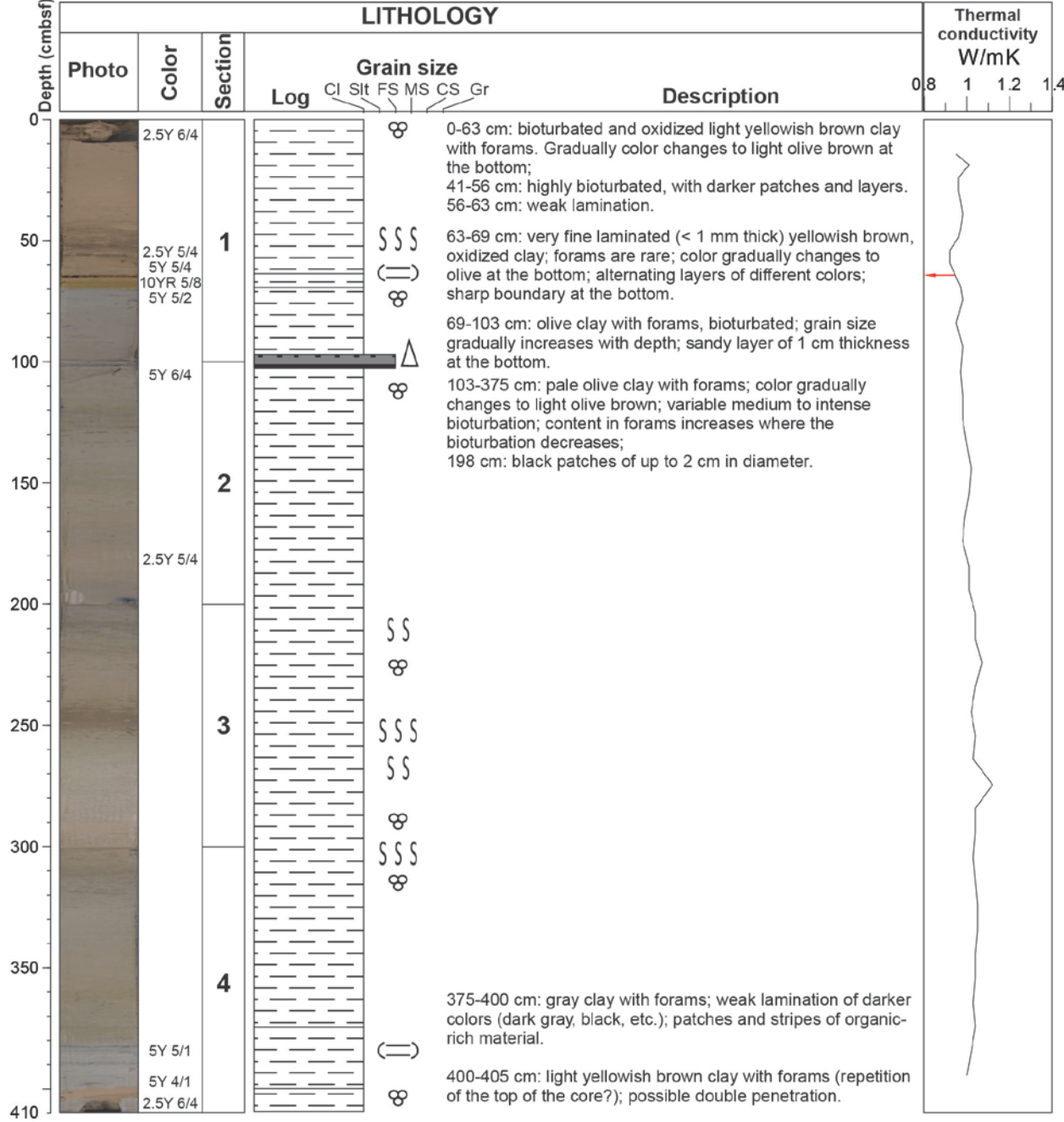


M86/5-37 GC-07
M86/5_340



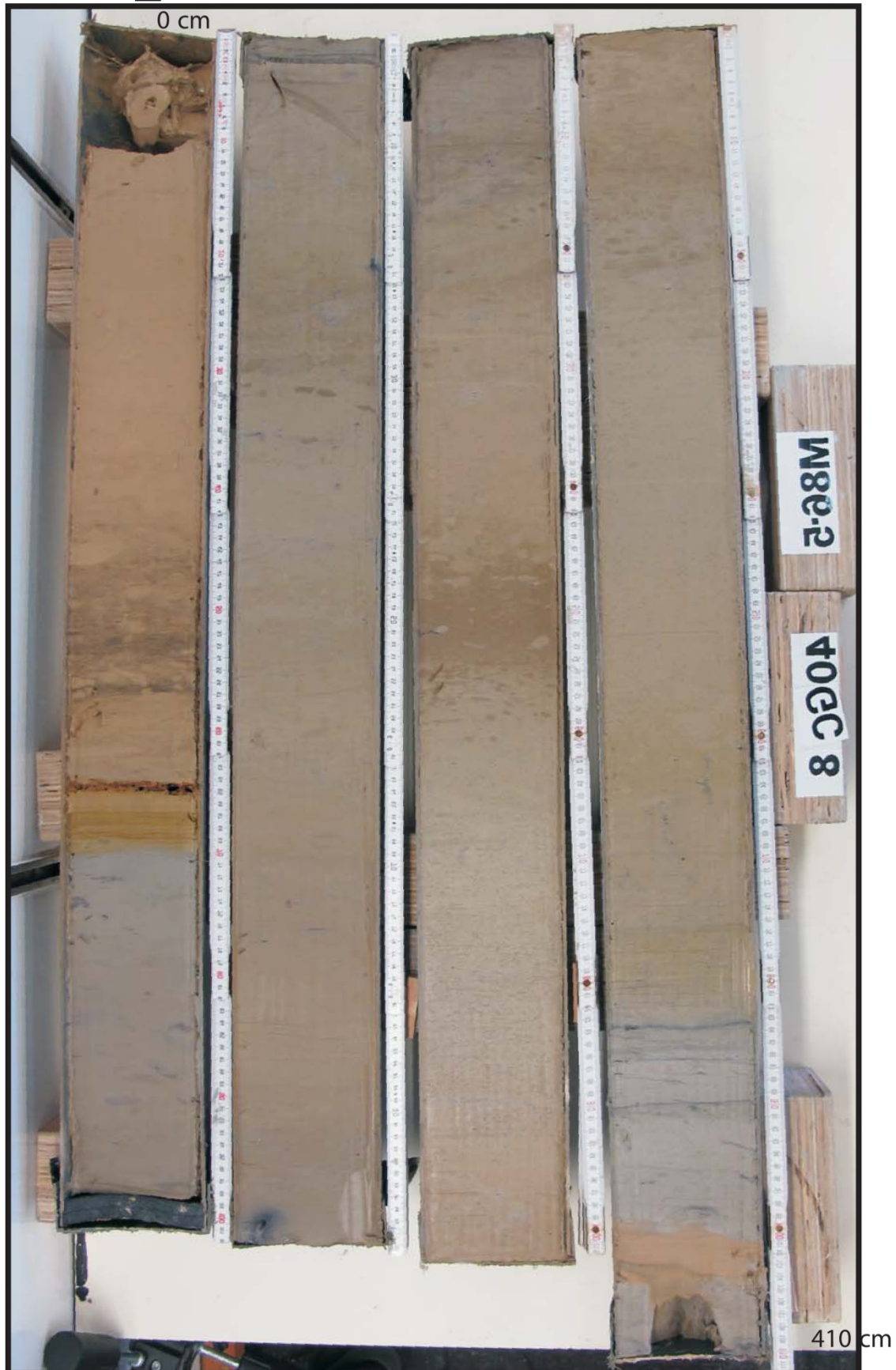
475 cm

R/V METEOR M86/5 Location: Gulf of Cadiz, reference station for heat flow, close to Michael Ivanov MV Latitude: 35°45.585' N Longitude: 10°11.729' W Water depth: 4584 m	Station: M86/5 - 40 GC08 M86/5_343 Date: 04.03.2012, 10:25 (UTC) Recovery: 410 cm
---	--



M86/5-40 GC-08

M86/5_343



R/V METEOR M86/5

Station: M86/5 - 42 GC10

Location: Gulf of Cadiz, Michael Ivanov mud volcano

M86/5_345

Latitude: 35°44.355' N
Longitude: 10°12.179' W
Water depth: 4481 m

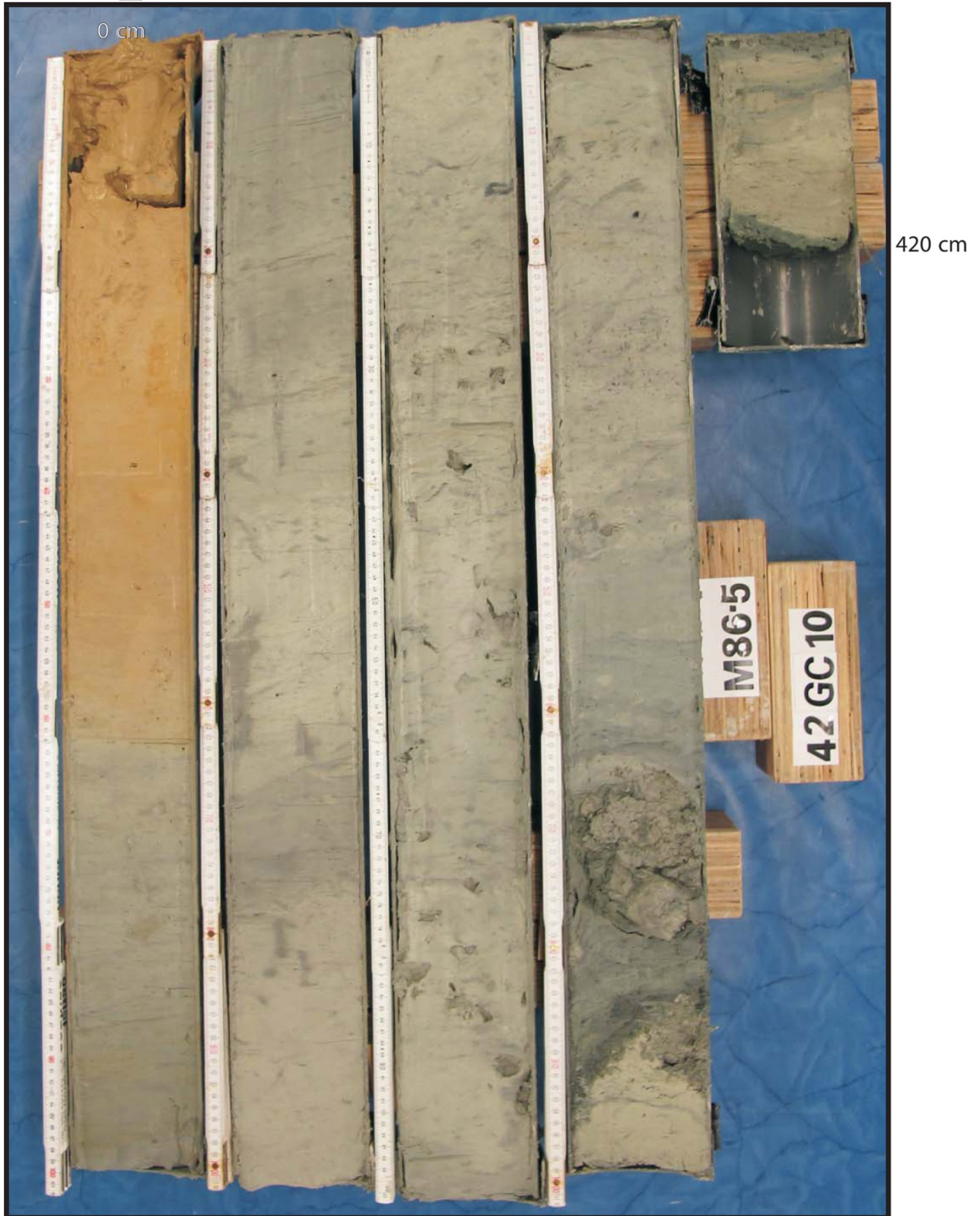
Date: 04.03.2012, 17:34 (UTC)

Recovery: 420 cm

Depth (cmbsf)	LITHOLOGY					Thermal conductivity	
	Photo	Color	Section	Log	Grain size		Description
					Cl Silt FS MS CS Gr		
0		10YR 6/8	1		☉	0-63 cm: oxidized light olive brown silty clay with forams, highly bioturbated, water saturated up to 10 cm, with brownish yellow patches of and with probable organic-rich material, patches of darker color; gradual color change to light yellowish brown.	not measured
50		2.5Y 6/4 5GY 5/1			SSS	63-389 cm: greenish gray clay; 94-140: vertical and continuous tube-like trace of black material with 0.7 cm in diameter (probably the trace of a frenulata tube), pseudolaminated in some areas, with patches of dark material;	
100			2		☉	145-180: frenulata tubes;	
150		5BG 6/1			☉	164-177: intense bioturbation;	
200		5B 4/1			☉	225-290 cm: patches of transparent gelly material, occurrence of carbonate concretions up to 3 cm in diameter;	
250			3		☉	225-290 cm: mud breccia with rare clasts of claystone very weak and dissolved into the matrix.	
300						☉	310-367: intense bioturbation;
350			4		☉	370-380: very large concretion of 12 cm in diameter, probably forming an extensive layer cut through by the corer, well consolidated at the bottom and weakly consolidated at the top;	
400		5GY 5/1				☉	380-389: clayey silt, greenish gray color, gradually changing to darker greenish gray at the bottom; sharp contact at the base.
420		5GY 7/1	5		☉	389-400 cm: light greenish gray clay carbonate concretion, with a sharp contact at the base;	
						☉	400-420: greenish gray clayey silt, alternating with light greenish gray layers of clayey silt.
					☉	Observations: 300-400 cm: section 4 was squeezed for He sampling.	

M86/5-42 GC-10

M86/5_345



R/V METEOR M86/5

Station: M86/5 - 47 GC11

Location: Gulf of Cadiz, target point 2 on the Horseshoe Abyssal Plain

M86/5_351

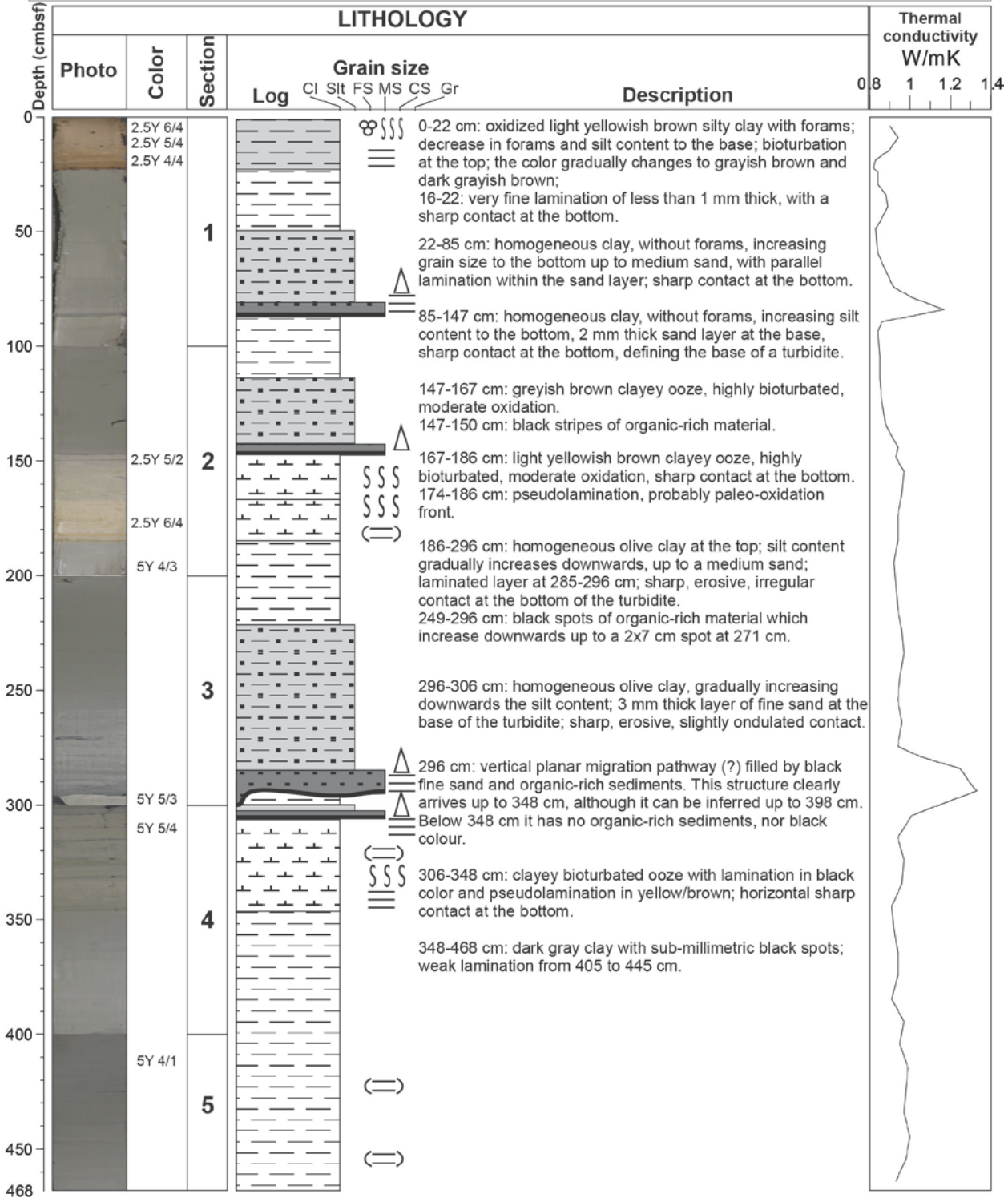
Latitude: 35°47.301' N

Date: 05.03.2012, 18:07 (UTC)

Longitude: 10°38.537' W

Water depth: 4874m

Recovery: 468 cm



M86/5-47 GC-11
M86/5_351



R/V METEOR M86/5

Station: M86/5 - 54 GC12

Location: Gulf of Cadiz, topographic high on Horseshoe Abyssal Plain

M86/5_356

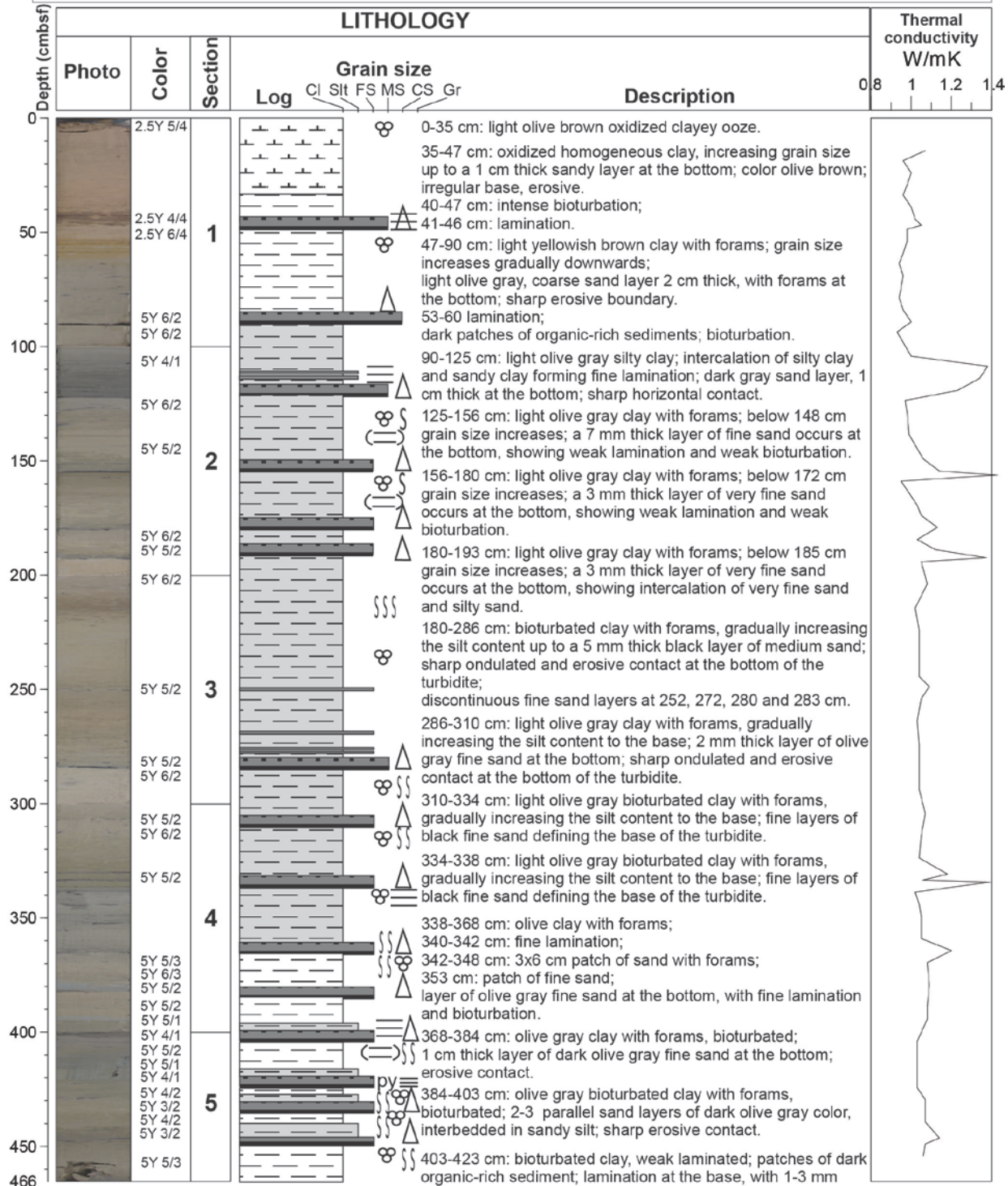
Latitude: 35°49.678' N

Date: 06.03.2012, 08:03 (UTC)

Longitude: 11°20.769' W

Water depth: 4823 m

Recovery: 466 cm



thick layers of fine sand interbedded within sandy silt sediment; irregular and discontinuous base;
 410-421 cm: vertical fracture 1 mm thick, filled with dark organic material and semiconsolidated claystone and sub-millimetric pyrites.
 423-430 cm: olive gray clay with forams and bioturbation; increasing grain size to bottom up to a medium sand discontinuous layer of dark olive gray color.
 430-448 cm: bioturbated clay with forams; grain size increases with depth up to a medium sand layer at the bottom of the turbidite.
 448-466 cm: olive gray bioturbated clay with forams.

M86/5-54 GC-12

M86/5_356



466 cm

R/V METEOR M86/5

Station: M86/5 - 62 GC13

Location: Gulf of Cadiz, target point 2 on the Horseshoe Abyssal Plain

M86/5_364

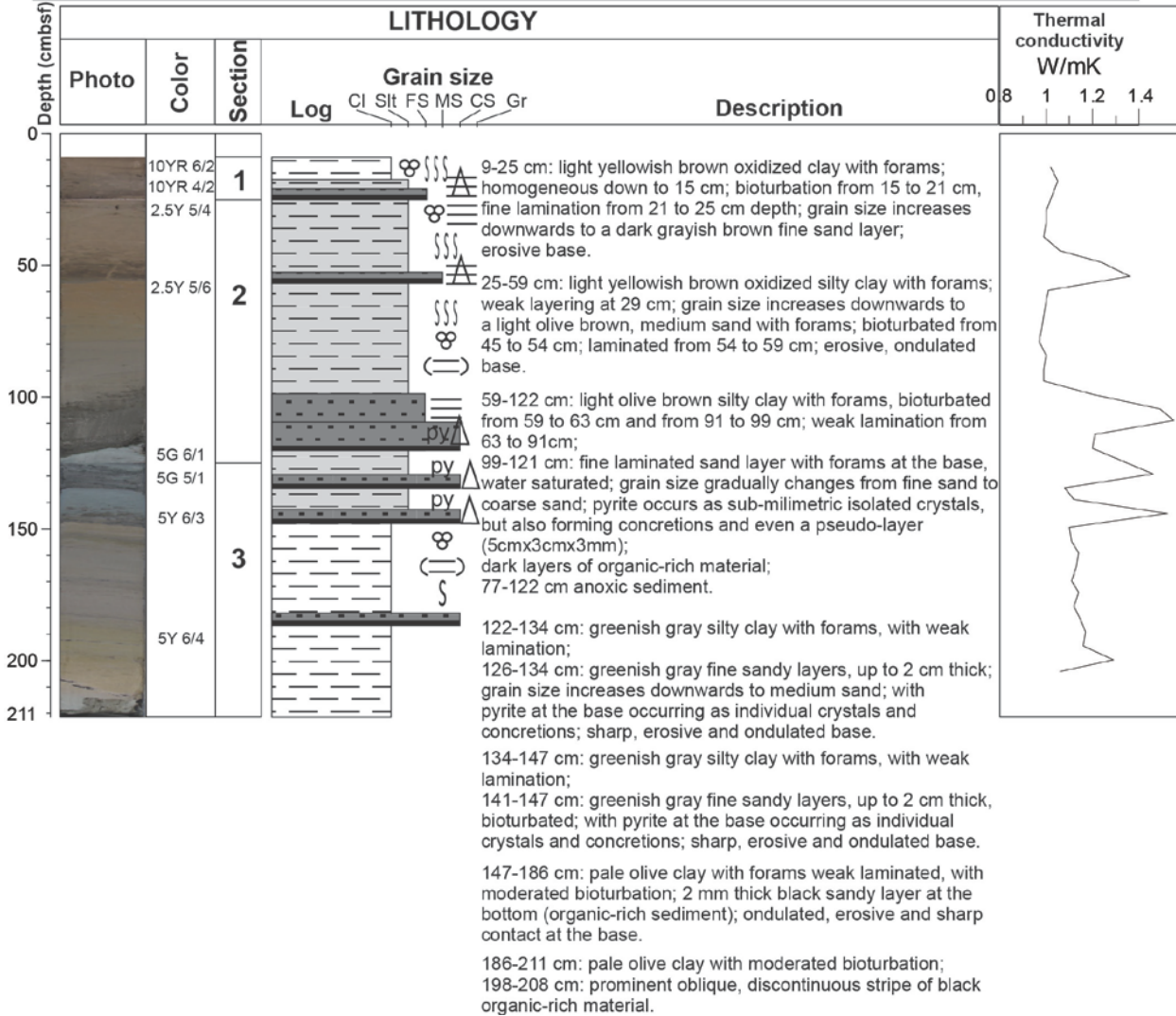
Latitude: 35°47.320' N

Date: 07.03.2012, 10:12 (UTC)

Longitude: 10°38.450' W

Recovery: 211 cm

Water depth: 4843 m



M86/5-62 GC-13

M86/5_364



R/V METEOR M86/5

Station: M86/5 - 63 GC14

Location: Gulf of Cadiz, target point 2 at the Horseshoe Abyssal Plain

M86/5_365

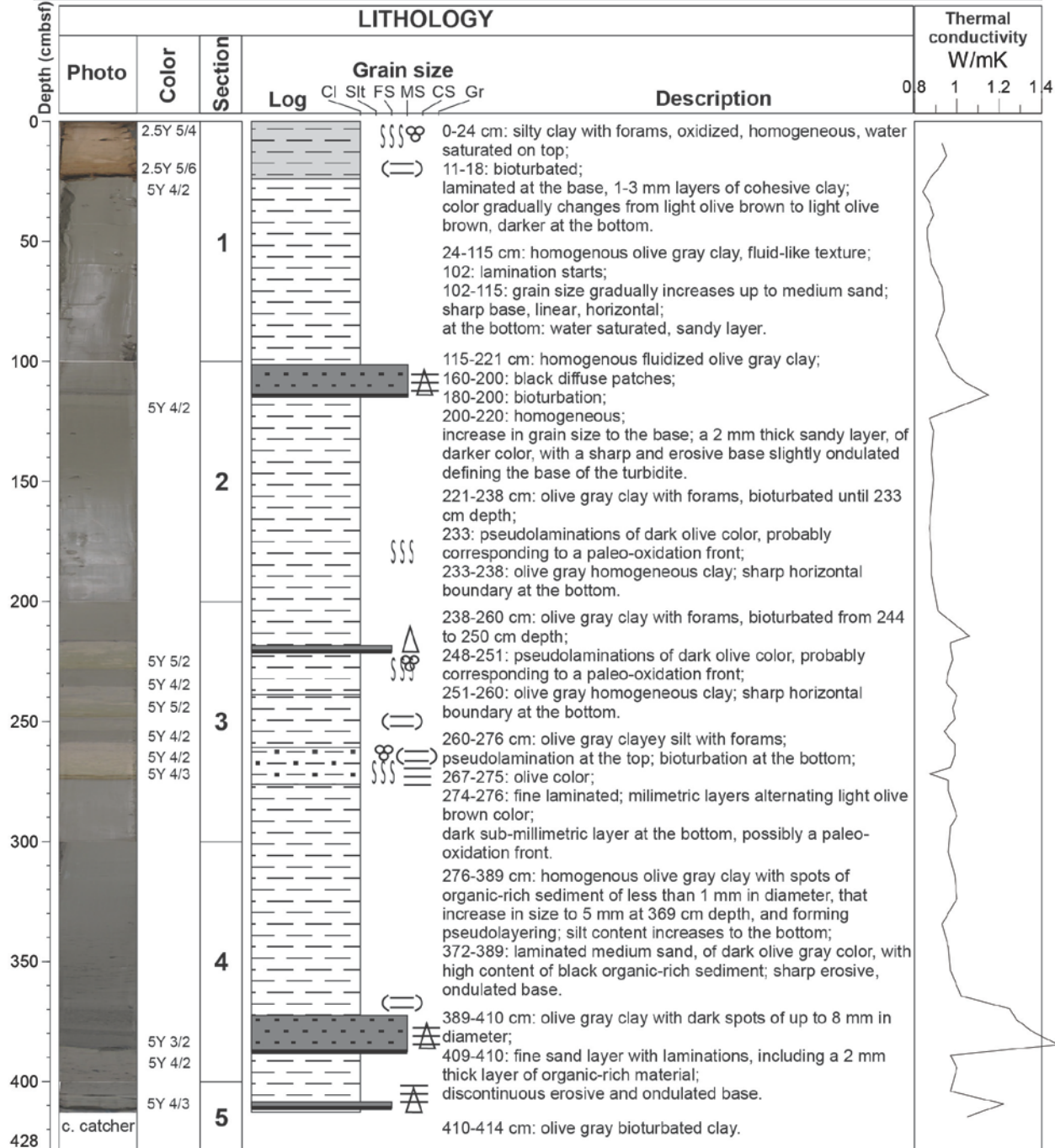
Latitude: 35°47.260' N

Date: 07.03.2012, 15:00 (UTC)

Longitude: 10°38.510' W

Water depth: 4865 m

Recovery: 428 cm



M86/5-63 GC-14

M86/5_365



428 cm

R/V METEOR M86/5

Station: M86/5 - 68 GC15

Location: Gulf of Cadiz, Abzu mud volcano

M86/5_370

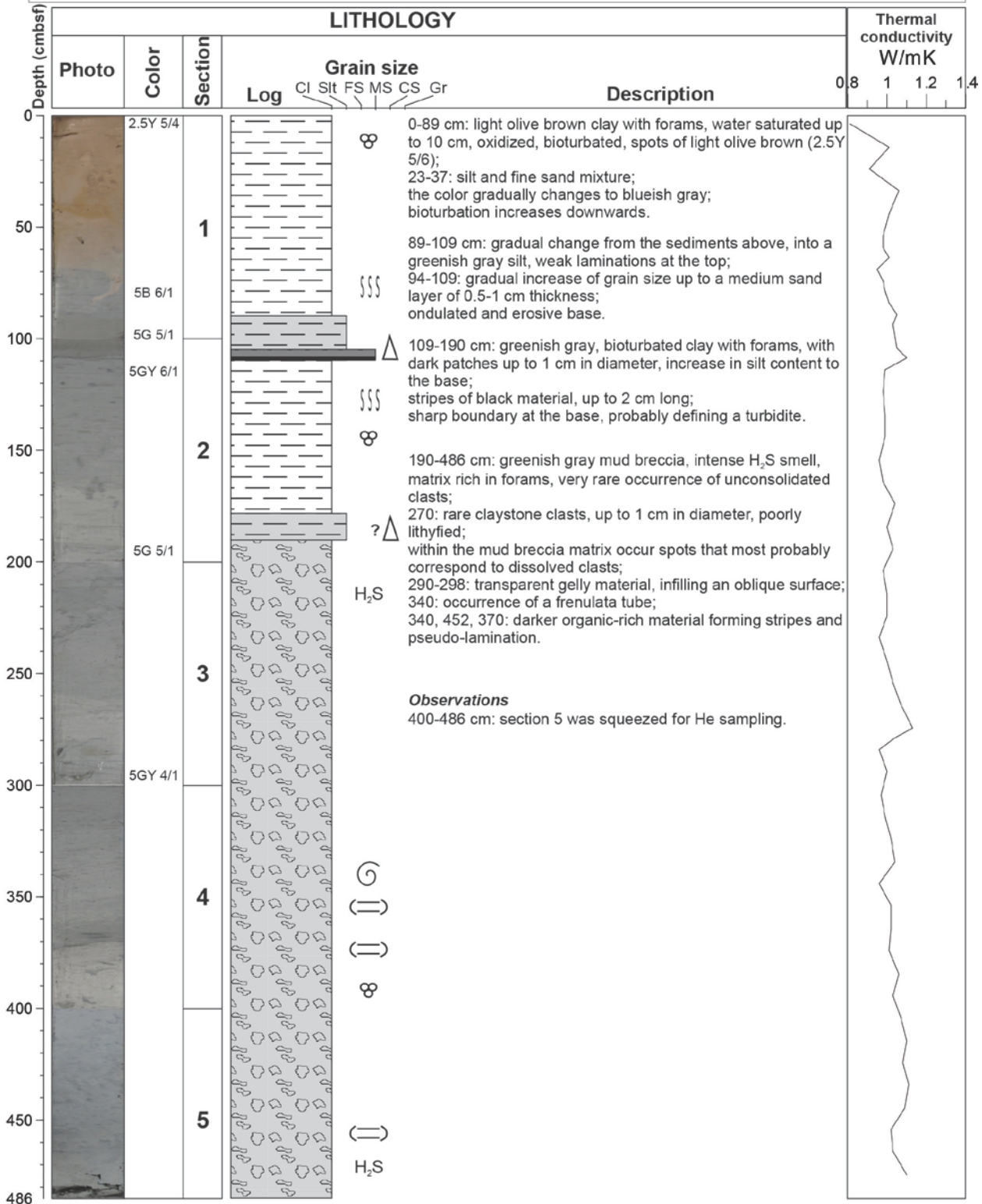
Latitude: 35°45.045' N

Date: 08.03.2012, 11:20 (UTC)

Longitude: 10°19.014' W

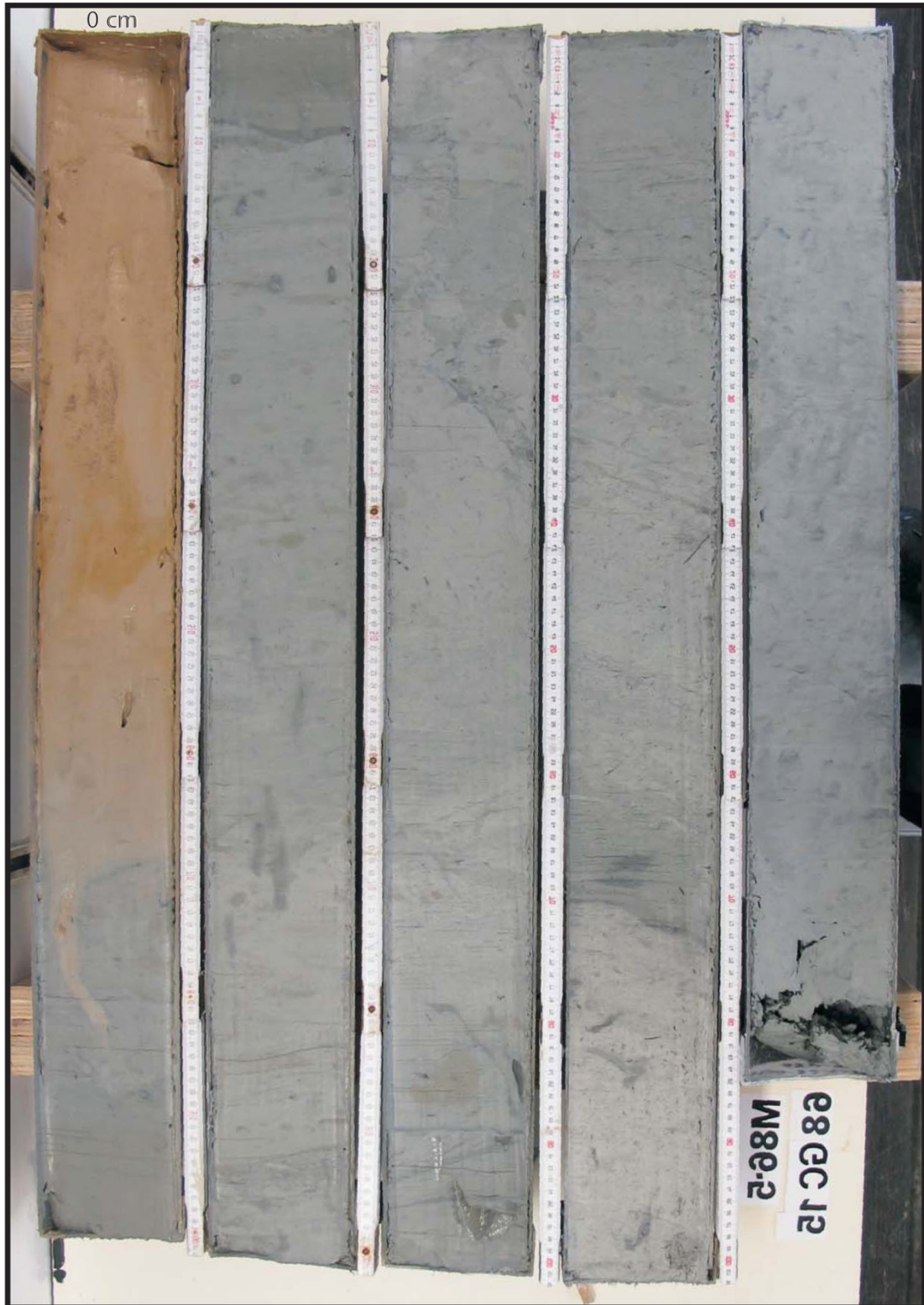
Water depth: 4549 m

Recovery: 486 cm



M86/5-68 GC-15

M86/5_370



486 cm

R/V METEOR M86/5

Station: M86/5 - 69 GC16

Location: Gulf of Cadiz, background reference core at the Horseshoe Abyssal Plain

M86/5_371

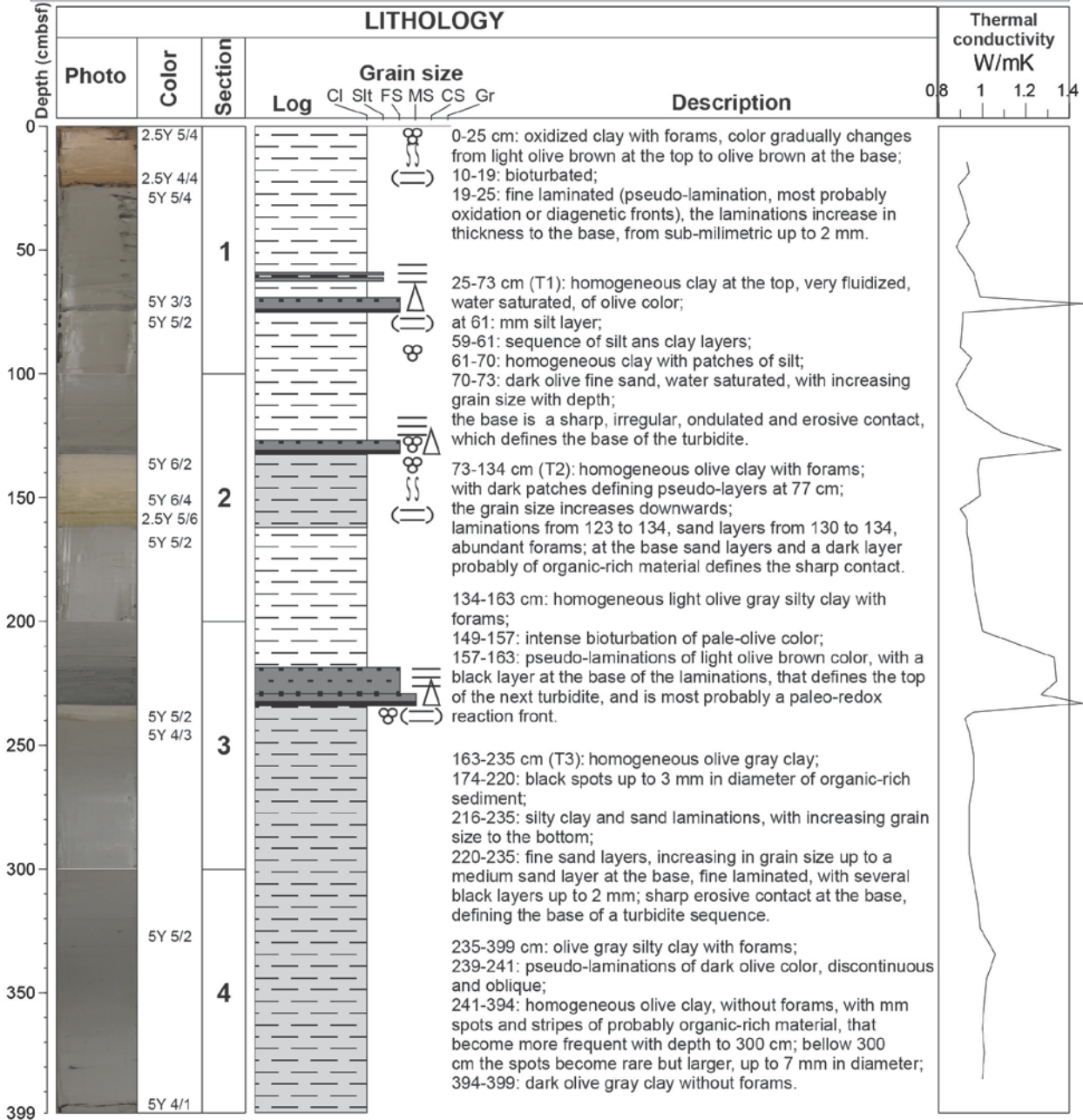
Latitude: 35°42.924' N

Date: 08.03.2012, 16:25 (UTC)

Longitude: 10°40.963' W

Water depth: 4864 m

Recovery: 399 cm



M86/5-69 GC-16

M86/5_371



R/V METEOR M86/5

Station: M86/5 - 73 GC17

Location: Gulf of Cadiz, topographic high at the Horseshoe Abyssal Plain

M86/5_375

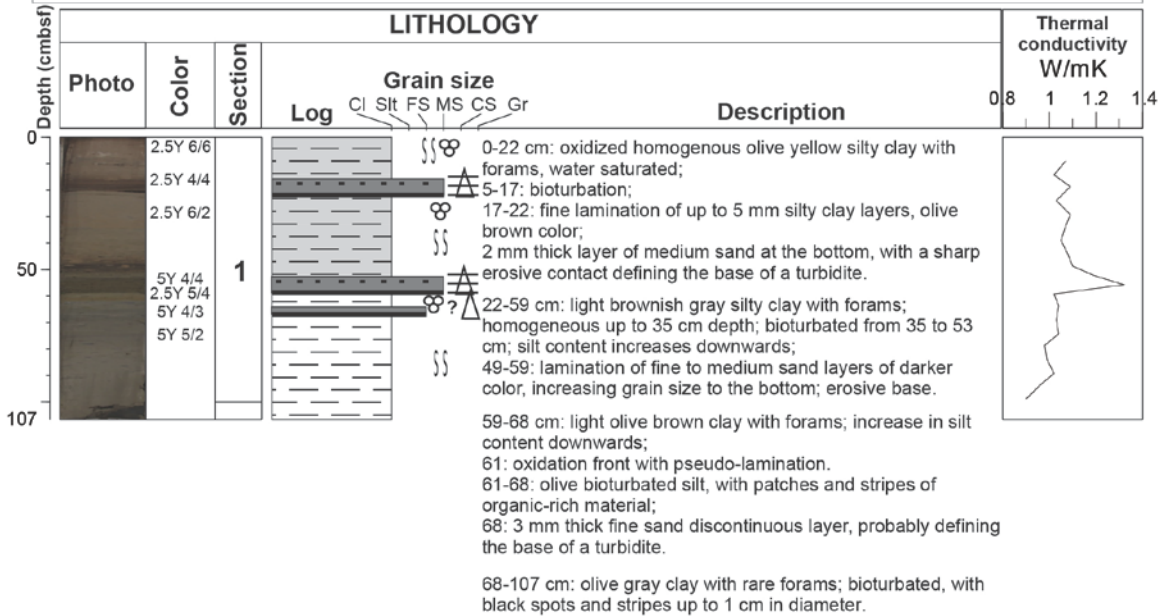
Latitude: 35°46.889' N

Date: 09.03.2012, 13:31 (UTC)

Longitude: 10°34.041' W

Water depth: 4856 m

Recovery: 107 cm



M86/5-73 GC-17

M86/5_375



M86/5-77 GC-18

M86/5_381



R/V METEOR M86/5

Station: M86/5 - 78 GC19

Location: Gulf of Cadiz, Horseshoe Abyssal Plain
North of Coral Patch Ridge

M86/5_382

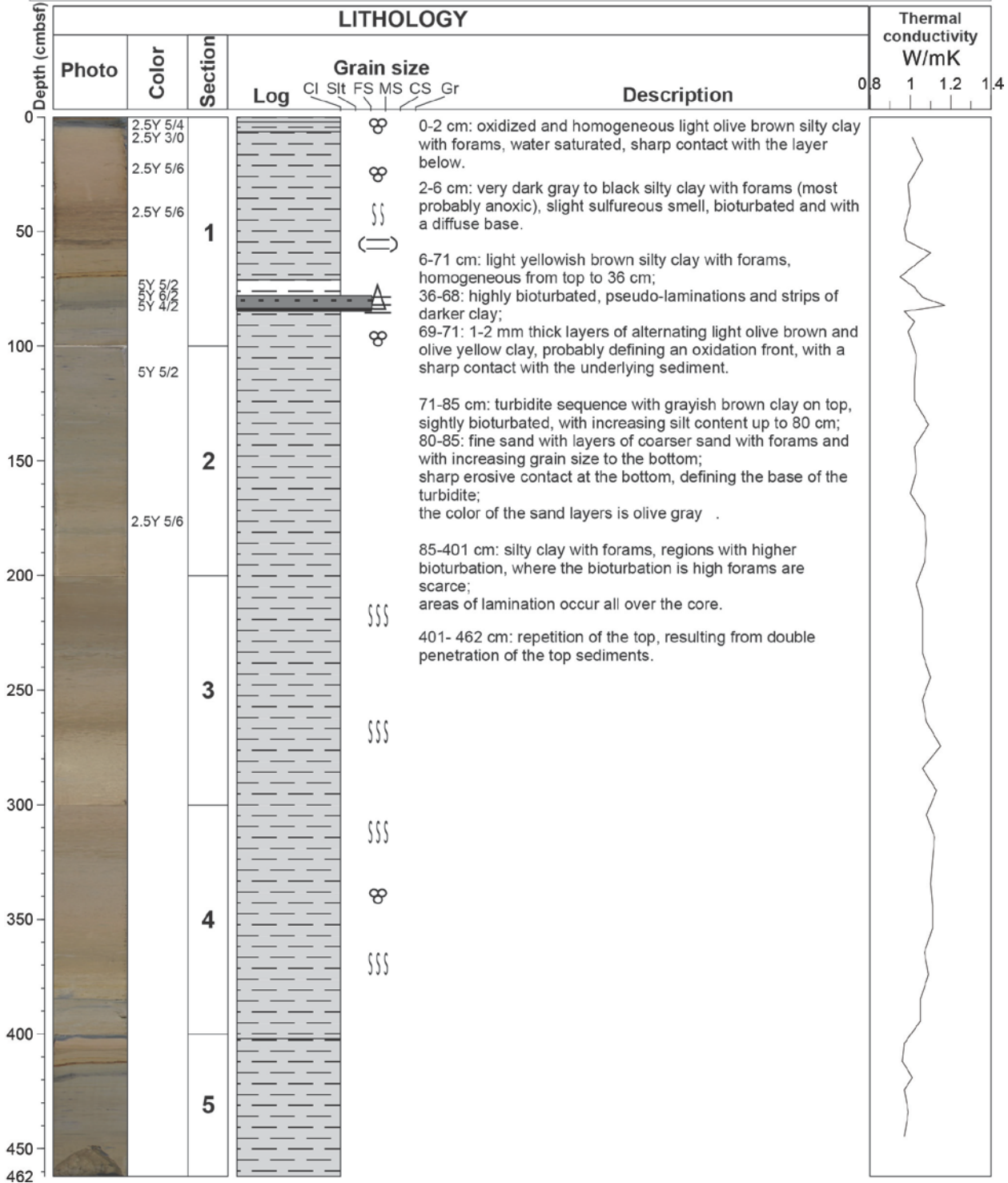
Latitude: 35°39.604' N

Date: 10.02.2012, 12:23 (UTC)

Longitude: 10°23.923' W

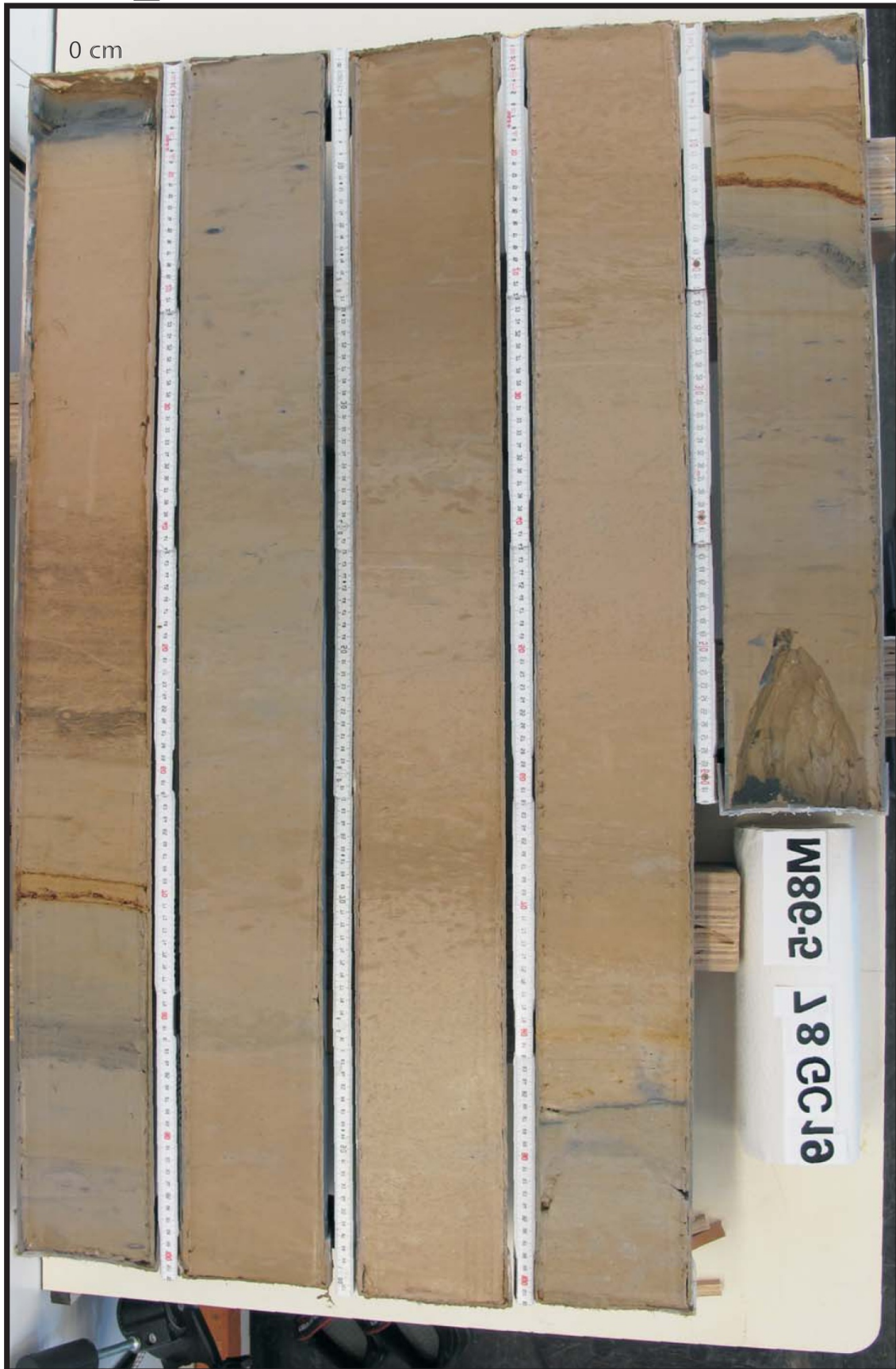
Water depth: 4642 m

Recovery: 462 cm



M86/5-78 GC-19

M86/5_382



0 cm

462 cm

M86-2 18 GC 19

R/V METEOR M86/5

Station: M86/5 - 92 GC20

Location: Gulf of Cadiz, Horseshoe abyssal Plain

M86/5_397

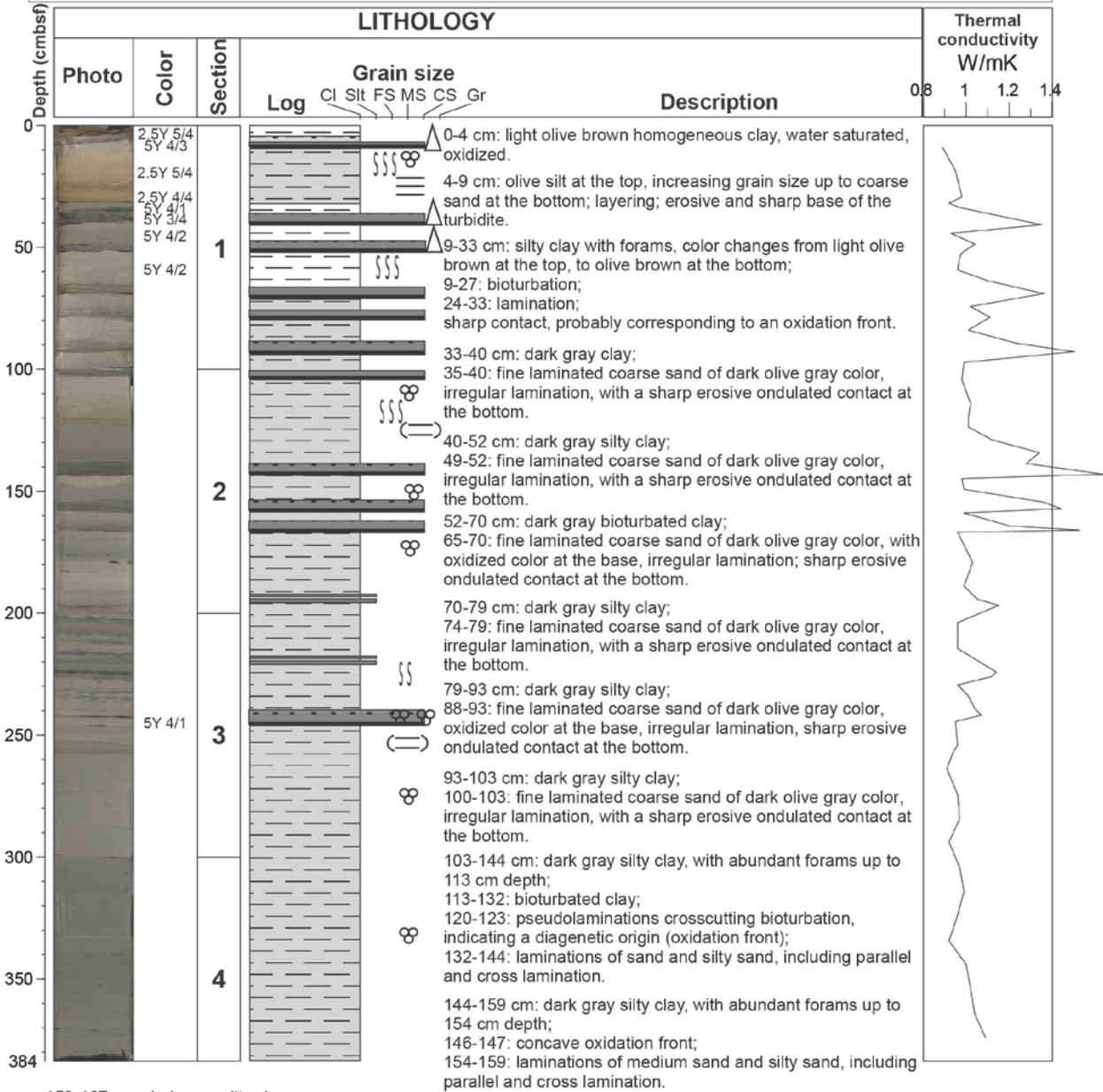
Latitude: 35°50.067' N

Date: 12.03.2012, 10:54 (UTC)

Longitude: 11°28.804' W

Water depth: 4848 m

Recovery: 384 cm



159-167 cm: dark gray silty clay;

163-167: fine laminated medium sand of dark olive gray color, irregular lamination, with a sharp erosive undulated contact at the bottom.

167-244 cm: clay with heterogeneous distribution of forams;

195-199 and 222-229: intercalations of silt and fine sand, with gradual diffuse boundaries at top and bottom;

spots, stripes and layer up to 2 cm thick of black organic-rich sediment, moderately bioturbated;

178: clast of 0.7 mm in diameter, probably gabbro;

240-244: foraminifera sandy layers with a sharp, erosive and slightly undulated base;

black color at the bottom due to the presence of black stained foraminifera and black minerals.

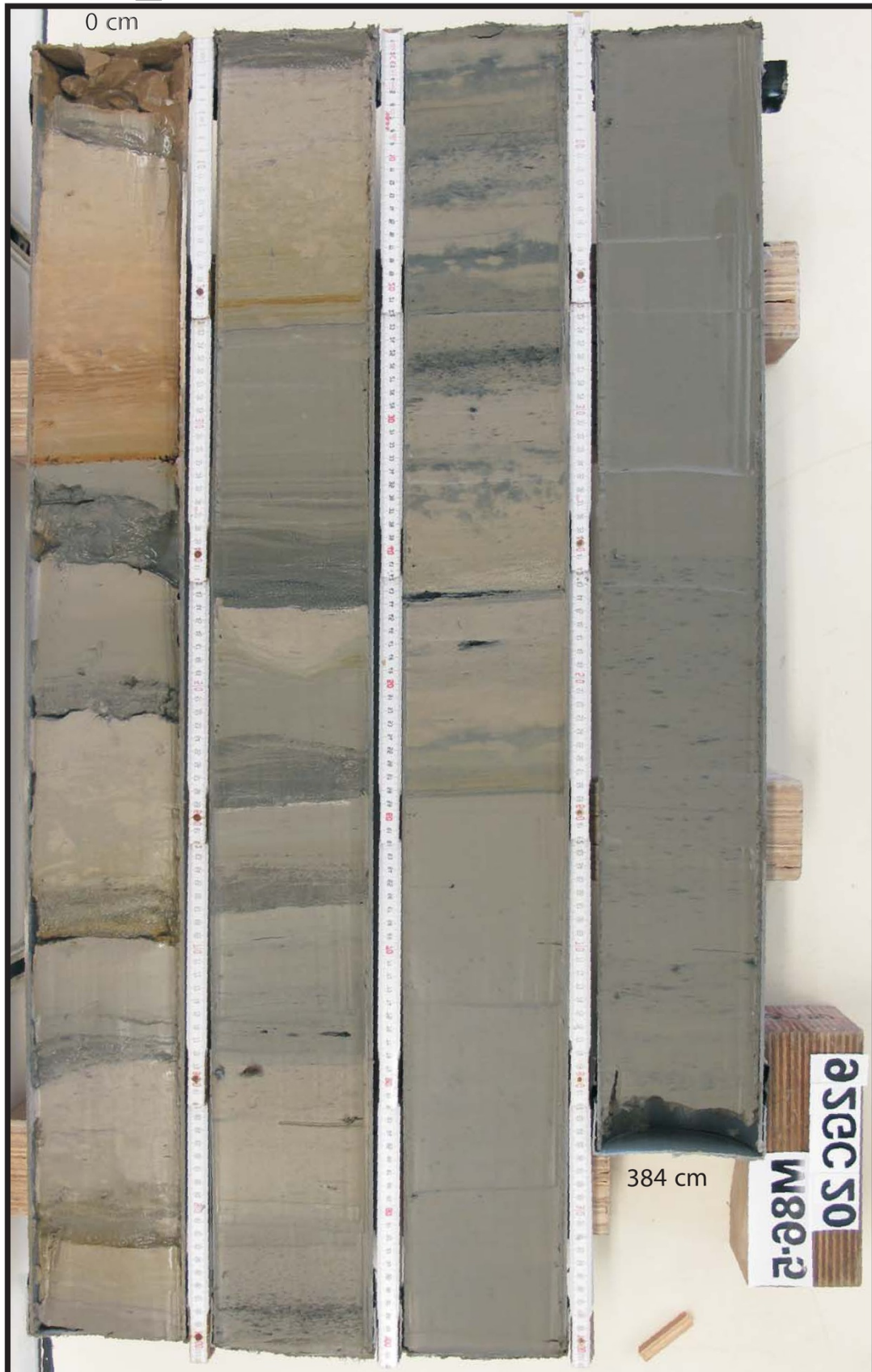
244-384 cm: homogeneous clay with forams, dark gray color;

254-257: pseudo-layers of paleo-oxidation fronts;

247: black clast of 5 mm in diameter, weak and with rubber smell; stripes and spots of black material up to 3 mm in diameter.

M86/5-92 GC-20

M86/5_397



R/V METEOR M86/5

Station: M86/5 - 93 GC21

Location: Gulf of Cadiz, topographic high at the Horseshoe Abyssal Plain

M86/5_398

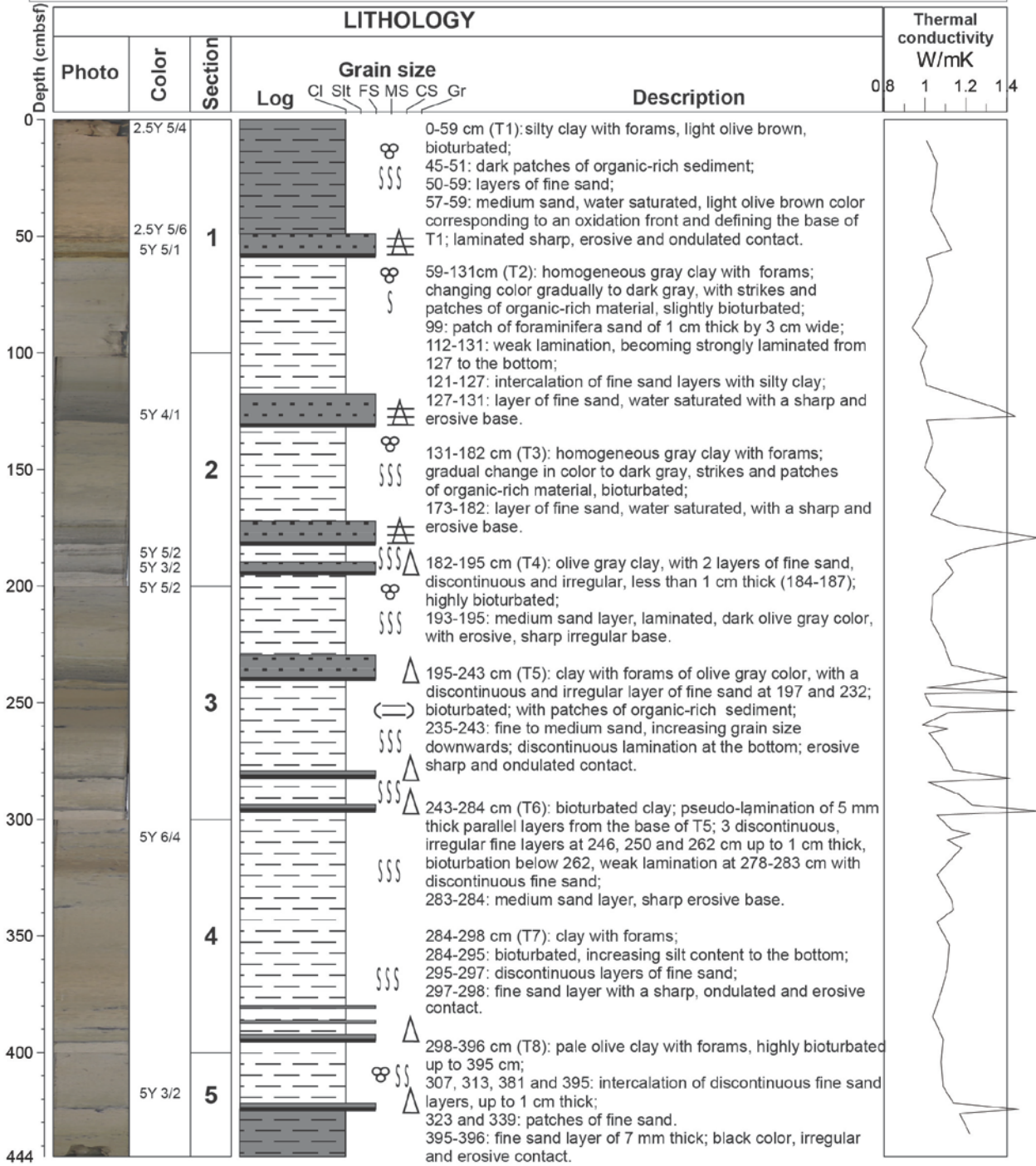
Latitude: 35°49.797' N

Date: 12.03.2012, 15:24 (UTC)

Longitude: 11°20.167' W

Water depth: 4825 m

Recovery: 444 cm



M86/5-93 GC-21

M86/5_398



0 cm

444 cm

M86-2

93GC21

R/V METEOR M86/5

Station: M86/5 - 95 GC22

Location: Gulf of Cadiz, topographic high at the Horseshoe Abyssal Plain

M86/5_401

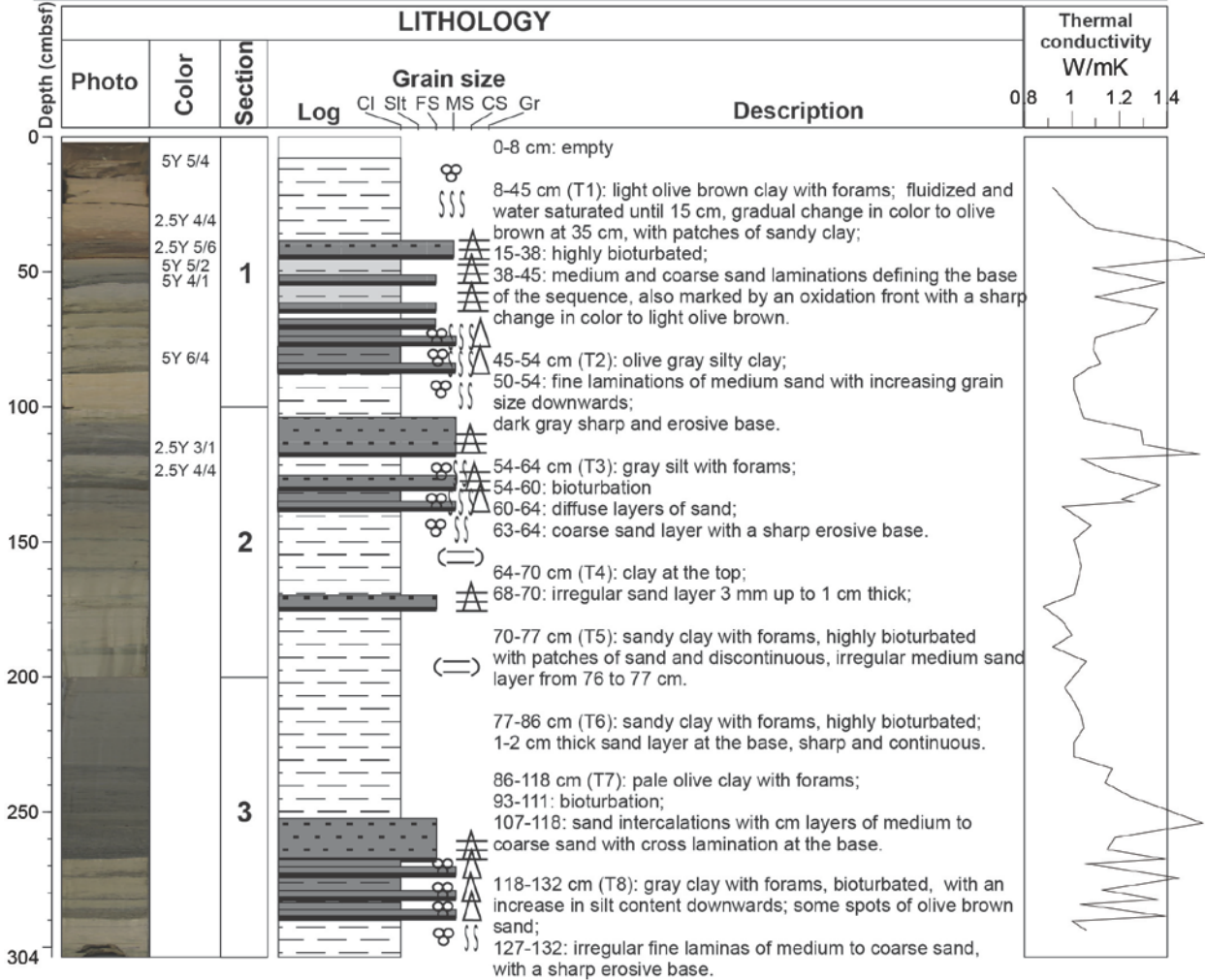
Latitude: 35°50.274' N

Date: 13.03.2012, 08:15 (UTC)

Longitude: 11°20.736' W

Recovery: 304 cm

Water depth: 4847 m



132-138 cm (T9): sandy clay with forams, highly bioturbated with patches of sand and discontinuous, irregular, medium sand layer at the base.

138-175 cm (T10): bioturbated clay with forams on top; with black spots and stripes of probable organic-rich sediment; with brown pseudolaminations, most probably marking a paleo-oxidation front; 170-175: layers and lenses of medium to coarse sand with forams.

175-268 cm (T11): clay with forams up to 182 cm; 182-234: clay with no forams; 185-199: pseudolamination, most probably marking paleo-oxidation front; 205-230: black spots of organic-rich material; 234-257: discontinuous layers of fine sand, increasing grain size downwards; 257-268: fine laminated sand with a sharp and erosive base.

268-275 cm (T12): sandy clay with forams, highly bioturbated with patches of sand and discontinuous, irregular medium sand layer at the base.

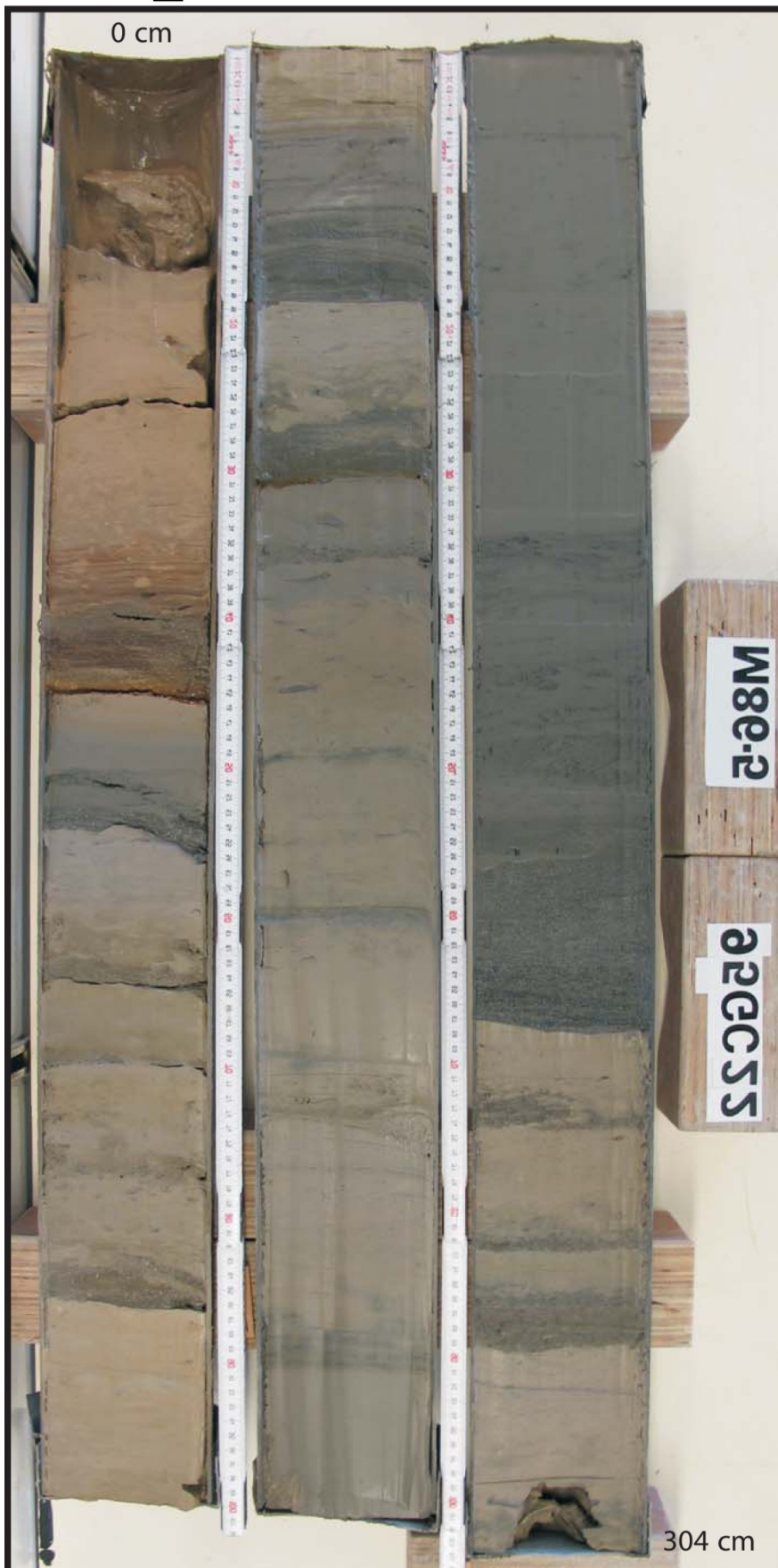
275-284 cm (T13): sandy clay with forams, highly bioturbated with patches of sand and discontinuous, irregular medium sand layer at the base.

284-290 cm (T14): sandy clay with forams, highly bioturbated with patches of sand and discontinuous, irregular medium sand layer at the base.

290-304 cm: bioturbated clay with forams, with spots and stripes of black organic-rich sediments.

M86/5-95 GC-22

M86/5_401



R/V METEOR M86/5

Station: M86/5 - 96 GC23

Location: Gulf of Cadiz, topographic high at the Horseshoe Abyssal Plain

M86/5_402

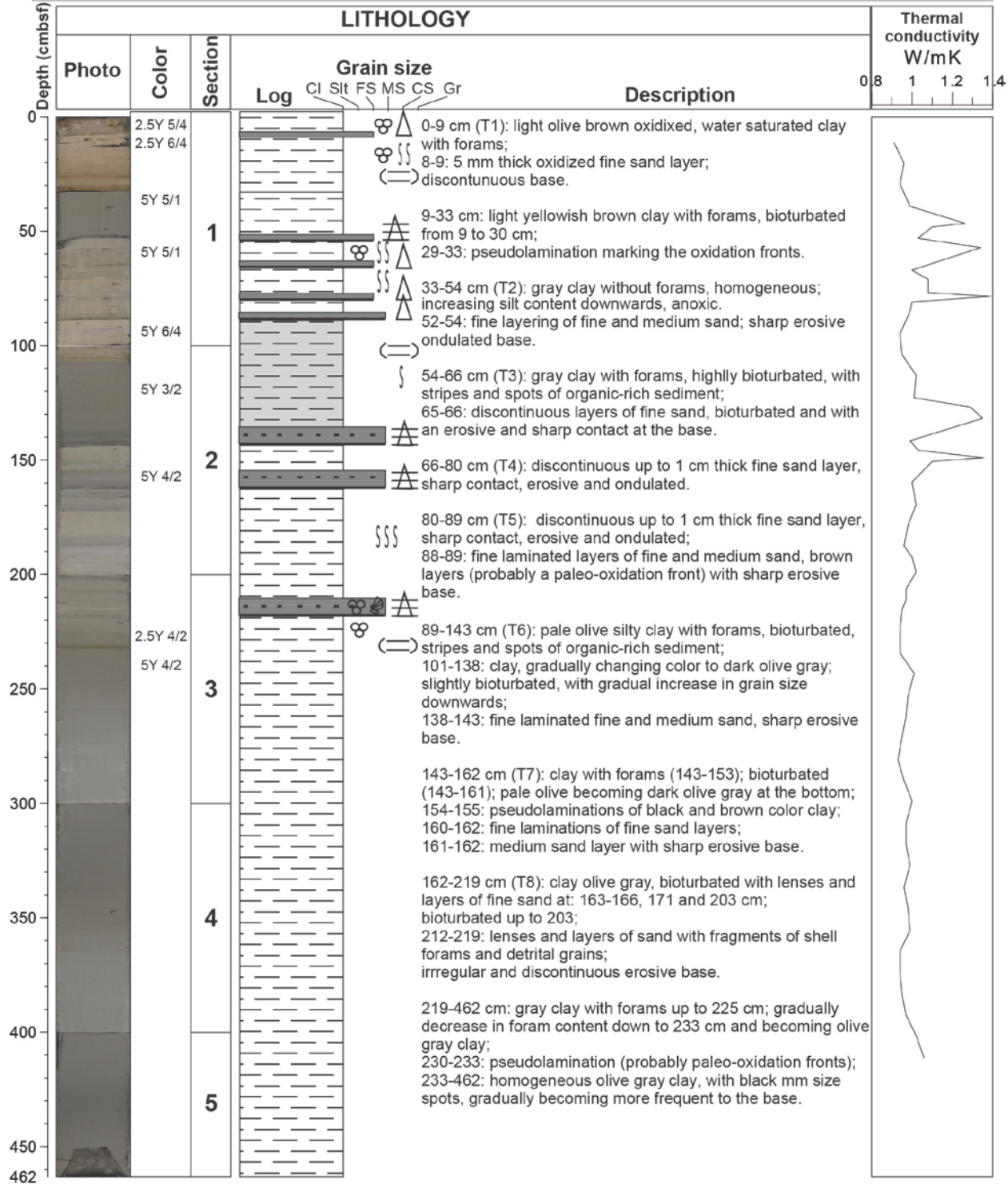
Latitude: 35°48.674' N

Date: 13.03.2012, 11:48 (UTC)

Longitude: 11°20.858' W

Water depth: 4860 m

Recovery: 462 cm



M86/5-96 GC-23

M86/5_402



R/V METEOR M86/5

Station: M86/5 - 97 GC24

Location: Gulf of Cadiz, (target point 9) topographic high at the Horseshoe Abyssal Plain

M86/5_403

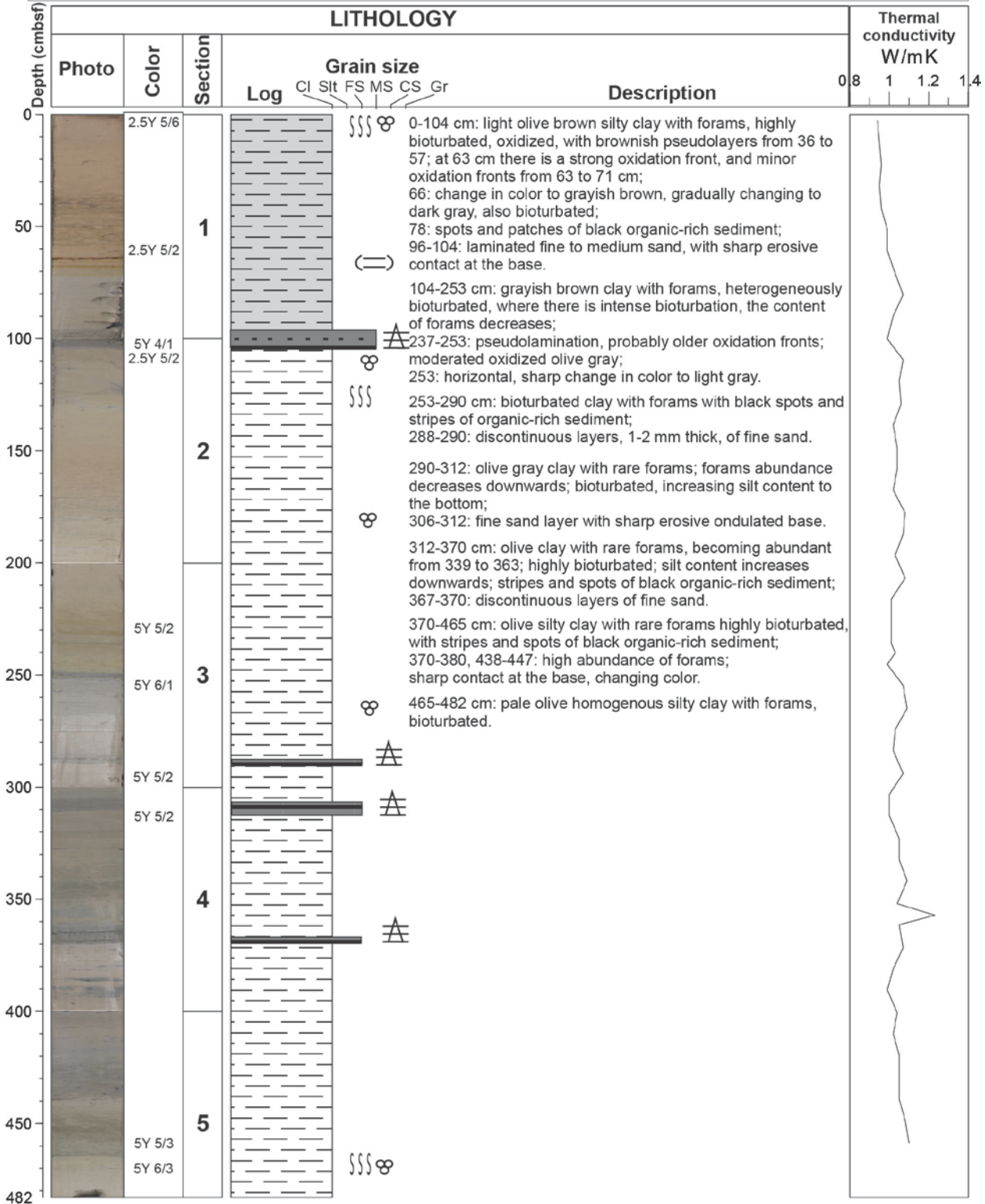
Latitude: 35°47.875' N

Date: 13.03.2012, 18:27 (UTC)

Longitude: 10°40.764' W

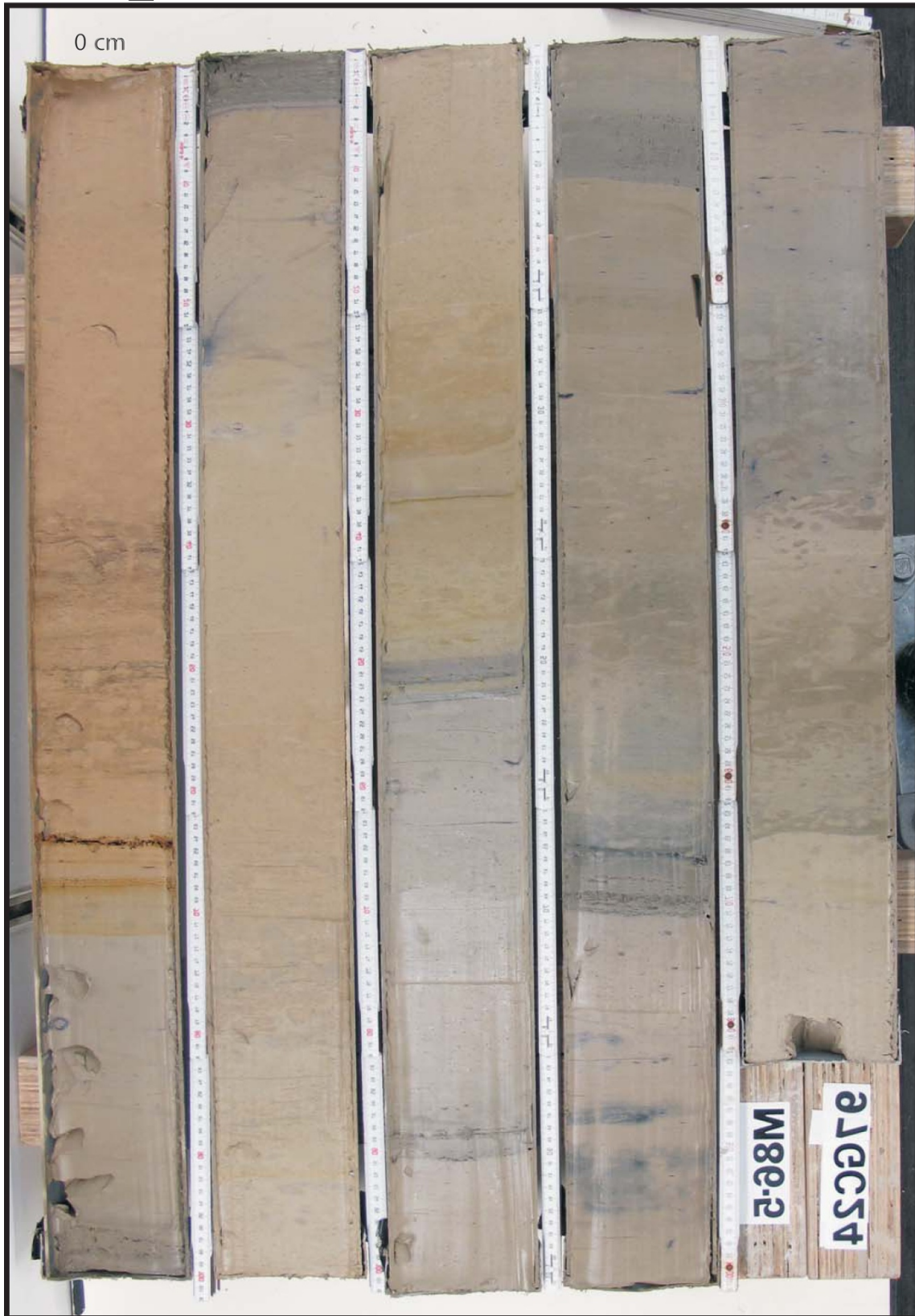
Water depth: 4814 m

Recovery: 482 cm




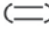
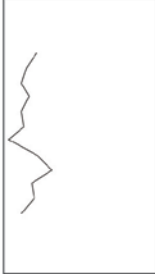


M86/5-97 GC-24

M86/5_403



R/V METEOR M86/5	Station: M86/5 - 100 GC25
Location: Gulf of Cadiz, M Ivanov mud volcano	M86/5_406
Latitude: 35°44.341' N	Date: 14.03.2012, 08:36 (UTC)
Longitude: 10°12.061' W	Recovery: 94 cm
Water depth: 4488 m	

Depth (cmbsf)	LITHOLOGY						Thermal conductivity W/mK							
	Photo	Color	Section	Log	Grain size									
				Cl	Silt	FS	MS	CS	Gr	Description	0.8	1	1.2	1.4
0		5G 4/1	1		H ₂ S  23 cm frenulata tube; 23 cm Acharax shell;  32 cm: changing color to greenish gray; 46 cm: claystone clast of 1 cm diameter; 48-49 cm: pseudo-lamination with a black layer of 0.5 cm thick and a brownish layer 2 mm thick. gh 65-76 cm: one gas hydrate chunk subrounded of 10x4x5 cm size. White milky color, with transparent, euhedric crystals of ice (?).									
50		5G 5/1												
94		5G 7/1												

Observations:
 20 cm: Section was squeezed for He sampling.

M86/5-100 GC-25

M86/5_406



M86/5-03TV-MUC-01

M86/5_307



M86/5-04MUC-02

M86/5_308

